(12)

VSC-TR-82-7

Q OF THE EARTH IN THE 0.5-10Hz BAND

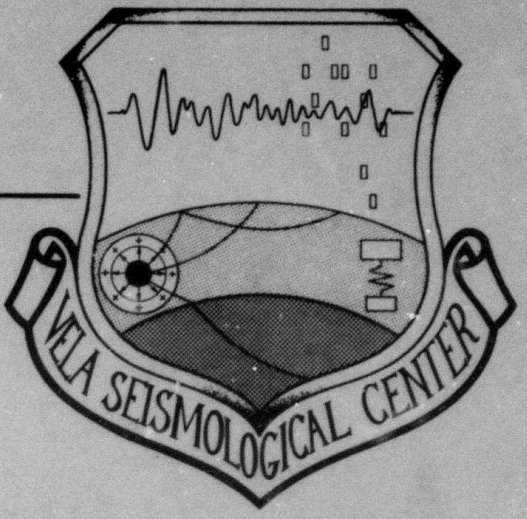

Z.A. Der, D.W. Rivers, T.W. McElfresh,
A. O'Donnell, P.J. Klouda, and M. Marshall

Seismic Data Analysis Center
Teledyne Geotech
314 Montgomery Street
Alexandria, Virginia 22314

16 OCT 1981

APPROVED FOR PUBLIC RELEASE; DISTRIBUTION UNLIMITED.

Monitored By:
VELA Seismological Center
312 Montgomery Street
Alexandria, VA 22314

Sponsored by

The Defense Advanced Research Projects Agency (DARPA)

DARPA Order No. 2551

Unclassified

SECURITY CLASSIFICATION OF THIS PAGE (When Data Entered)

REPORT DOCUMENTATION PAGE		READ INSTRUCTIONS BEFORE COMPLETING FORM
1. REPORT NUMBER VSC-TR-82-7	2. GOVT ACCESSION NO. AD A117712	3. RECIPIENT'S CATALOG NUMBER
4. TITLE (and Subtitle) Q OF THE EARTH IN THE 0.5-10 HZ BAND		5. TYPE OF REPORT & PERIOD COVERED Technical 6. PERFORMING ORG. REPORT NUMBER SDAC-TR-81-11
7. AUTHOR(s) Z. A. Der — A. O'Donnell D. W. Rivers — P. J. Klouda T. W. McElfresh — M. Marshall		8. CONTRACT OR GRANT NUMBER(s) F08606-79-C-0007
9. PERFORMING ORGANIZATION NAME AND ADDRESS Teledyne Geotech 314 Montgomery Street Alexandria, Virginia 22314		10. PROGRAM ELEMENT, PROJECT, TASK AREA & WORK UNIT NUMBERS VT/0709
11. CONTROLLING OFFICE NAME AND ADDRESS VELA Seismological Center 312 Montgomery Street Alexandria, Virginia 22314		12. REPORT DATE 10/16/81 13. NUMBER OF PAGES 98
14. MONITORING AGENCY NAME & ADDRESS(if different from Controlling Office) Defense Advanced Research Projects Agency 1400 Wilson Boulevard Arlington, Virginia 22209		15. SECURITY CLASS. (of this report) Unclassified 15a. DECLASSIFICATION/DOWNGRADING SCHEDULE

16. DISTRIBUTION STATEMENT (of this Report)

APPROVED FOR PUBLIC RELEASE; DISTRIBUTION UNLIMITED.

17. DISTRIBUTION STATEMENT (of the abstract entered in Block 20, if different from Report)

18. SUPPLEMENTARY NOTES

omega

19. KEY WORDS (Continue on reverse side if necessary and identify by block number)

Upper Mantle Attenuation

t*

Magnitude-Yield

20. ABSTRACT (Continue on reverse side if necessary and identify by block number)

The study of spectral characteristics of short period body waves using a worldwide data set indicates that the high frequency fall-off rates of body wave spectra correlate with the tectonic regime of the upper mantle structures traversed. The study also shows, in a consistent manner, that this is due to lateral variations of Q in the mantle. The magnitude of the worldwide Q variations in the mantle is of the same order as that previously observed for the United States. The internal consistency of the observations is such that

DD FORM 1 JAN 73 1473 EDITION OF 1 NOV 65 IS OBSOLETE

Unclassified

SECURITY CLASSIFICATION OF THIS PAGE (When Data Entered)

crustal and site effects and instrument nonlinearity can be ruled out as factors significantly affecting the t* estimates obtained. The results indicate low attenuation under shields and old oceans and high attenuation under tectonic areas and new oceans. While t* in the long-period band is approximately 1.0 sec, most of the short-period t* values are considerably less than 1.0 sec, even for paths involving a low Q mantle, such as the mantle under the western United States. The high frequency fall-off rates of P and S wave spectra, the shapes of spectral ratios as functions of frequency, and the sizes of the regional body wave amplitude anomalies impose tight limits on the possible values of short-period t*, in spite of uncertainties in the source properties. The presently available long-period and short-period Q studies cannot be reconciled by any reasonable value of constant Q, thus requiring a Q that is frequency dependent.

Q OF THE EARTH IN THE 0.5-10 HZ BAND

SEISMIC DATA ANALYSIS CENTER REPORT NO.: SDAC-TR-81-11

AFTAC Project Authorization No.:	VELA VT/0709
Project Title:	Seismic Data Analysis Center
ARPA Order No.:	2551
Name of Contractor:	TELEDYNE GEOTECH
Contract No.:	F08606-79-C-0007
Date of Contract:	1 October 1980
Amount of Contract:	$1,538,055
Contract Expiration Date:	30 September 1981
Project Manager:	Robert R. Blandford (703) 836-3882

P. O. Box 334, Alexandria, Virginia 22313

APPROVED FOR PUBLIC RELEASE; DISTRIBUTION UNLIMITED.

ABSTRACT

The study of spectral characteristics of short period body waves using a worldwide data set indicates that the high frequency fall-off rates of body wave spectra correlate with the tectonic regime of the upper mantle structures traversed. The study also shows, in a consistent manner, that this is due to lateral variations of Q in the mantle. The magnitude of the worldwide Q variations in the mantle is of the same order as that previously observed for the United States. The internal consistency of the observations is such that crustal and site effects and instrument nonlinearity can be ruled out as factors significantly affecting the t* estimates obtained. The results indicate low attenuation under shields and old oceans and high attenuation under tectonic areas and new oceans. While t* in the long-period band is approximately 1.0 sec, most of the short-period t* values are considerably less than 1.0 sec, even for paths involving a low Q mantle, such as the mantle under the western United States. The high frequency fall-off rates of P and S wave spectra, the shapes of spectral ratios as functions of frequency, and the sizes of the regional body wave amplitude anomalies impose tight limits on the possible values of short-period t*, in spite of uncertainties in the source properties. The presently available long-period and short-period Q studies cannot be reconciled by any reasonable value of constant Q, thus requiring a Q that is frequency dependent.

TABLE OF CONTENTS

LIST OF FIGURES

LIST OF FIGURES (cont.)

LIST OF FIGURES (cont.)

INTRODUCTION

Anelastic attenuation in the mantle is closely related to the evolution of continents and oceans and is thus of great geophysical interest. Before we can understand the attenuation properties of the mantle, there are a number of facts which must be established. We must put limits on the absolute value of energy losses due to attenuation in the mantle, delineate the frequency dependence of absorption, outline regional variations as well as depth distribution of anelasticity, and correlate these with other relevant geophysical variables.

We shall discuss anelastic attenuation in terms of the quantity $t^* = \int \frac{dt}{Q}$ where Q is the quality factor and the integral involving travel time t is taken along the seismic ray path. The t* is a path dependent quantity, being a function of the Q variation in the Earth as a function of depth and region, and it is also frequency dependent. t* appears to be a convenient parameter for characterizing attenuation because it changes little with epicentral distances greater than 25 degrees. It can therefore be used as a single (although frequency dependent) parameter to characterize regional differences for various types of paths described in terms of upper mantle structures under the source and receiver. For distances less than about 20 to 25 degrees, t* increases with epicentral distance due to the fact that the body waves penetrate the low-velocity-low Q layer in the upper mantle. The contributions from the low velocity zone (LVZ) that are coincident with the low Q layer dominate the integral, and thus t* becomes a property that depends almost entirely on the types of upper mantle structures the ray path crosses. Thus:

$$t^* = \int_D \frac{dt}{Q} + \int_U \frac{dt}{Q} + t_r^* \qquad (1)$$

where D is the integral along the downgoing leg of the ray path through the LVZ and U is the upgoing part. t_r^* is the contribution from the rest of the path through the crust and the lower mantle.

Although reports of significant energy in teleseismic arrivals in the 1-10 Hz band have appeared frequently in the literature since the earliest days of seismology, systematic studies of attenuation in this frequency range were, in general, either nonexistent or sketchy. There are several reasons for this. Theoretical seismology, as it developed, was more suited to describe and explain seismic phenomena in the long-period band, since it was easier to describe the earth in terms of mathematically tractable models. As a consequence, development since the earliest days concentrated on long-period seismology. Another reason was the lack of suitable instrumentation, especially recording media for analyzing high frequency waves. The establishment of the WWSSN network accelerated the development of seismology by the wide coverage of the network and the availability of the data to a large number of scientists, but it did little to advance knowledge in the field of high-frequency seismology. The photographic recording utilized in this network is not suitable for frequencies beyond 3 Hz. Digital analyses of such data are tedious and impractical. Early data on high-frequency energy was obtained by special systems with responses peaked at high frequencies, or in the case of some Japanese and Russian investigations, with systems recording simultaneously in a number of overlapping frequency bands.

The introduction of analog tape recording and, later, direct digital recording, opened the way for the study of high-frequency seismic energy beyond regional distances. In spite of these advances in recording technology, much of the new data was still analyzed in the established fashion in the time domain, and seismic energy at teleseismic distances was considered insignificant at frequencies above 2-3 Hz by many researchers. Nevertheless, there have been important studies of attenuation in island arc regions using instruments similar to those of the WWSSN which detected the major, visually noticeable variations in the frequency content of short-period body waves at regional distances. Examples of such studies are Barazangi et al.(1971,1972,1974,1975,1978), Mitronovas and Isacks (1971), Mitronovas et al. (1969) and Mooney (1970), to name a few. Molnar and Oliver (1969) showed that there

are consistent patterns in the efficiency of propagation of this phase that are reflected in the amplitude and frequency content of S_n phases. These studies, although largely qualitative in nature, did much to dispell the widespread but mistaken notion that short-period body-wave spectra are dominated by local crustal and scattering effects and that Q values derived from short-period data are inherently less reliable than those obtained from long-period data. While it is true that crustal and site effects are large in the short-period band, this is more than counterbalanced by the extreme sensitivity of the high frequency energy to variations of Q.

These studies are, of course, relevant only to the 1-3 Hz range of frequencies visually detectable on the WWSSN records. One would expect that similar variations would also be detectable in the frequency content of seismic body waves at teleseismic distances. The regions near island arcs are quite anomalous in many respects; the lateral velocity contrasts are large and the variations of Q are larger than an order of magnitude. For some regions, Q as low as 20 is reported (Baranzangi et al., 1975). For other regions of the world, however, Q variations are less drastic, and the corresponding spectral and amplitude anomalies are more subtle. Furthermore, the increasing popularity of time domain waveform simulation methods and the acceptance by many researchers of such techniques as sole standards for data analysis at the expense of spectral methods further decreased awareness of the existence of high frequency energy in teleseismic arrivals.

During the last twenty years, several networks and arrays applying analog and digital recording systems came into use. The LRSM network employed a large number of mobile seismic stations covering mostly the contiguous United States. LASA and NORSAR and the Commonwealth arrays ESK, YKA, WRA, and GBA provided worldwide coverage with high dynamic range and a frequency band up to 10 Hz. More recently, the SRO network, with even better data quality, came into existence. With the introduction of better recording systems, reports of high frequency observations at teleseismic distances became more frequent. As soon as the first reliable reports of significant energy in the 3-10 Hz band

from teleseismic waves were published, a major discrepancy between the Q estimates in the short- and long-period bands became apparent. We quote Asada and Takano (1964);

> "The most satisfactory explanation for the existence of a high frequency component in the spectra is that the value of Q for P waves is not as small as one would expect from the results of studies of surface waves."

The above quote shows that awareness of possible frequency dependence of Q surfaced quite early. It actually was first stated by Gutenberg (1958) in a somewhat oblique fashion.

Besides stating the discrepancies between short- and long-period Q estimates, early studies of Q for short-period body waves have concentrated mostly on the average vertical distribution of Q in the Earth without regard to regional variations (Kurita 1968; Takano 1971).

Accumulation of large amounts of data at seismic arrays and at high quality seismic stations opened the way for the recognition of patterns of regional variations in the frequency content of teleseismic body waves in the short period band. It soon became apparent that P waves traveling through the mantle under shields suffer little loss, and the spectral shapes are also left unaltered after propagating over long paths. On the other hand, waves traversing the upper mantle under tectonic regions were observed to lose most of the high frequency content in their spectra (Filson and Frasier 1972, Frasier and Filson 1972, Noponen 1975, Der and McElfresh 1976, 1977, Der, Masse and Gurski 1975). Some of the older digital systems used a 10 Hz sampling rate with the associated anti-alias filter which cut off the energy at 5 Hz; therefore, they were not too well adapted to study high frequency waves. Newer systems such as the SDCS, SRO and new NORSAR use 20 Hz sampling and an anti-alias filter with a cut-off at 10 Hz. These systems are thus able to detect higher frequencies. Work with such systems soon revealed the existence of extremely high-frequency energy in seismic waves propagating over shield paths.

The existence of seismic energy near 10 Hz in teleseismic body waves can be shown easily by several methods. For example, one can compute body wave spectra by windowing the teleseismic arrival, Fourier transforming it, and comparing the resulting spectrum with that of the preceding noise. Figure 1 shows an example of such a pair of spectra; on the top we show the spectrum of the signal window and at the bottom, that of the preceding noise window. The signal is a mantle arrival from a suspected nuclear explosion in Russia at an epicentral distance of 23°as recorded at NORSAR. In the example shown, the signal spectrum is above the noise level at frequencies up to 10 Hz, indicating a high Q path. Alternatively, the seismic trace can be bandpass filtered and the amplitudes in the various bands measured. This, although equivalent to computing spectra, has several advantages. Inspecting bandpass filtered records like those shown in Figure 2 shows that the high-frequency content of short-period P waves is considerable and is not due to spikes or noise. Moreover, the envelope shapes at the various frequencies are similar. Thus the spectral methods are not biased by scattered energy in the coda, as is claimed by some. (For spectral computations, several seconds of the P wave need to be windowed and Fourier analyzed.) It is also obvious that the high-frequency content is not due to windowing or truncation effects in the spectral methods. The seismogram shown in Figure 2 is a Kazakh nuclear explosion recorded at NORSAR, and it has considerable signal energy at 6 Hz. It can also easily be shown by Fourier analyzing the calibration signals applied to the total system that nonlinearities in the system cannot cause generation of high-frequency energy at this level (Der, McElfresh and O'Donnell, 1980). We must therefore accept the high frequency content of short-period seismograms as real seismic energy. We do not use the bandpass filter approach to estimate t* because of the variability of the frequency content of the outputs due to the interactions of the signal spectra with the filter bands and fall-offs at the flanks of the bands. We have found, however, that we can obtain similar t* values to those obtained by the more precise spectral methods by using bandpass filtering.

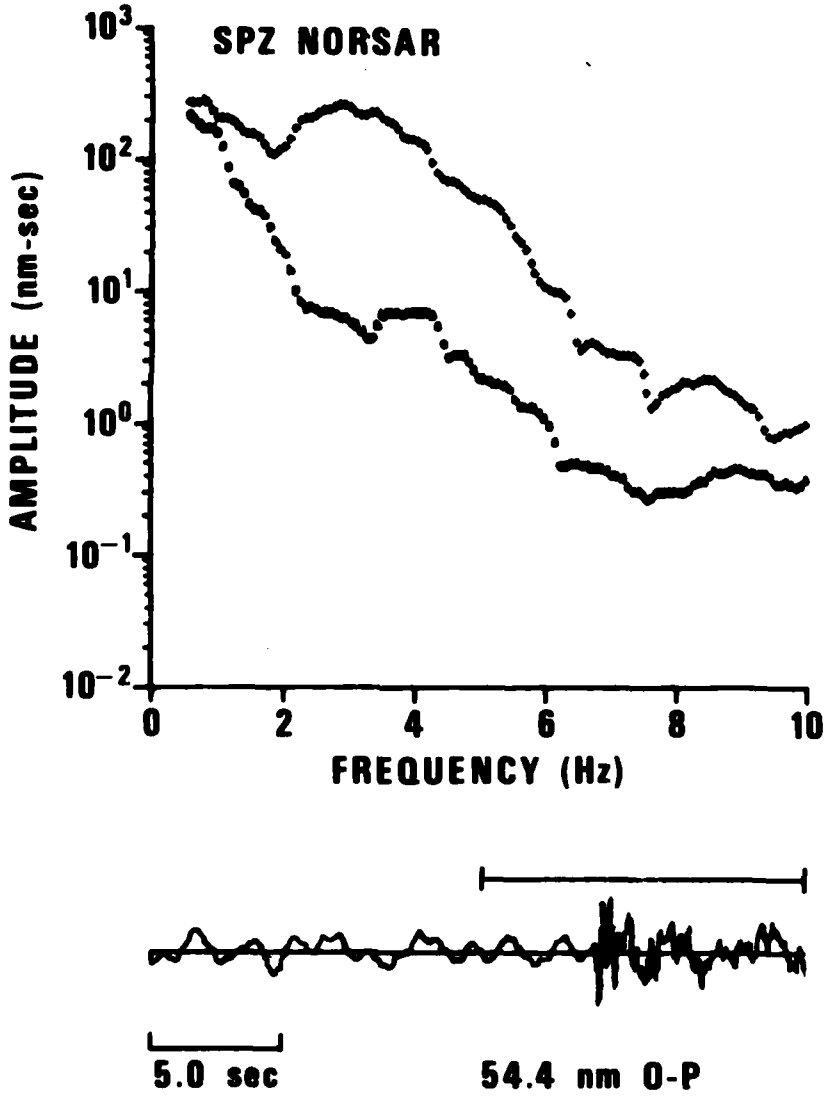

Figure 1. Amplitude spectrum of a P wave from a suspected nuclear explosion (top trace) observed at a distance of 23° at NORSAR. The lower curve is the spectrum of noise preceding the arrival. The P wave spectrum is above the noise level up to 10 Hz.

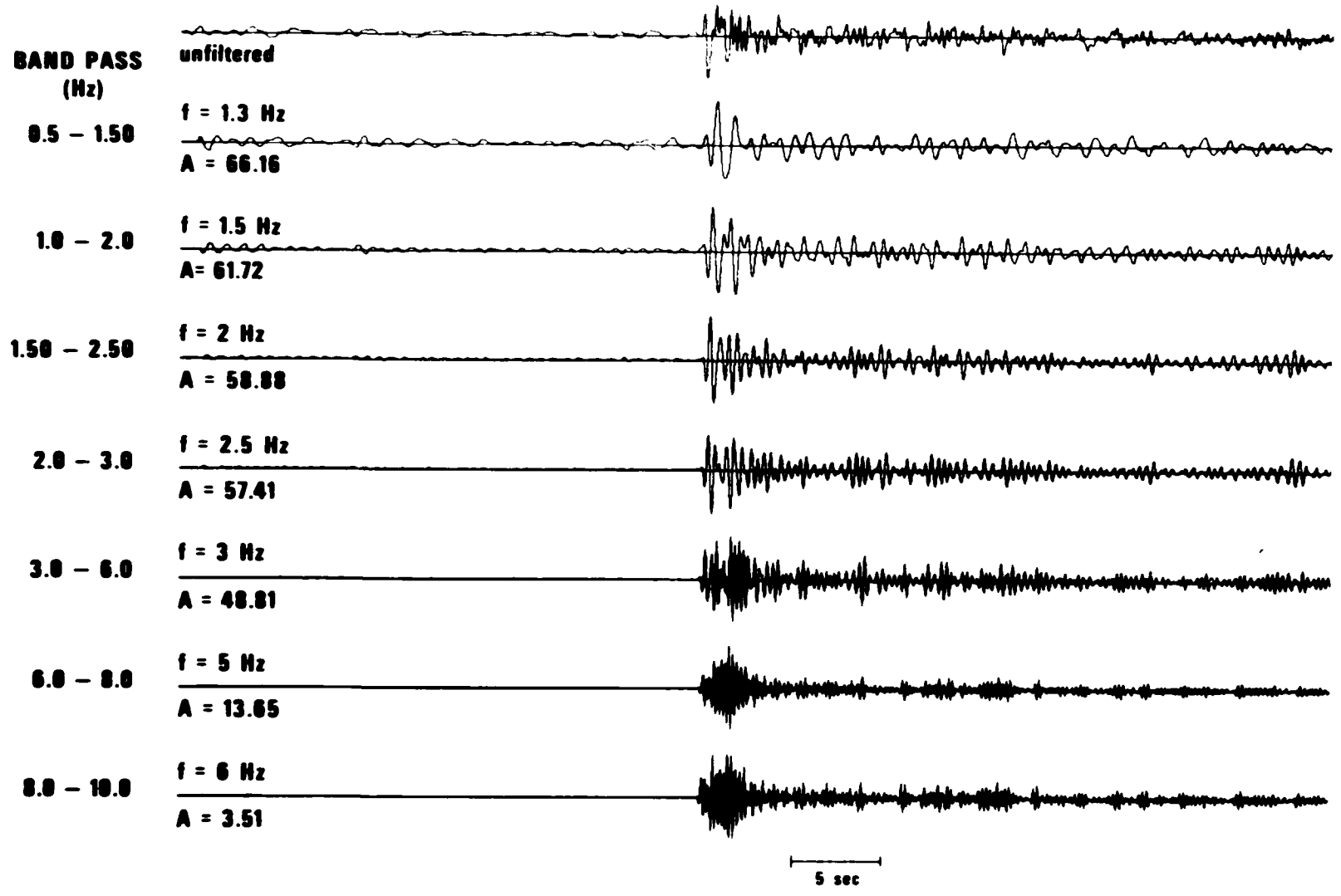

Figure 2. Bandpass filtered P waves of a Kazakh nuclear explosion observed at NORSAR. The bandpass settings are indicated on the left. The relative trace amplitudes and the actual dominant frequencies seen are indicated on each trace.

Although regional variations of Q in the short-period band have been repeatedly commented upon, only a few studies of selected regions or compilations of results exist for teleseismic body waves. Several of the authors of this report have done extensive studies of Q within the United States. Two regionalized compilations of short period Q estimates were given by Noponen (1975) and Der and McElfresh (1977) for limited data sets. There has been no exploratory study of the various regions of the world of the type done for long period surface wave attenuation (Nakanishi 1979, Mills 1978), studies of Q_{ScS} (Sipkin and Jordan 1980), travel time residuals (Julian and Sengupta (1976) and many other geophysical parameters. In this report we shall attempt to accomplish this by compiling existing spectral information on teleseismic P waves. Most of the data comes from various studies performed by our group, but we shall include selected results by other workers. Before we present the results, we shall discuss briefly the basic methods of measuring attenuation in the short period band.

METHODS OF MEASURING t* IN THE SHORT-PERIOD BAND

In principle, the measurement of t* should be simple. If one knows the amplitude of any sinusoidal signal component at the source, one could measure the amplitude of the same component at a distant observation point, and after correcting for geometrical spreading effects, t* could be found directly from the ratio A of the two amplitudes at the receiver and the source respectively, by the formula

$$A = \exp(-\pi f t^*) \qquad (2)$$

Frequency dependence of t* causes no difficulty with this approach, since t* can be computed separately for each frequency component. Unfortunately, absolute signal amplitudes at the source are highly uncertain, and near receiver effects also cause great fluctuations in the absolute signal levels observed in the short-period band. Therefore, the simple approach outlined above is not practical.

Most published t* estimates pertaining to the short-period band were obtained either by utilizing the fall-off rates of spectral ratios derived from the observed and estimated source spectra, or by attempting to match observed waveform shapes with synthetic seismograms disregarding the absolute amplitude. Such methods involve comparison of the spectral shapes, i.e., the measurement of the decrease of high frequency content in the signal relative to the lower frequencies. This approach to measuring attenuation is advantageous because the spectral shape of the seismic source does not change rapidly with event magnitude (Aki, 1969; von Seggern and Blandford, 1972), and the shape of observed spectra is not sensitive to the local focusing that severely affects absolute amplitudes of signals (Der, McElfresh and O'Donnell, 1980). Practically all t* estimates obtained thus far by such methods assume a constant, frequency-independent Q. If Q, or t*, is frequency-dependent, then all such results will be biased and will yield an apparent t*, $\overline{t^*}$, which is related to the absolute t* in equation (2) by the formulas

$$\overline{t^*} = \frac{-1}{\pi}\frac{d(\log A)}{df} = t^* + f\frac{dt^*}{df} \qquad (3)$$

where A is the spectral ratio and f is frequency. All terms in these formulas are assumed implicitly to be functions of frequency throughout this paper. The slope of the logarithm of the spectral amplitude ratio in a linear frequency plot, d(log A)/df, is commonly used to determine $\overline{t^*}$. In principle, t* can be determined by solving the differential equation (3) using some appropriate absolute values of t* at some frequency, as well as the values of $\overline{t^*}$ determined for each frequency. Since spectral ratios determined from data are quite variable in shape, only averages of $\overline{t^*}$ over limited frequency bands can be obtained in practice. Although the spectral ratios A are corrected for instrument response, the requirement that $\overline{t^*}$ be averaged over limited frequency bands results from the fact that spectral ratios have to be smoothed heavily for stability in the measured slope, and the limited bandwidth of instruments does not allow the estimation of $\overline{t^*}$ outside the main band of the instrument due to system noise. Empirical t* versus frequency relationships can be derived by drawing curves that conform to the measured average of $\overline{t^*}$ in various frequency bands along with some bounding values of absolute t*, usually at the long-period end of the spectrum.

In the rest of this report we shall use the notation $\overline{t^*}$ for averages of this quantity in various frequency bands. In each case, the frequency band in question will be clearly implied. We are somewhat reluctant to introduce the new symbol $\overline{t^*}$, but we find it necessary in order to connect new frequency-dependent models of Q to historical Q estimates. $\overline{t^*}$ is an easily and directly measurable quantity, whereas t* is not, at least in the short-period band, if Q depends on frequency. Furthermore, the differences in the frequency and waveform characteristics of signals due to attenuation can be more easily described in terms of an average $\overline{t^*}$ over the band of an instrument than in terms of a frequency dependent t*. For the case of frequency independent Q, $\overline{t^*}$ and t* are the same.

Similar arguments apply to estimates of path t* differentials. Assuming a constant Q, we obtain relative $\overline{t^*}$ that may also be biased by the frequency dependence of the absolute t* differentials between the paths in question.

The reader may regard the notation $\overline{t^*}$ as a device to identify those results which have been obtained by comparing the relative amplitudes of various spectral components and which may be biased relative to the absolute t* by the frequency dependence of Q. The possibility of bias does not imply, however, that the bias is very large. Although equation (3) allows great differences between $\overline{t^*}$ and t* for rapidly changing Q with frequency, the available evidence discussed in more detail in the rest of this paper indicates that the frequency dependence is fairly gradual and the difference between $\overline{t^*}$ and t* is not likely to exceed a few tenths of a second. Moreover, $\overline{t^*}$ appears to be fairly constant over wide frequency bands, as evidenced by the long history of attenuation studies in limited frequency bands using constant frequency independent Q, in which no indications of frequency dependence were detected. It also appears that differentials of $\overline{t^*}$, with respect to tectonic regimes of the paths, reflect the regional variations of t* as well, and also correlate with other types of geophysical variables diagnostic of the temperature of the upper mantle.

DISCUSSION OF THE WORLDWIDE MEASUREMENTS OF t_p^*

Description of the Data Set

As mentioned above, t* is determined from the ratio of the observed body-wave spectrum to that of the estimated source spectrum. Source spectra are usually not very well known, but this poses little difficulty for the broadband estimation of $\overline{t^*}$ involving high frequencies, since the sensitivity of the spectra to $\overline{t^*}$ is extremely high. There are several general descriptions of source spectra for earthquakes and explosions (Aki 1969, von Seggern and Blandford 1972) that can be used for estimating $\overline{t^*}$. The basic methods used for computing t_p^* in this paper differ somewhat.

One procedure we used to determine $\overline{t_p^*}$ was to correct the spectra until the ω^{-2} falloff rate was achieved, and the corner frequency was fitted independently. An example of this procedure is shown in Figure 3. In other cases (mostly for explosions), spectral shapes derived from reduced displacement potentials were fitted with t* to match the observed spectra. Large events were used with the assumption that the spectra falloff as ω^{-2}. A large number of t* estimates for explosions was also obtained from detailed spectral fitting using the surface reflection coefficients and delay times as free parameters in addition to $\overline{t^*}$. For some events we used Aki's (1969) ω^{-2} scaling law to derive a set of source spectra with various t_p^*. These were matched with the observed P wave spectra using templates such as that shown in Figure 4 to estimate $\overline{t_p^*}$, considering only the parts of the signal spectra that were significantly above the noise level in each case.

Since events of relatively high magnitude are required to obtain spectra which are above the noise level over wide frequency ranges, most of the P wave spectra were dominated by the high-frequency falloff rate of the source spectrum (which we assumed to be ω^{-2}), and the corner frequencies were probably below 0.5 Hz for most events. Despite the differences of approach in estimating $\overline{t_p^*}$ used by various workers, we have found that the estimates usually differ by less than 0.1 sec if a

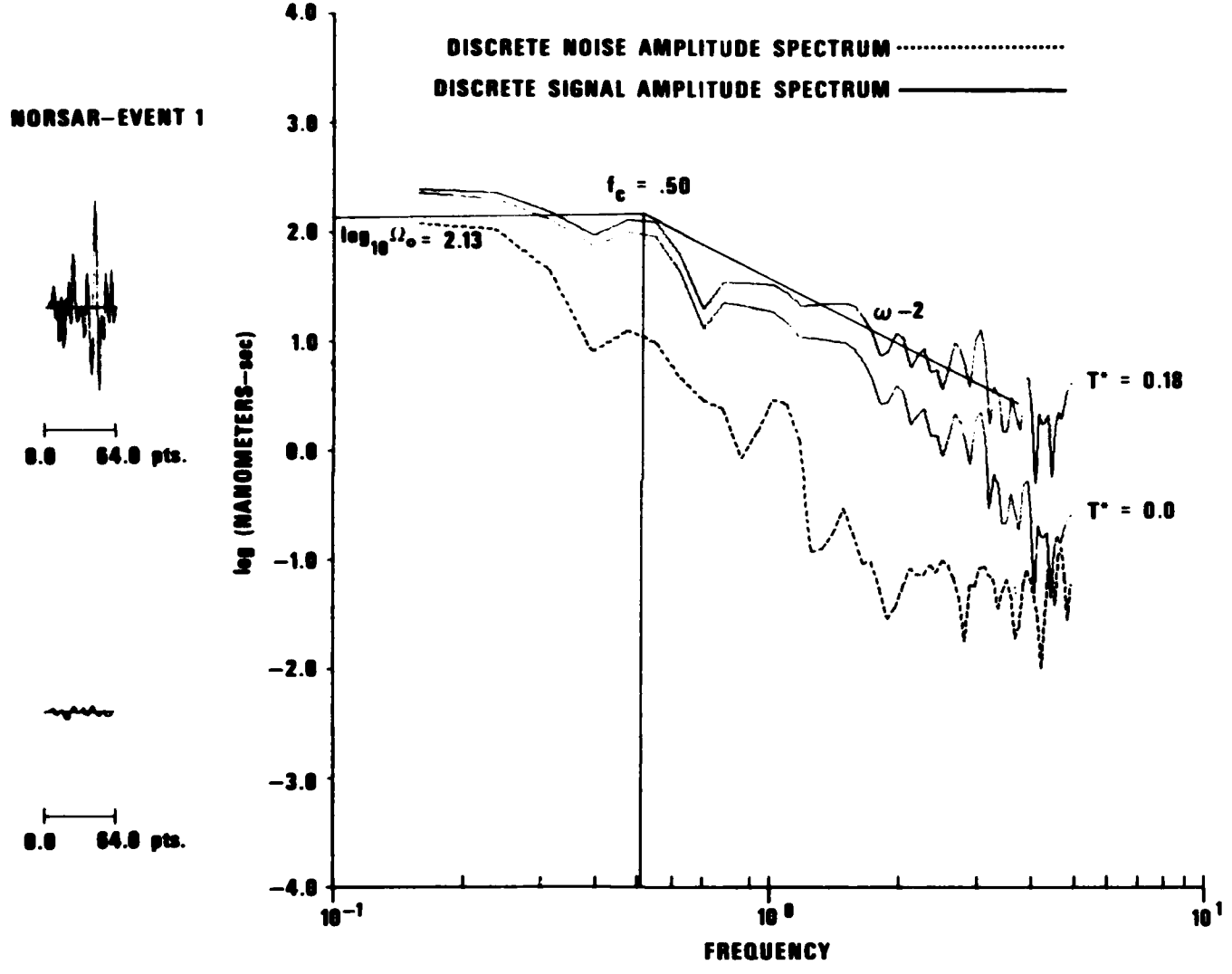

Figure 3. A procedure to determine $\overline{t^*_p}$ by fitting a corner frequency and simultaneously correcting the falloff of spectra to a ω^{-2} slope. The lowest curve is the noise spectrum as observed. The signal spectrum corrected to an ω^{-2} falloff is shown on the top. In this case $\overline{t^*_p}$ of 0.18 sec was found to be appropriate. In determining $\overline{t^*_p}$ the parts of spectra that are near the noise level are disregarded.

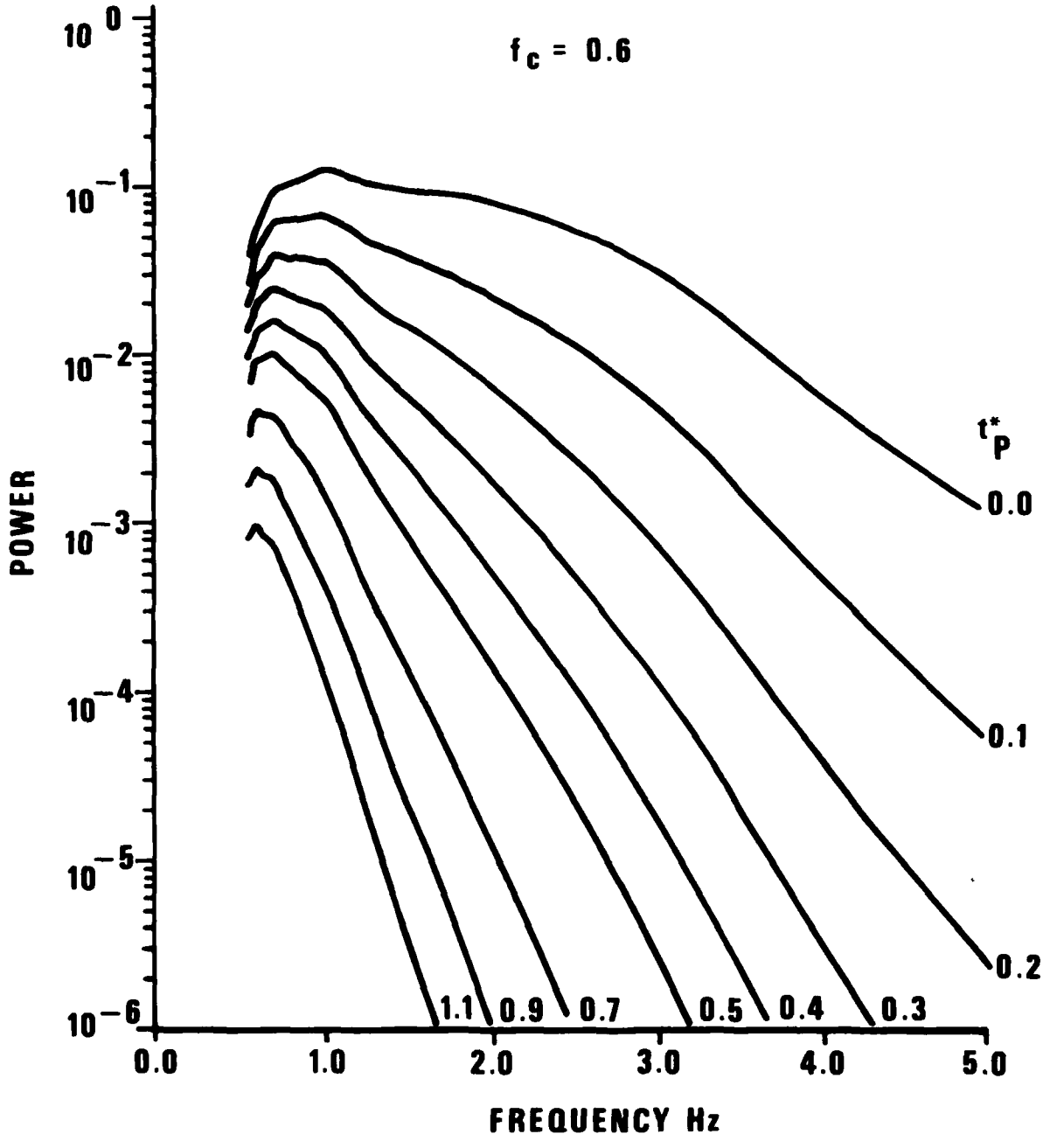

Figure 4. Template for reading $\overline{t^*_p}$ from power spectra produced by assuming an SDCS instrument response and a corner frequency of 0.6 Hz.

wide frequency band in the spectrum is utilized to compute $\overline{t^*_p}$. The probable reason for the agreement is that we all measured essentially the general falloff rate of observed P spectra relative to the theoretically assumed ω^{-2}. We also compiled results in the literature using similar approaches to estimate $\overline{t^*_p}$ or Q (Noponen, 1975, Asada and Takano, 1963) and included these in our data set. Results by other workers constitute no more than 15% of the $\overline{t^*_p}$ estimates that we compiled.

A skeptical reader may doubt the validity of the $\overline{t^*_p}$ results presented, recalling the extensive literature on spectral differences due to variable stress drops and partial stress drops, as well as the uncertainties due to possible ω^{-3} falloff rates in earthquake source spectra at the high frequency end and a transitional ω^{-1} falloff due to partial stress drops at intermediate frequencies. At this point, he may regard $\overline{t^*_p}$ to be a parameter describing the deviations of the P wave frequency content from the standards given by Aki's (1969) ω^{-2} model for earthquakes and the model of von Seggern and Blandford (1972) for explosions in granite. These deviations could be due to a variety of causes that may include some of the factors listed above besides Q. We shall discuss the relative importance of these other factors later in this report and present evidence that favors the interpretation of $\overline{t^*_p}$ as being primarily determined by mantle Q variations.

Variations of mantle Q under the United States have been studied in great detail (Der, Massé and Gurski, 1975; Der, McElfresh, and O'Donnell, 1980, 1981; Lay and Helmberger, 1981) and the available $\overline{t^*_p}$ data set is extremely large for the western United States (WUS). Therefore, in order to avoid the domination of the total data set by tectonic paths by the western United States, we excluded all paths involving the WUS from our analysis of worldwide events. The results concerning the lateral variations of Q under the United States will be summarized in the latter part of this report. The worldwide data set contains only paths involving the eastern United States and other areas of the world.

The sources of the seismic waves used in the analysis of worldwide data are plotted on the map in Figure 5. The data set contains earthquakes with various source depths in various areas of the world and some nuclear explosions outside the United States. The recording stations shown in Figure 6 cover a large part of the northern hemisphere and also include two stations in Australia. The events in this data set are listed in Appendix A, and the $\overline{t_p^*}$ for the individual paths are listed in Appendix B. In order to classify the seismic paths with respect to the tectonic regimes of the upper mantle structures traversed by the P waves, we have subdivided the world into shield, tectonic, island arc, and old and new ocean provinces. All subdivisions of this kind are somewhat arbitrary, but they are sufficient to study the gross regional variations of Q in the mantle. The subdivision we used is shown in Figure 7. The $\overline{t_p^*}$ values in the data set were sorted with respect to source type, path type, and source depth, and compiled into histograms to extract information necessary to interpret the data.

The first histogram in Figure 8 shows all the data, consisting of 562 worldwide seismic paths. This histogram shows dramatically the disagreement between the short- and long-period $\overline{t^*}$ estimates. While our data set has a mean $\overline{t_p^*}$ value of 0.269 sec, the long-period data give a value on the order of 1 sec, worldwide. There are only two values in our data set near 1 sec, involving paths from Tibet to KSRS. The overwhelming majority of $\overline{t_p^*}$ fall below 1 sec and are inconsistent with values of 1 sec, even if one assumes a flat source spectrum and a constant, frequency independent Q.

Figure 9 shows a set of histograms of $\overline{t_p^*}$ from shallow ($h < 40$ km) events for 1) shield-to-shield paths (called "shield type paths" in the rest of this report), 2) shield-to-tectonic paths (including tectonic-to-shield), and 3) tectonic-to-tectonic paths (called "tectonic type paths" in the rest of this report). The means of the $\overline{t_p^*}$ for the populations increase as the proportion of the tectonic type of upper mantle included in the paths increases. There is also an increase in the standard deviations of the populations, indicating that the tectonic subdivision in our mantle types is considerably more heterogeneous than the shield. The standard deviation of the shield population (0.1 sec)

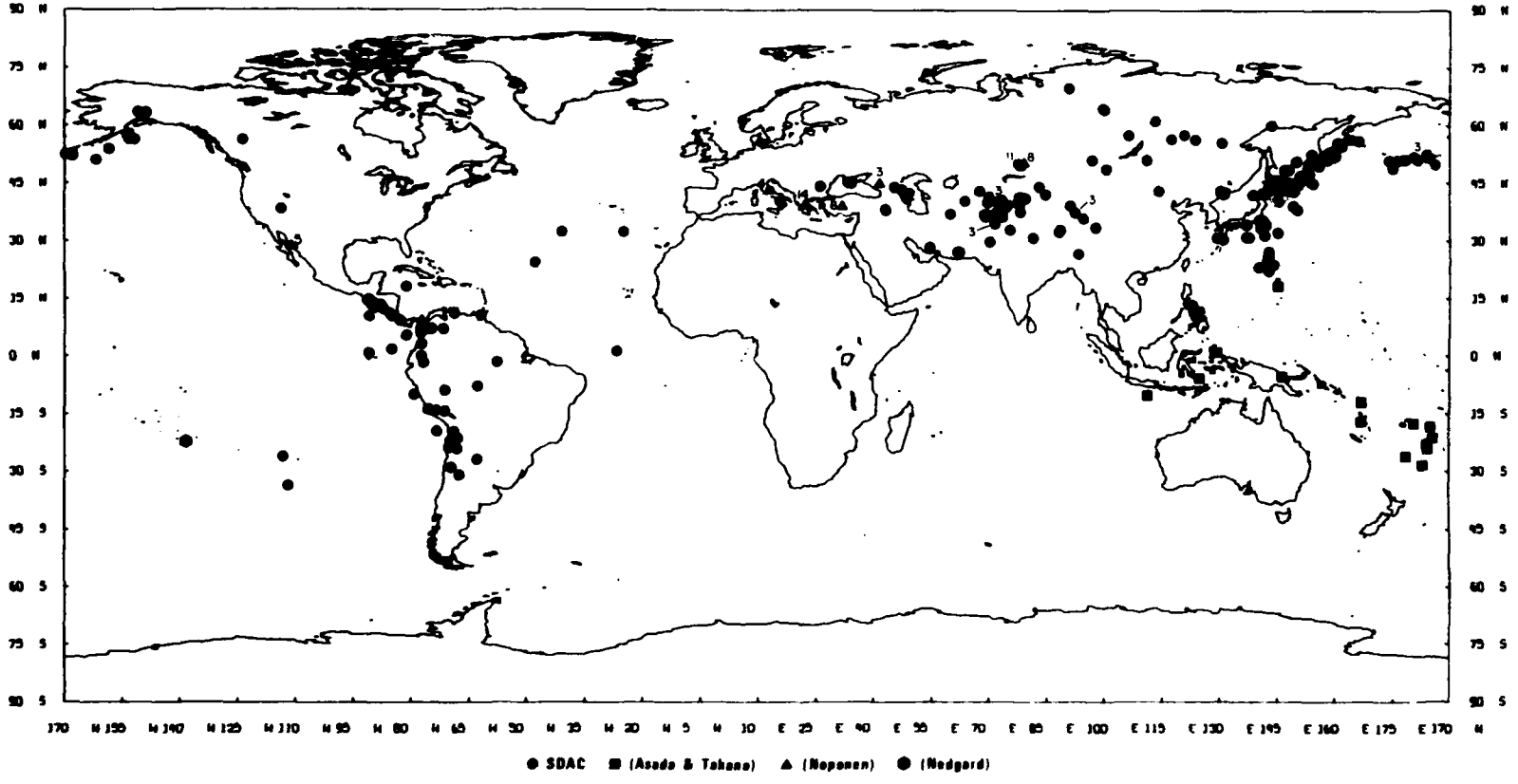

Figure 5. Location of the events used for the worldwide t_p^* compilation.

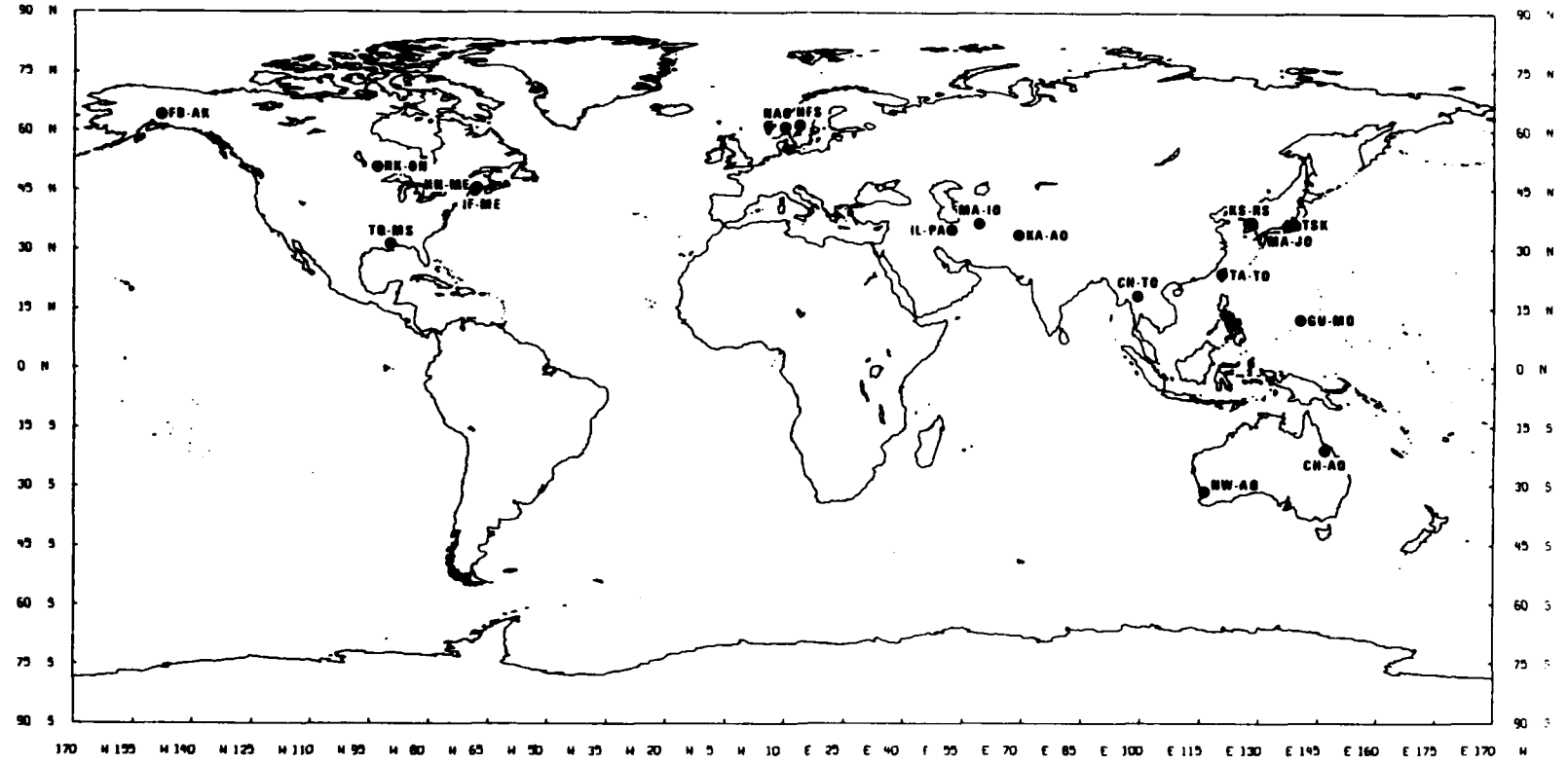

Figure 6. Recording sites for the short-period P waves studied.

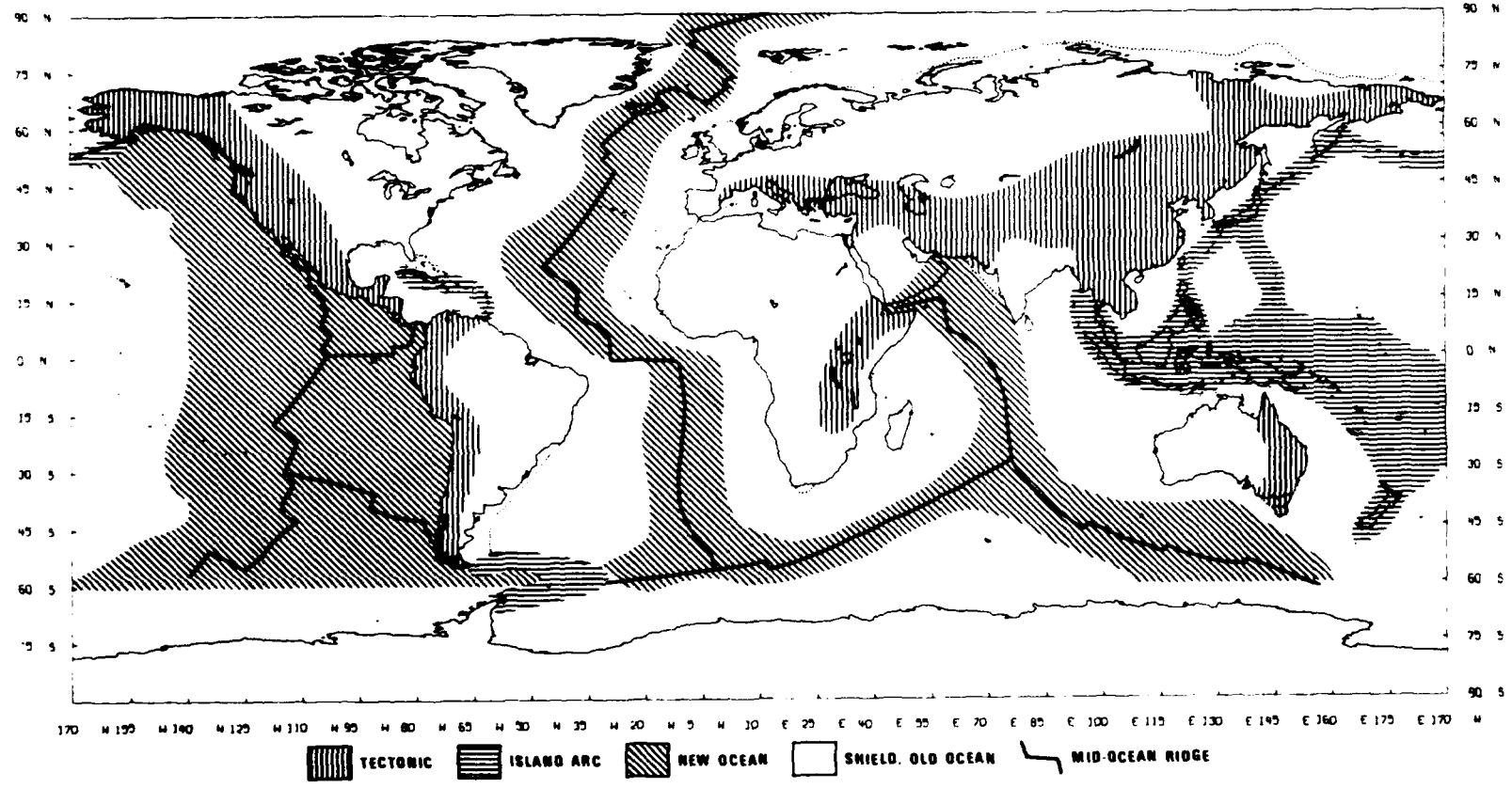

Figure 7. Subdivision of the world into shield, tectonic, island arc, new and old ocean provinces.

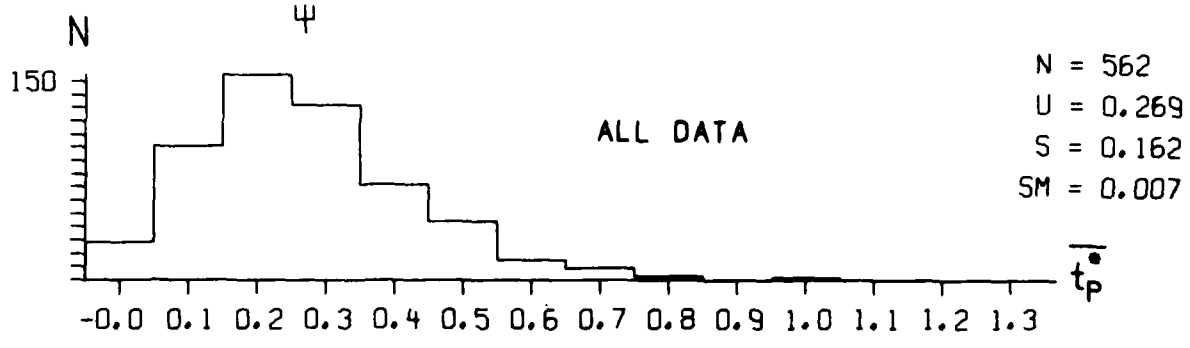

Figure 8. Histogram of all $\overline{t_P^*}$ values compiled. (Explanation for all histograms N = total number of data points, U = mean, S = standard deviation, SM = standard deviation of the mean.)

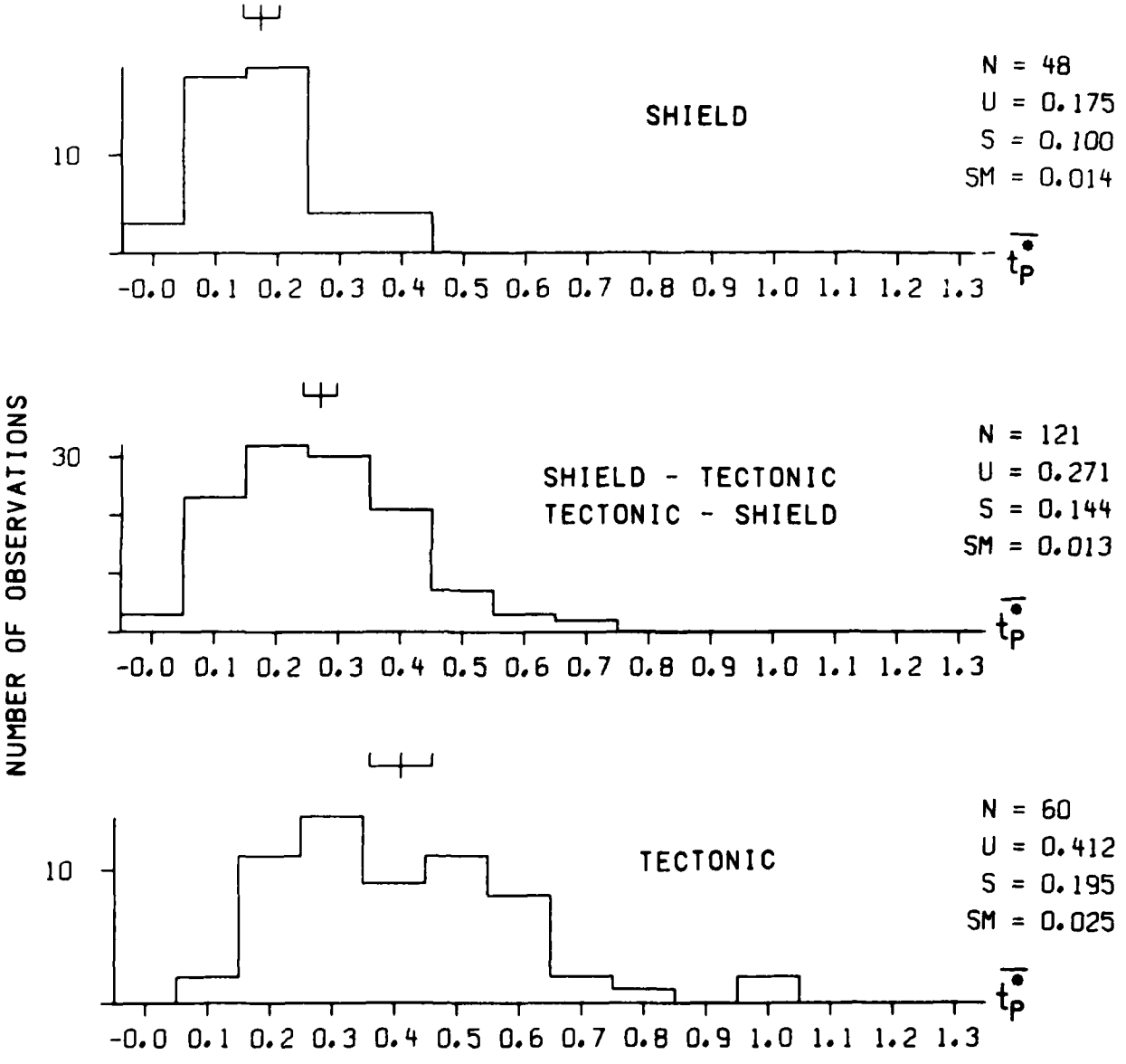

Figure 9. Comparison of $\overline{t_p^*}$ populations for shield, tectonic-to-shield and tectonic paths using shallow events only.

is only slightly more than the .06 sec caused by the inherent fluctuation of $\overline{t_p^*}$ due to lateral inhomogeneities under NORSAR (Der, McElfresh and O'Donnell, 1980).

The set of histograms in Figure 10 shows the populations of all events observed on shields sorted with respect to source depth. The deep events are either from island arcs or from South America. The shift of the populations towards higher $\overline{t_p^*}$ as the source depth decreases is consistent with the assumption that raypaths from shallower events traverse increasing portions of the low-Q zone in the upper mantle, resulting in increased $\overline{t_p^*}$. It is interesting to note that the mean $\overline{t_p^*}$ for the events with source depth exceeding 150 km is about the same as that for shallow events along shield type paths. This seems to indicate that the extra path length for the shallow events in shields does not contribute significantly to $\overline{t_p^*}$ --thus implying high Q in the upper mantle under shields.

A subdivision of the island arc-to-shield population of $\overline{t_p^*}$ with respect to source depth yields similar results, as shown in Figure 11. This shift in the frequency content of the island arc events with respect to source depth was also documented by Marshall et al (1975) for both P and S waves in a manner that is consistent with our interpretation of this phenomenon in terms of the mantle Q.

In Figure 12 we compare the $\overline{t_p^*}$ populations for shield-to-shield, old ocean-to-shield, and new ocean-to-shield paths. The old ocean-to-shield group contains only three events due to the lack of seismicity in such areas. This population also includes a French nuclear event in the Pacific observed at HFS (Hagfors, Sweden). This is the only event in the data set beyond the distance of 85°, and the seismic P wave from this event contains a significant amount of 4 Hz energy after traveling through the mantle and the core (Nedgard, 1978). The new ocean-to-shield population includes mostly ocean ridge events, five of which come from the Gulf of California. While the new ocean-to-shield population has a relatively high t_p^* in agreement with an earlier study of Solomon (1973), the old ocean-to-shield population has $\overline{t_p^*}$ values no higher than those for shield-to-shield paths.

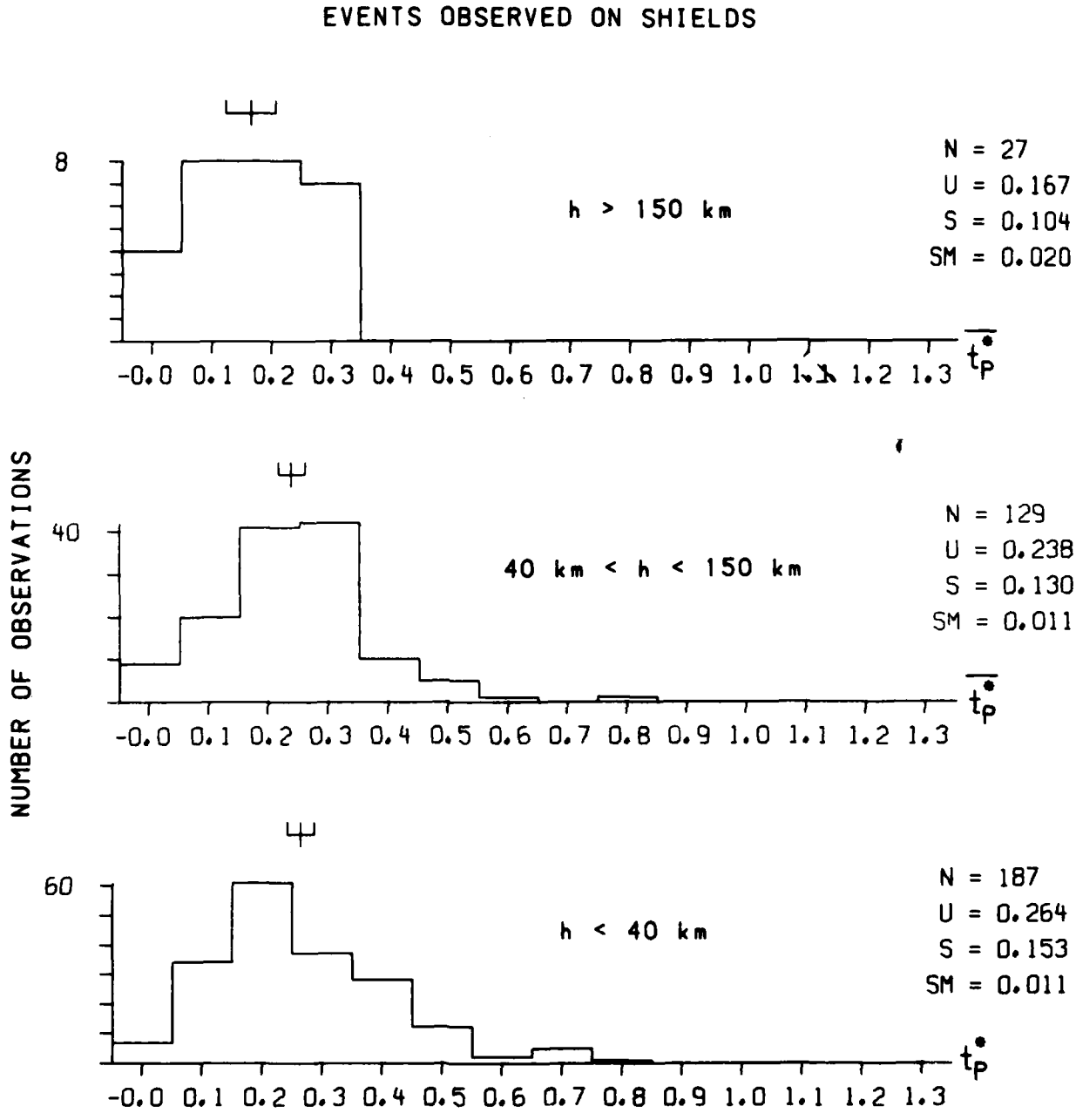

Figure 10. $\overline{t_P^*}$ for all events observed on shields sorted with respect to source depth.

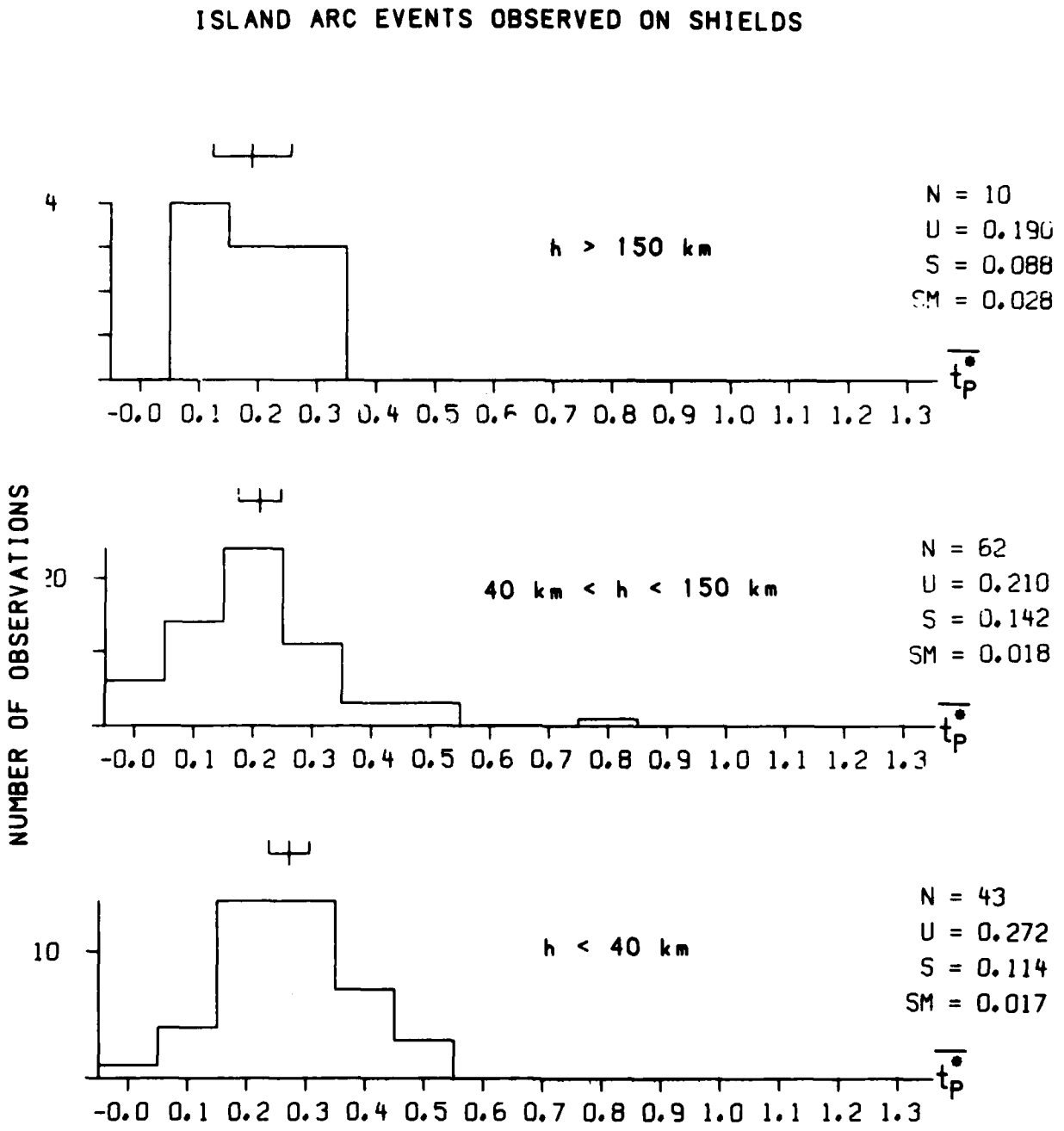

Figure 11. Comparison of $\overline{t_P^*}$ values for shield paths and island arc-to-shield paths for various source depth ranges.

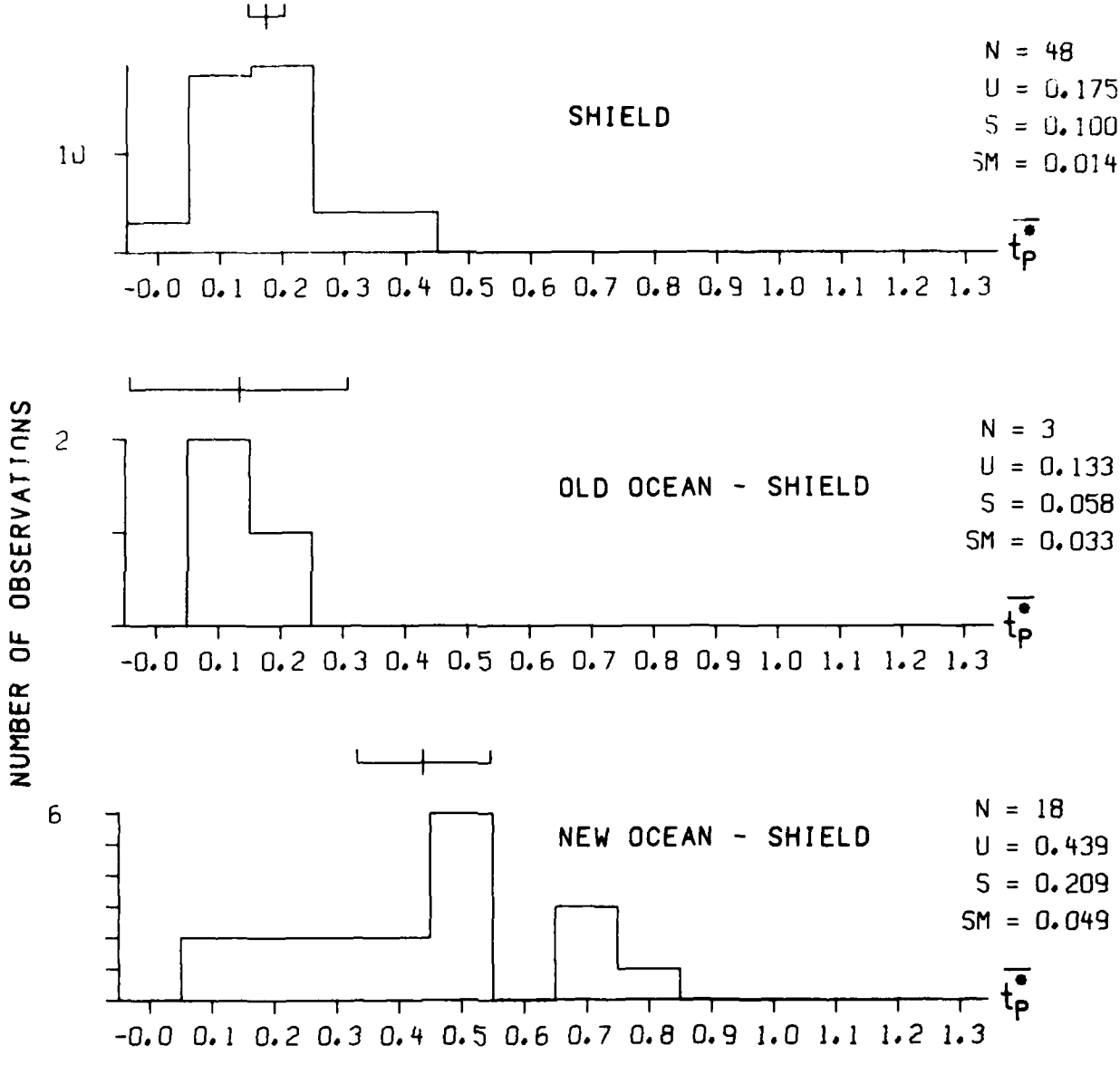

Figure 12. Histograms of $\overline{t^*_P}$ for shield, new ocean-to-shield, and old ocean to shield type paths. All events used are shallow.

A Digression to the Interpretation and Internal Consistency of Worldwide $\overline{t^*_p}$ Measurements

As we mentioned before, there are a number of factors besides variations of Q that may, conceivably, influence $\overline{t^*_p}$. Consequently, some critical evaluation of the data is necessary to separate Q effects from possible source related effects. Some of the possible factors that may influence the falloff rates of P wave spectra are:

a) Earthquake source spectra may fall off at a ω^{-3} rate instead of the assumed ω^{-2}.

b) Stress drops of the events in various regions may differ considerably.

c) Deep earthquake source mechanism and spectral characteristics may differ considerably from those implied by Aki's scaling laws.

d) Surface reflections may bias t^*_p for shallow events.

Let us examine these possible factors one by one.

a) An ω^{-3} falloff rate in the actual spectrum when an ω^{-2} rate is assumed leads to an over-estimation of t^*_p of the order of 0.15 sec (Noponen 1975, Lundquist and Cormier 1980). That this does not happen often is indicated by the fact that earthquakes and nuclear explosions yield similar t^*_p estimates over similar types of paths if one assumes an ω^{-2} falloff. Thus while for individual events an ω^{-3} falloff may occur occasionally, it appears that most earthquake source spectra fall off as ω^{-2} (Hank, 1979).

b) Variable stress drops of events from region to region are partially eliminated by the procedure of fitting corner frequencies and spectral asymptotic falloff rates independently, but partial stress drops may cause an intermediate ω^{-1} falloff.

If Aki's (1967) source spectrum is used, as it was for some $\overline{t^*_p}$ presented here, there may be some effect of stress drop on $\overline{t^*_p}$, although the fitting range in its determination is above the corner frequency,

regardless of stress drop for most events. Anomalously low stress drops were claimed for some ocean ridge events (Burdick and Kaufman, 1980) and high stress drops for intraplate events (Liu and Kanamori, 1980). On the other hand, the reduction and enhancement of high-frequency content in P waves from sources located in these regions can be explained entirely in terms of lateral Q variations in the mantle, without the need for any anomalous stress drops reflected in the falloff rates. For instance, we see not only a reduction of high-frequency content of P waves from ocean ridges as shown in Figure 12, but also a reduction of high frequency content in teleseismic arrivals in new ocean areas such as Iceland. Figure 13 compares SH waves for common events at AKU (in Iceland) to those observed at COP (Copenhagen, Denmark) on the Baltic shield. The plots show clearly the reduction of high frequency content and amplitudes of signals at AKU. Such reciprocal observations do not support low stress drop as the sole explanation for high $\overline{t^*_p}$ in new ocean areas.

By the same token, the high stress drop of intraplate events is not the sole explanation for their higher m_b and higher frequency character. The m_b differential in the populations of M_s-m_b for worldwide and intraplate events, shown in Figure 14, was used in support of the stress drop differential explanation by Liu and Kanamori (1980). On the other hand, Figure 14 can be explained fully in terms of the known attenuation differences between shield, old ocean and tectonic regions. In fact, there exists a similar m_b differential for nuclear explosions in tectonic (WUS) and shield areas well known to workers in the field of seismic discrimination that clearly has nothing to do with stress drops (Marshall and Basham, 1972).

c) There have been studies that indicated unusual source characteristics for deep earthquakes involving phase transitions in addition to the conventional model of displacements along fault planes (Randall, 1964; McGarr, 1977; Balakina and Golubyeva, 1979). While we have no objections to the results of such studies, the available evidence indicates that such source mechanisms do not imply any unusual characteristics in the falloff rates of the spectra from deep earthquakes. The fact that the frequency content of S waves from deep sources changes more with source depth than that of P favors the interpretation of this phenomenon as a Q effect (Marshall et al., 1975). The

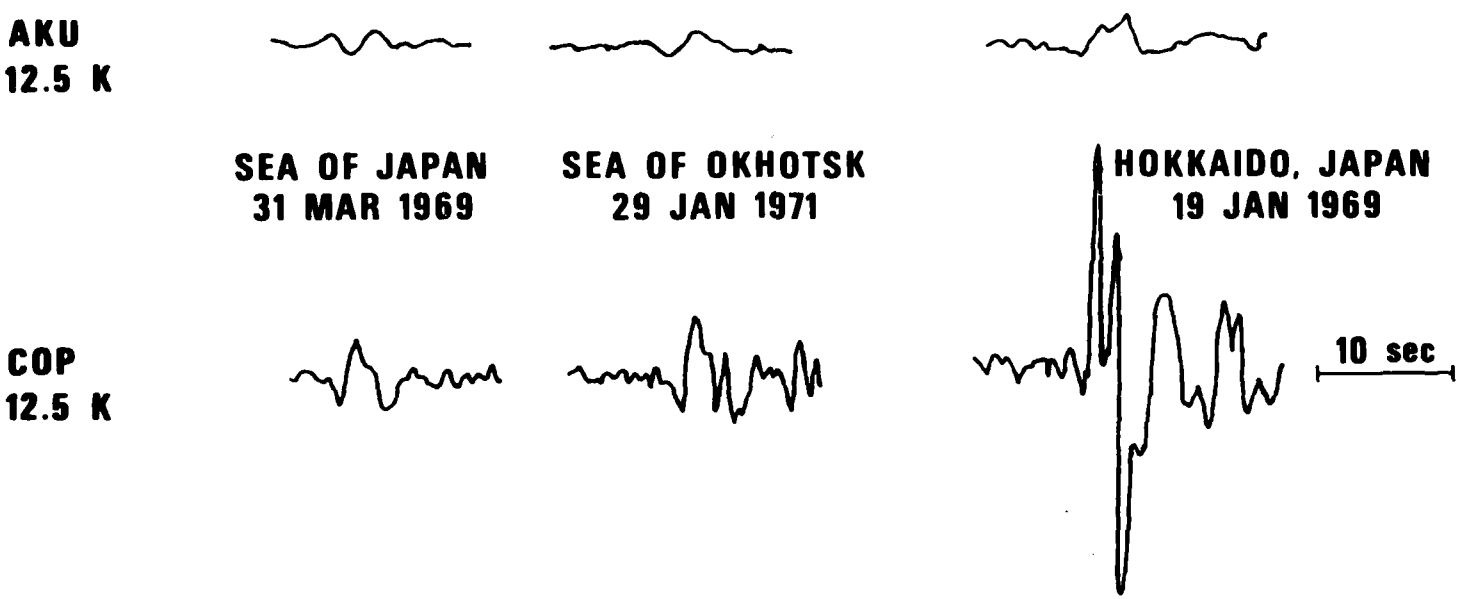

Figure 13. Comparison of SH waveforms for common events at AKU, Iceland (new ocean) and COP, Copenhagen, Denmark (shield).

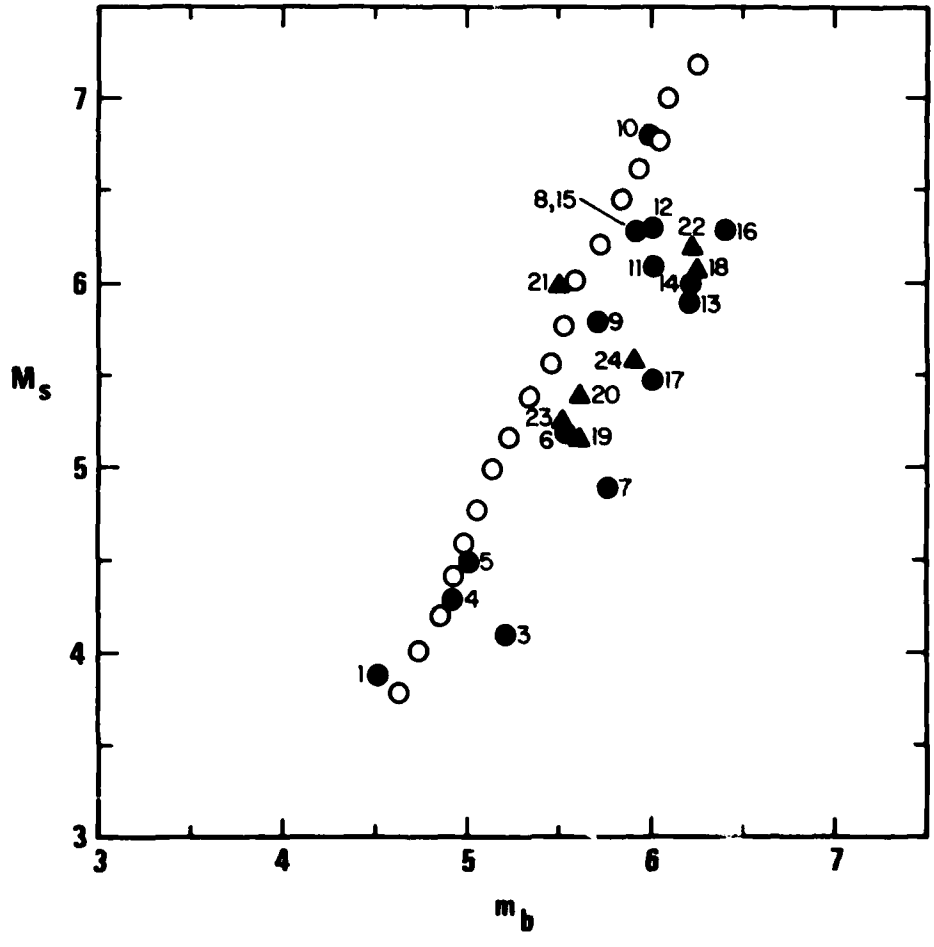

Figure 14. Comparisons of the M_s-m_b populations for mid-plate events (solid dots) and worldwide average (circles) (after Liu and Kanamori, 1980).

enhancement in the high frequency content of short period body waves from deep earthquakes relative to the average earthquake when both are observed in shields is again consistent with the size of the additional contribution of a tectonic upper mantle to $\bar{t}^*$, without the need to invoke unusual source spectra for deep earthquakes.

d) The effect of surface reflections on the spectral estimation of falloff rates (and thus of t*) was emphasized by Langston (1978). On close examination, most of the additional uncertainty claimed in defining the corner frequency due to the surface reflections is actually due to the source spectrum used. Although surface reflections may contribute to the uncertainties in determining corner frequencies or t*, they are not important factors at high frequencies.

The fact that the $\overline{t_p^*}$ estimates are similar along similar paths for earthquakes and explosions is demonstrated by Figure 15, which compares histograms of $\overline{t_p^*}$ determined from explosions and shallow earthquakes along paths that involve a shield and tectonic type upper mantle. The two populations have the same mean (the difference is statistically insignificant), indicating that the ω^{-2} falloff rate for earthquakes must be approximately correct. If we had assumed an ω^{-3} falloff in the spectra of earthquakes, the corresponding $\overline{t_p^*}$ means would have been lower for the earthquake population, as compared to the explosion population. Comparing the $\overline{t_p^*}$ population for the shield type paths including explosion data only causes a reduction of the mean $\overline{t_p^*}$, which appears to be statistically significant. This reduction is to be expected if one interprets the changes in terms of attenuation. In comparing the explosion and earthquake populations of $\overline{t_p^*}$ for similar paths, it was necessary to use shield-to-tectonic paths for explosions and tectonic-to-shield paths for earthquakes, since shields are not seismic. The $\overline{t_p^*}$ populations involving the propagation in the reverse direction are too scarce to make convincing comparisons in a similar vein, although even this scarce data set do s tend to support the above conclusions (Figure 16). As we shall discuss later, comparisons involving almost exactly reversed paths were actually made within the United States, which confirms that $\overline{t_p^*}$ determined by the simple approaches used in this report must indeed be interpreted in terms of Q in the mantle.

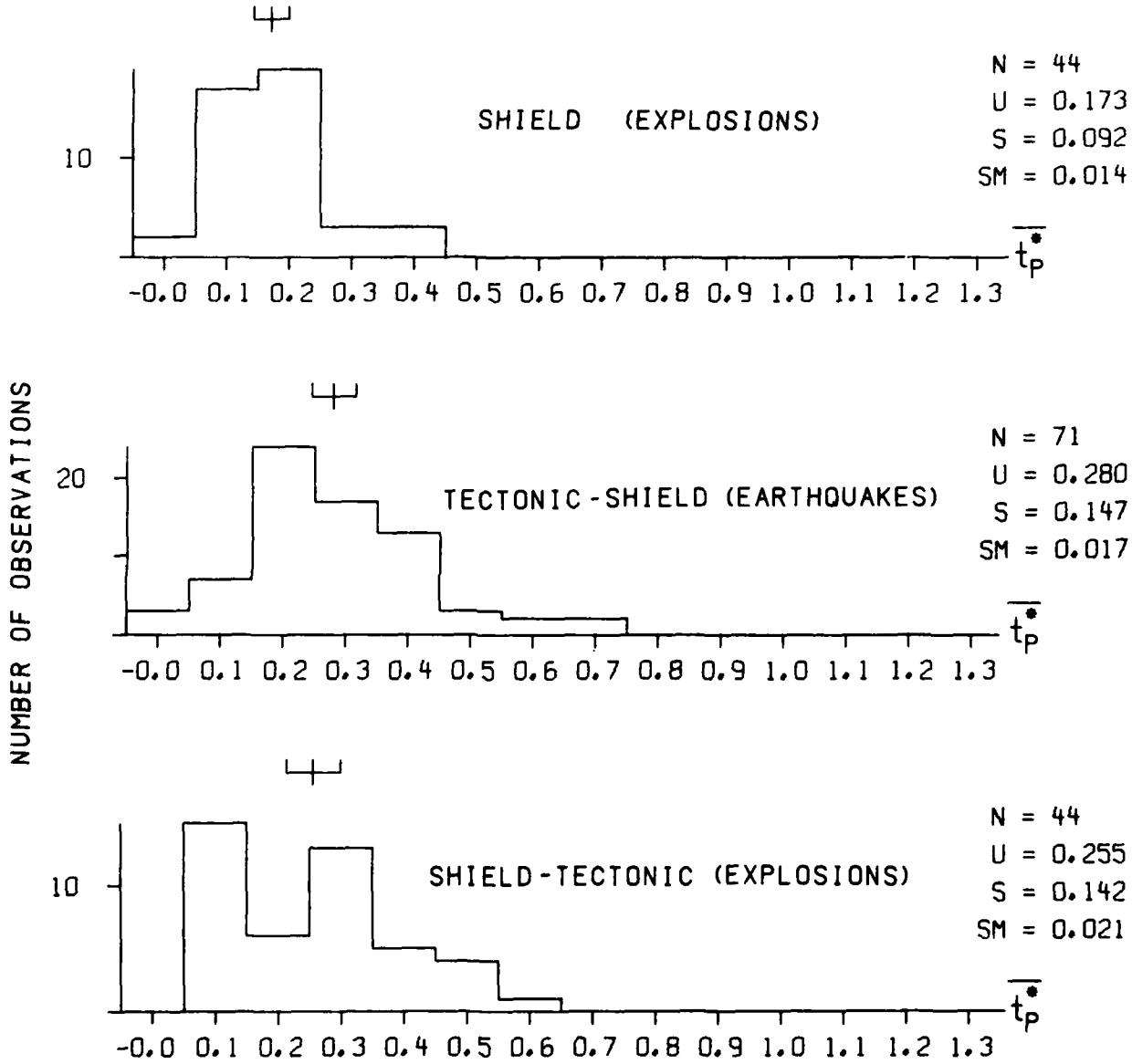

Figure 15. Comparison of $\overline{t_p^*}$ populations for shield type paths derived from explosion data, and paths involving combined shield and tectonic type upper mantle structures separated with respect to source type into explosion and earthquake populations.

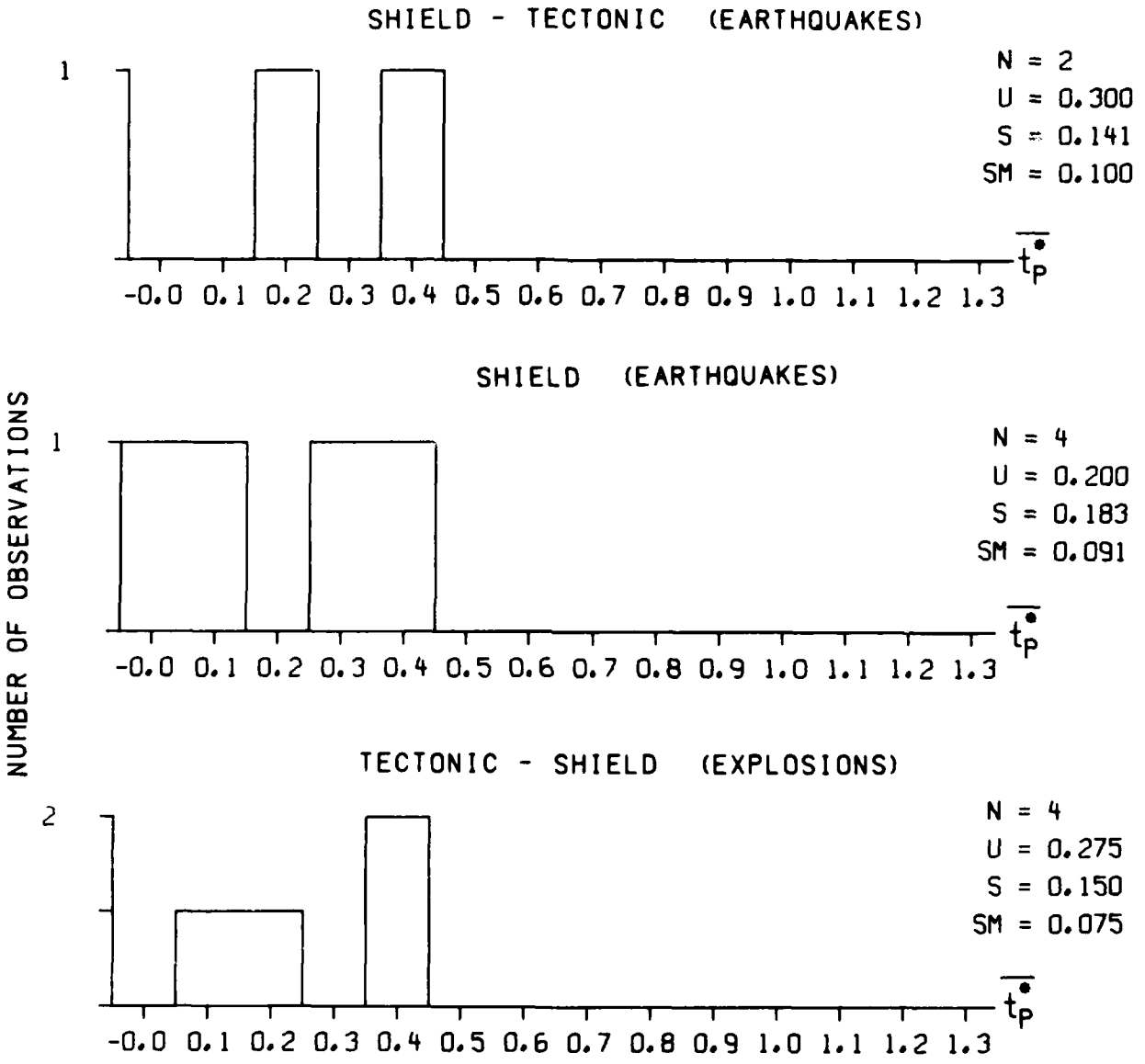

Figure 16. $\overline{t_P^*}$ populations for (from top to bottom); a) shallow earthquakes originating in shields and observed in tectonic areas.
b) shallow earthquakes in shields observed in shields.
c) explosions in tectonic areas observed in shields.

A Preliminary Investigation of t^*_p Variations in Eurasia

A region of special interest in nuclear monitoring is Eurasia. To obtain some idea of the mantle Q variation under Eurasia, we have plotted all of the available $\overline{t^*_p}$ estimates obtained at NORSAR for shallow events on a map of Eurasia at the locations of the events. The resulting map is shown in Figure 17. In this map, we have rounded off the $\overline{t^*_p}$ values to the nearest 0.1 sec and multiplied the values by 10. The resulting numbers are plotted on the map. Thus a value of 1 means that the $\overline{t^*_p}$ is between 0.05 and 0.15, etc. Despite the scarcity of data, a good agreement with the existing ideas about mantle attenuation is evident. The low values in $\overline{t^*_p}$ are associated with the shield areas (see Figure 7 for tectonic subdivisions), the Kazakh test site, Novaya Zemlya, Azgir and the regions adjoining the shield. The only other values of 1 on the main part of the continent are in the Hindu-Kush - Pamir area, where a downgoing slab may reduce attenuation for teleseismic distances (Khalturin it al., 1977). High values of $\overline{t^*_p}$ characterize eastern Tibet and Southern Iran, which are areas of high attenuation according to some other studies (Toksöz and Bird, 1977). The circled numbers in southern Europe are regional averages found by Noponen (1975) and are also high. Moderate values characterize the rest of the tectonic areas of Asia, and mixed values are shown in the Kamchatka-Kuriles region, reflecting the extreme heterogeneity of subduction zones. Clearly more data are needed to map mantle Q in detail, but even this map illustrates that it can be done easily.

Summary of Upper Mantle Attenuation Studies in the United States in the Short Period Band

Prior to the worldwide study of attenuation presented above, we conducted extensive research on upper mantle attenuation under the United States (Der, Massé and Gurski, 1975; Der and McElfresh, 1976a, 1976b, 1977; Der, Smart and Chaplin, 1980; Der, McElfresh and O'Donnell, 1981; Der, 1981). The methodology was similar to that used for the worldwide study; in fact, the basic approach to the analysis of the data was developed during the course of these earlier investigations. We analyzed earthquake and explosion data at both teleseismic and regional

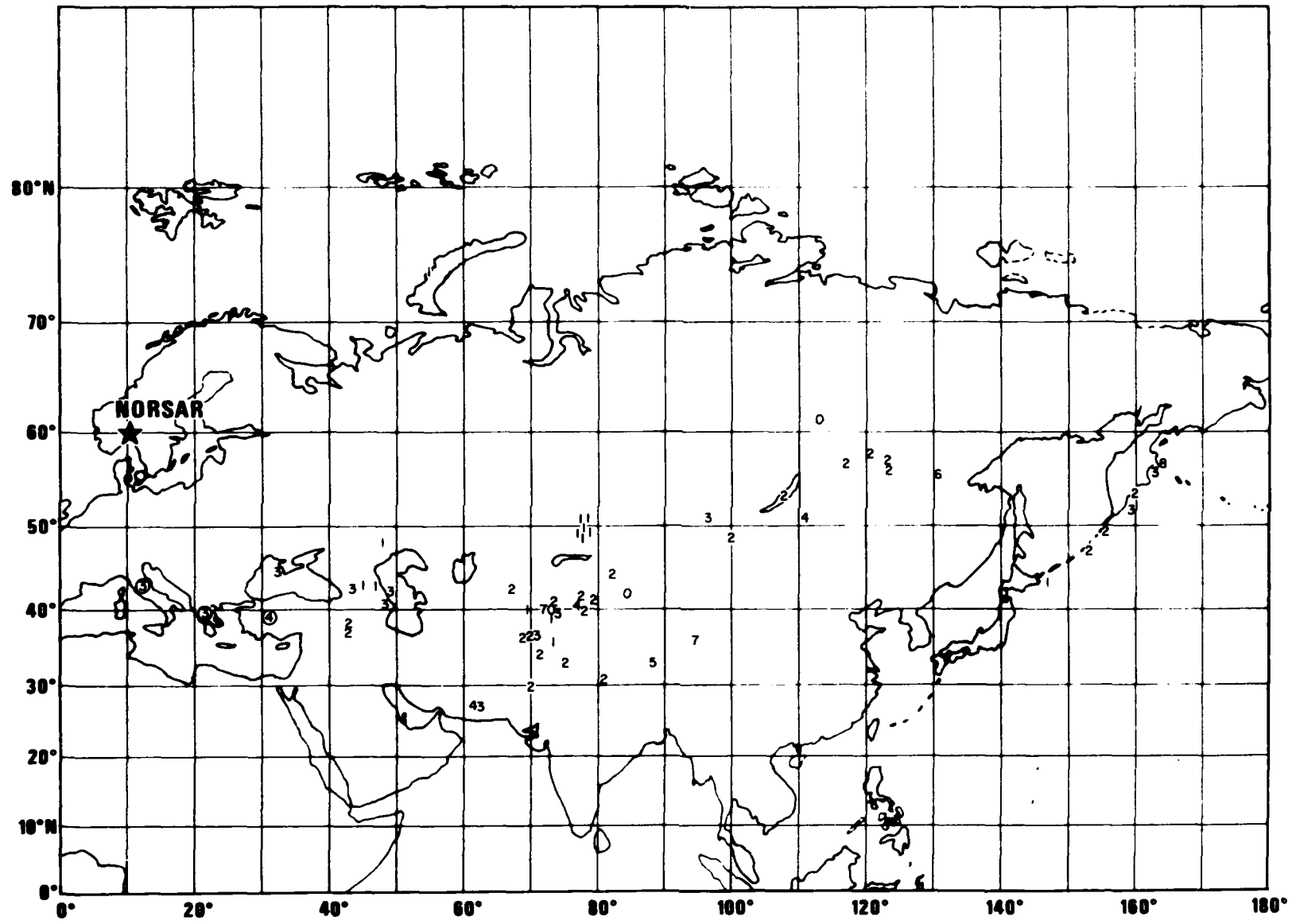

Figure 17. A plot of our $\overline{t_p^*}$ data for Eurasiaa with NORSAR as the observation point. The numbers are $\overline{t_p^*}$ rounded off to the nearest 0.1 sec and multiplied by a factor of 10.

distances, involving both short period P and S waves. The result was a detailed, internally consistent picture of the lateral mantle Q variations under the United States. The main findings of these studies can be summarized as follows:

- Much of the WUS is characterized by a low Q layer in the mantle, whereas this layer is absent under most of the eastern United States (EUS). The northeastern U.S. has mantle attenuation intermediate between the WUS and EUS. The low Q under the western U.S. causes an increase in $\overline{t^*_\beta}$ of 0.2-0.3 sec relative to ray paths that traverse the mantle under shields (EUS).

- The contribution of the low Q upper mantle to $\overline{t^*_\beta}$ is about four times that of $\overline{t^*_\beta}$ (Der, Smart and Chaplin, 1980; Solomon and Toksoz, 1970; Lay and Helmberger, 1981), indicating that the losses in the mantle are predominantly in shear deformation.

- The totality of long and short period data in the region seems to require a frequency dependent Q. (Archambeau, Flinn and Lambert, 1969; Solomon, 1972; Der and McElfresh, 1977; Der, McElfresh and O'Donnell, 1981, Der, 1981).

- $\overline{t^*_\beta}$ for shield type paths in North America (and elsewhere) are typically in the 0.1-0.2 range (Der and McElfresh, 1977,;Noponen, 1975), whereas paths of the WUS to shield (or reciprocal paths) are usually between 0.4-0.5 sec.

Due to the wide areal coverage of the U.S. and parts of Canada by WWSSN and LRSM stations and the long operational life of these stations, it was possible to accumulate sufficient data to verify the above findings by various independent checks. Some of the results that show the internal consistency of the findings above are:

- The relative regional differentials in mantle Q are of the same order when estimated from regional data and teleseismic arrivals (Archambeau, Flinn and Lambert, 1969; Der, McElfresh and O'Donnell, 1981; Der and McElfresh, 1976, 1977).

- When measured using the spectral technique, $\overline{t^*_\beta}$ has a regional variation that agrees in detail with the regional variations of $\overline{t^*_\beta}$ except for the factor of four multiplier in size (Der, McElfresh and O'Donnell, 1981; Lay and Helmberger, 1981).

- The regional amplitude anomalies of P and S waves after crustal corrections are in agreement with those predictable

from the variations of $\overline{t^*_p}$ and $\overline{t^*_s}$ (Der, McElfresh and Mrazek, 1979; Der, McElfresh and O'Donnell, 1981; Lay and Helmberger, 1981).

- o Reciprocity in Q estimates can be demonstrated. The estimates of t^*_p are of the same order regardless of whether outgoing or incoming P waves over similar paths were used for their estimation. For example, the nuclear explosion SALMON (in the EUS) observed in the WUS gives t^*_β which is similar to t^*_β estimates of NTS explosions observed in the EUS (Der and McElfresh, 1976a,b).

- o The estimates of $\overline{t^*_p}$ obtained from the best source functions available for nuclear explosions and from Aki's (1967) ω^{-2} model for earthquakes are about equal for tectonically similar paths.

- o In all of these studies the effect of the local crust on the estimates of $\overline{t^*_p}$ was found to be small or negligible (Der, McElfresh and O'Donnell, 1981).

The internal consistency illustrated by these results encouraged us to apply the spectral approach to the worldwide data readily available to us. The results of the study which followed are given above. Although our worldwide data set is less complete than that for the U.S., the available data are also quite consistent internally. The U.S. data fits quite naturally into the picture presented by the worldwide data, and the WUS appears to be just one of the numerous tectonic regions in the world underlain by low Q in the upper mantle.

General Remarks

The picture of regional variations of mantle Q presented above is in sharp contrast with the picture given by a large body of literature that uses mostly time domain simulations to derive Q. In this literature the same Q is often used for a wide variety of tectonic environments, and all spectral differences are usually attributed to source effects. As we have shown above, such assumptions are no longer tenable. Instead, it appears that short-period body wave analyses at teleseismic distances indicate strong lateral variations of Q in the mantle that are in good agreement with the ideas of plate tectonic theory concerning the lateral variations of the asthenosphere and the mantle temperature. The existence of systematic variations in the frequency content of teleseismic body waves with respect to the tectonic types of the upper

mantle regions traversed has been common knowledge to those working in the field of high-frequency seismology for more than a decade. Such variations have been pointed out and discussed, correctly, in terms of mantle Q by many investigators. The writers of this report are indebted to many of the early workers in this field. The major contribution of this report is the quantitative demonstration of the mantle Q effect using a more extensive $\overline{t^*_p}$ data set than that contained in any previous work. The occurrence of such effects is not surprising in the light of the extensive prior studies of attenuation in various regions.

Claims of $\overline{t^*_p} = 1$ in the short period band based on time domain studies for all kinds of tectonic environments started to appear in the literature in the early seventies; in recent years a large number of such papers have appeared. From the beginning, these papers have been in conflict with most of the preexisting knowledge of the spectral characteristics of short-period body waves.

Although the lateral variations of mantle Q indicated by this study are moderate (a few tenths of a second in $\overline{t^*_p}$), we must point out that the paths investigated may not cross some of the most anomalous regions of the mantle with respect to Q. Back-arc basins and magma chambers existing beneath many volcanic areas (Ryall and Ryall, 1981; Matumoto, 1971; Pitt, 1974; Fedotov and Potapova, 1974) are typical examples. Such areas provide ideal settings for a special type of seismic test ban evasion, because P waves from events located in such areas may be suppressed relative to surface waves thereby rendering the M_s-m_b discriminant ineffective. Fedotov and Potapova (1974) describe such extensive zones of anomalously highly attenuation in the mantle under Kamchatka associated with magma chambers under active volcanoes. It may be that $\overline{t^*_p}$ for paths crossing such regions is quite large, perhaps far exceeding 1 sec.

THE FREQUENCY DEPENDENCE OF Q

The mantle Q apparently has regional variations that correlate with other diagnostics indicating the presence or absence of the upper mantle low-velocity--low-Q layer. Nevertheless, $\overline{t^*_p}$ is a true measure of attenuation only if either t* is frequency independent or if t* changes with frequency in a similar fashion in the various regions of the world. If the terms $f \frac{dt^*}{df}$, are roughly the same throughout a wide band in the short period range, then the differentials in $\overline{t^*_p}$ will reflect differences mostly in t^*_p. Moreover, if t* changes only slowly with frequency, the bias term in equation 3 may be small relative to t*, and again $\overline{t^*}$ will be diagnostic of the relative attenuation along various paths. On the other hand, if the form of frequency dependence of Q varies drastically from region to region, then $\overline{t^*_p}$ may not be a measure of attenuation along a path at all. Lundquist (1981) has shown several possibilities of this type, and several investigators have proposed a model of "absorption band shift" that would allow only for a change in the parameter τ_m in the Minster absorption band model, while keeping the long period t* level constant for various types of paths (Lay and Helmberger 1980). In the following we shall show that the available data do not support such models. The data rather favor t* versus frequency relationships in various regions that change gradually with frequency and run nearly parallel to each other such that the frequency bias term, although it may not be negligible, roughly cancels in making a relative $\overline{t^*_p}$ measurement. This would make $\overline{t^*_p}$ a fairly good measure of global attenuation differences. The fact that $\overline{t^*_p}$ apparently correlates well with regional variations of m_b indicates that this is the case, since m_b variations must be roughly proportional to the absolute t* (Der, McElfresh and Mrazek, 1979). This of course does not obviate the need for further research to determine the exact t* vs. frequency relationships for various regions, and the dependence of Q may be quite complex in some areas.

In determining the frequency dependence of Q, the shield areas of the world provide a convenient starting and reference point, because the high level of detectable high frequency seismic energy in teleseismic body waves observed in these areas, as we shall show later, imposes

narrow limits on the acceptable t* versus frequency models. In addition, the shield areas of the world, in all their characteristics, appear to be fairly similar on the various continents, and a large number of high quality seismic stations are located in them. Other major types of regions, such as tectonic areas, new oceans, and island arcs are laterally quite variable, while old ocean areas are hardly instrumented at all. Having outlined the limits on the frequency dependence of Q in shields, the Q versus frequency relationships in other areas may be determined by relative t_p^* and t_s^* measurements in various frequency bands by using regional amplitude anomalies of P and S waves as well as regional measurements of surface wave attenuation.

To outline the frequency dependence of t*, we shall solve the differential equation (3) approximately by determining averages of $\overline{t_s^*}$ and $\overline{t_p^*}$ in the 0.5-5 Hz range, at frequencies near 1 Hz and roughly in the 0.3-2 Hz range. We will then draw curves of t* that conform to these and to a set of t* estimates derived by other workers in the long-period band. In drawing regional curves of t* versus frequency, we shall also utilize a number of other constraints derived from regional amplitude anomalies of P and S waves, as well as relative spectral measurements. The validity of the frequency-dependent t* models presented will strongly depend on the correctness of the long-period studies we used.

The t* versus frequency curves we shall derive will be for shield type and shield-to-WUS type paths. We chose these because the most data are available for such paths. A similar approach can be used to determine such curves for other types of paths. Typical values of $\overline{t_p^*}$ in the 0.5-5 Hz band have been found to be 0.2 sec for shields and 0.4-0.5 sec for shield-to-WUS paths (Der and McElfresh 1977). In addition to these values, we shall need $\overline{t_p^*}$ and $\overline{t_s^*}$ estimates near 1 Hz to further define the frequency dependence of t*.

The Values of t_p^* and t_s^* For Shield Type Paths Near 1 Hz

To examine what $\overline{t_p^*}$ and $\overline{t_s^*}$ should be at frequencies at and above 1 Hz, we have computed a set of spectra from deep earthquakes for P and S

waves observed at hard rock sites in the southern edge of the Canadian shield. Figure 18 shows some representative examples of these. Noise spectra preceding the arrival of the respective phases are also plotted. For S phases, the noise spectra also include the scattered energy preceding the S arrival. The P spectra up to at least 5 Hz are above the background noise. The solid curves show the expected falloff of spectra assuming a rate of source spectrum decrease of ω^{-n} for $\overline{t^*_p} = 0.5$ and $\overline{t^*_s} = 2$ sec, one half the values for shallow events commonly used in synthetic simulations. Since the events in question are large, ω^{-2} most likely characterizes the source spectrum. The discrepancy between the observed and predicted spectra with ω^{-2} exceeds two orders of magnitude at the high-frequency end for both P and S waves. Even if one assumes an ω^0 falloff rate for the S-wave sources, which corresponds to a delta function source, the discrepancy between the 2 Hz amplitude level and the line computed for ω^0 with $\overline{t^*_s} = 2$ sec is about a factor of 200.

The dashed lines superimposed on the spectra correspond to $\overline{t^*_p} = 0.2$ and $\overline{t^*_s} = 0.8$, assuming a ω^{-2} falloff in the source spectra. Even at these low $\overline{t^*}$ values the spectra do not fit well, and lower attenuation is indicated. We must also add that even a frequency-dependent t^*_s that assumes the value of 2 sec at 1 H_z would be inconsistent with these data (with ω^{-2} falloff), since the t* needs to change faster than frequency to explain these spectra and present physical Q models do not allow for this (Minster, 1978).

Arguments based on spectral falloff rates are, of course, somewhat imprecise. The ω^{-2} falloff argument is for large unspecified frequencies (Brune, 1970), and smaller falloff rates are possible. On the other hand, observational evidence is such that source spectra actually fall off as ω^{-2} for events of the size analyzed here, and theoretical modeling using triangular or trapezoidal source pulses also implies ω^{-2}. It appears, therefore, that the spectra presented here cannot be reconciled with $\overline{t^*_s} = 2$ for any presently accepted source model, theoretical or observational, even for an ω^0 falloff in the

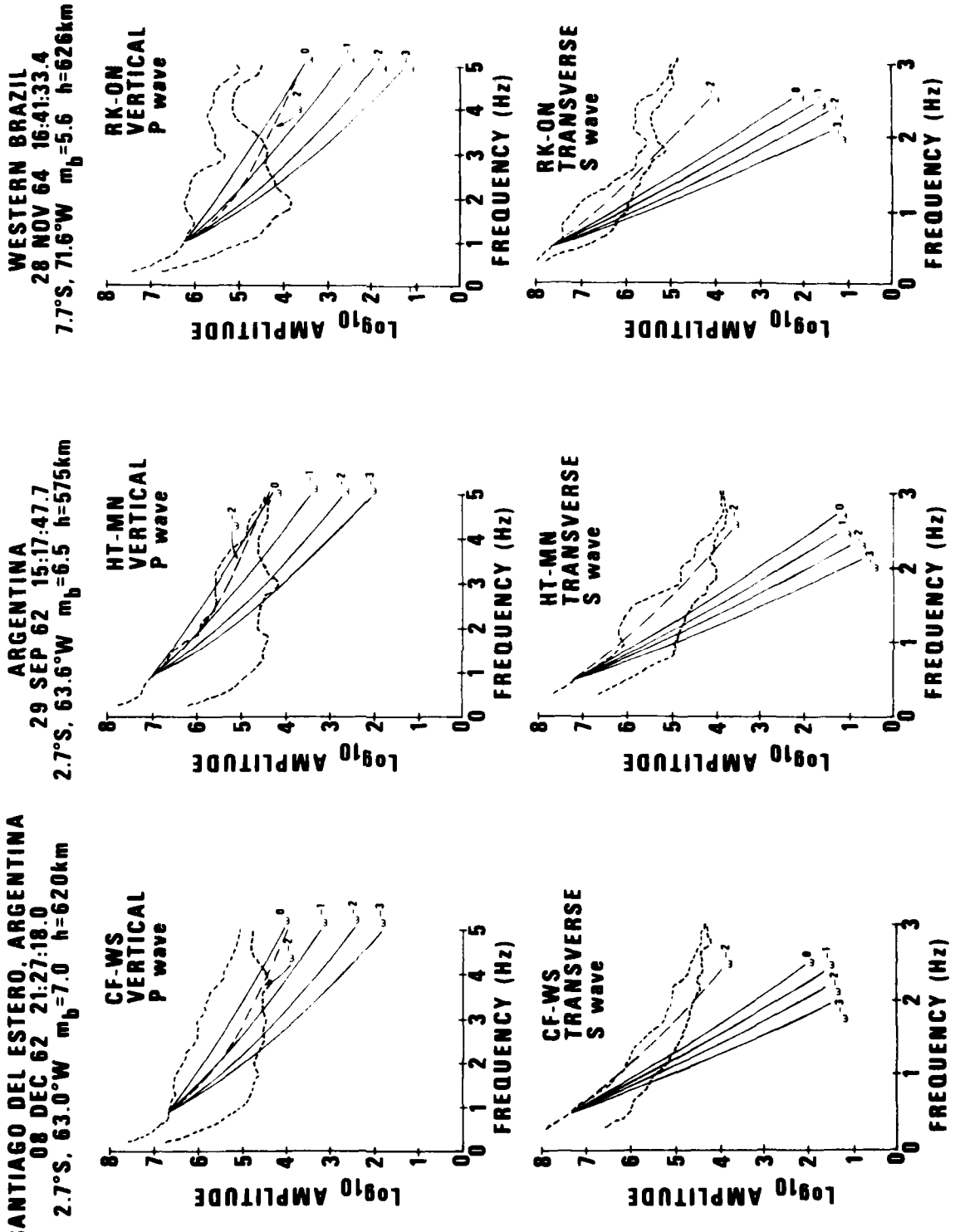

Figure 18. Spectra of short-period P and SH waves from deep South American earthquakes observed at hard rock sites in the north central U.S. (shield).

source spectra. These spectra clearly demonstrate that the discrepancy is prevalent in the vicinity of 1 Hz, and that the high t* values frequently used in many studies are not valid for these data.

It also appears that even if one adopts the time domain approach, a good case can be made against the $\overline{t^*_s}$ value of 3.2 sec of Burdick (1978). In Figure 19 we show observed and synthetic SH waveforms for several events and various model source time histories. The top set of traces shows SH waveforms of about 1 sec period from several South American deep earthquakes compared to synthetic waveforms for a triangular pulse of 1 sec duration and a delta function. Both source models were passed through the LRSM instrument response and attenuated with the $\overline{t^*_s}$ values of 3.2, 2.0 and 0.8. For the 1 sec triangular source appropriate for these earthquakes of about 5.6 body wave magnitude, all synthetics have longer period than the observed data. This source function was used by Lay and Helmberger (1980). With $\overline{t^*_s}$ = 3.2, or even $\overline{t^*_s}$ = 2.0, such short-period (1 sec) observed waveforms are not possible even with the assumption of a delta function which represents the extreme, unlikely example of a high frequency source. The bottom set of traces shows the comparison of synthetic waveforms for a 3 sec triangular source appropriate to a large event with the observed waveforms from a magnitude 7 deep earthquake. Again the $\overline{t^*_s}$ = 0.8 provides the best fit.

Note that the LRSM stations BXUT, WINV and DRCO are located in the WUS, ruling out the value of $\overline{t^*_s}$ = 3.2 even for this low Q region. While our spectral arguments based on Figure 18 limit the value of $\overline{t^*_s}$ in the 0.5-2 Hz range, the time domain simulation constrains t* at lower frequencies, roughly in the 0.3-1 Hz range. The fact that both estimates give a $\overline{t^*_s}$ much less than 3.2, indicates that this value is unacceptable for deep earthquake S phases observed in the EUS. Since impulsive source functions are physically unlikely, the short-period SH waves shown here rule out $\overline{t^*_s}$ values of 2-3 sec. However, SH waveforms with considerably less high frequency content between .3-2 H_z have also been observed, and S waves observed at close range commonly contain less high frequency energy than P waves. It is therefore not permissible to attribute all or most of the spectral differences between P and S to

anelastic attenuation (as was done in the past in many time domain studies of waveforms), since source effects also contribute to these differences (Molnar et al., 1973; Hanks, 1981). Besides the assumption of near equality of P- and S-wave spectra at the source, the reason for some of the high $\overline{t^*_s}$ estimates was non-representative data selection that overlooked the high-frequency S waves in a search for "simple" events (Burdick, 1978).

In an examination of worldwide data, we have found that $\overline{t^*_p}$ values for deep events observed on shields are of the same size as those derived for shallow events following paths confined to shields. One would therefore expect to see short-period S waves from such events. This observation is very hard to make, however, since there are very few intraplate events in shield areas of the necessary magnitude to be seen at large distances. If observed on the same continental block, the seismograms are dominated by crustal phases that obscure such arrivals. Nevertheless, we have found an event on the southern edge of the shield in Russia that produced a visible short-period S phase at NPNT at the northern edge of the Canadian shield. The dominant period of this S wave is 1 second. The magnitude computed from the P wave shows that the station is not close to a nodal line for P. With this size of P arrival, the 1 Hz S wave should be invisible if the high $\overline{t^*_p}$ near 1 sec claimed by some researchers were true (Figure 20).

The three types of evidence presented above apply to various frequency ranges: the spectra in the 0.5-2 Hz range, the waveform matching to the dominant frequencies of the waves in the 0.4-1 Hz range and the short-period S to 1 Hz. All of these are consistent with a low $\overline{t^*_s}$ on the order of 0.8 sec which implies a t^*_p near 0.2 sec. These data preclude any values of t^*_s near 3.2 and the corresponding $\overline{t^*_p} = 0.8$ in the neighborhood of 1 Hz claimed by Burdick (1978) and Lay and Helmberger (1980).

Q Under the Russian Shield

The Russian shield is an important area for seismic monitoring, and the value of the apparent and absolute t* involving teleseismic paths through the mantle under this region is of great importance. It is a

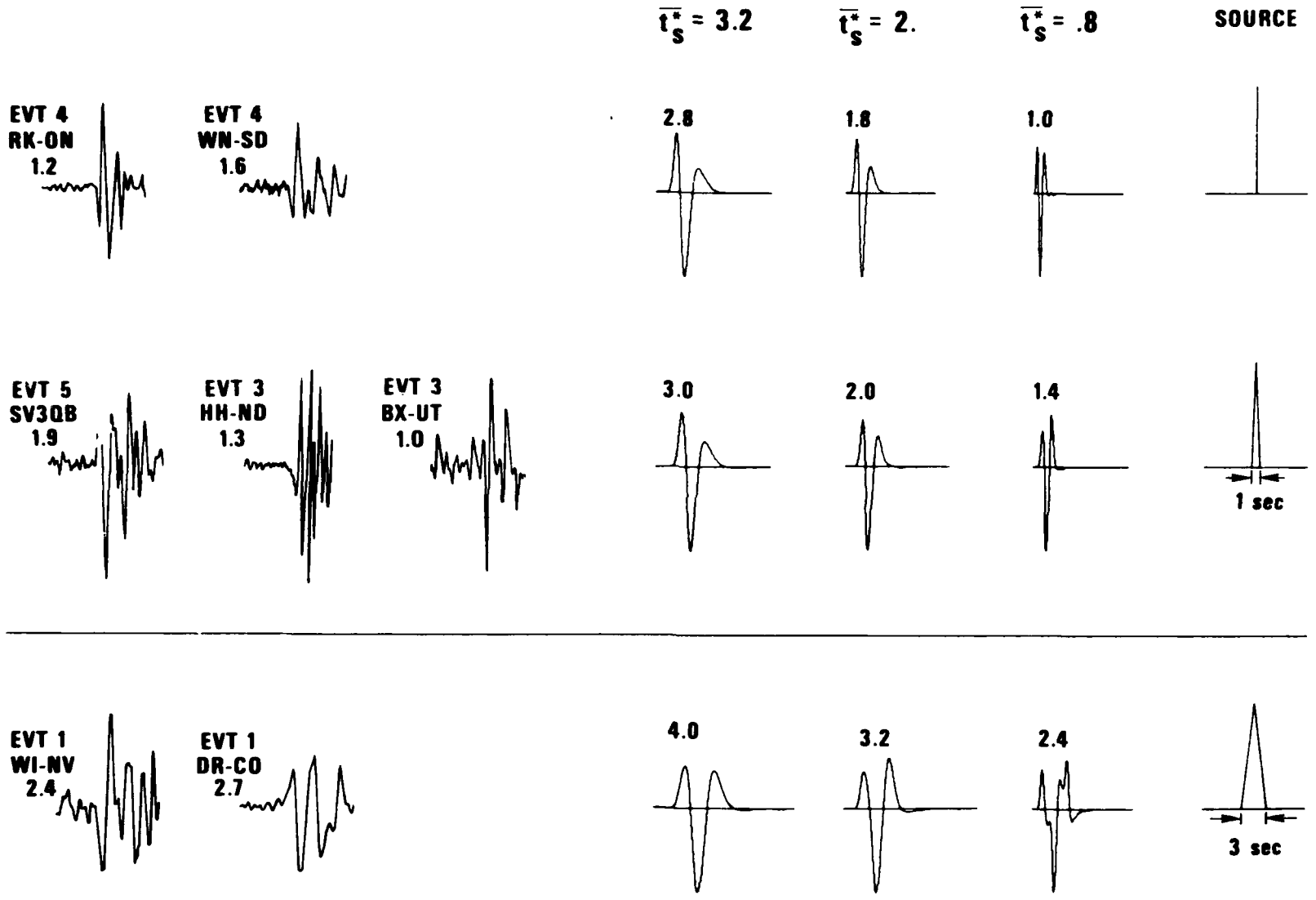

Figure 19. Matching of observed SH waveforms to synthetic waveforms using various source functions and $\overline{t_s^*}$ of 3.2, 2.0 and 0.8. The periods of the first cycle of the wave are written above each trace.

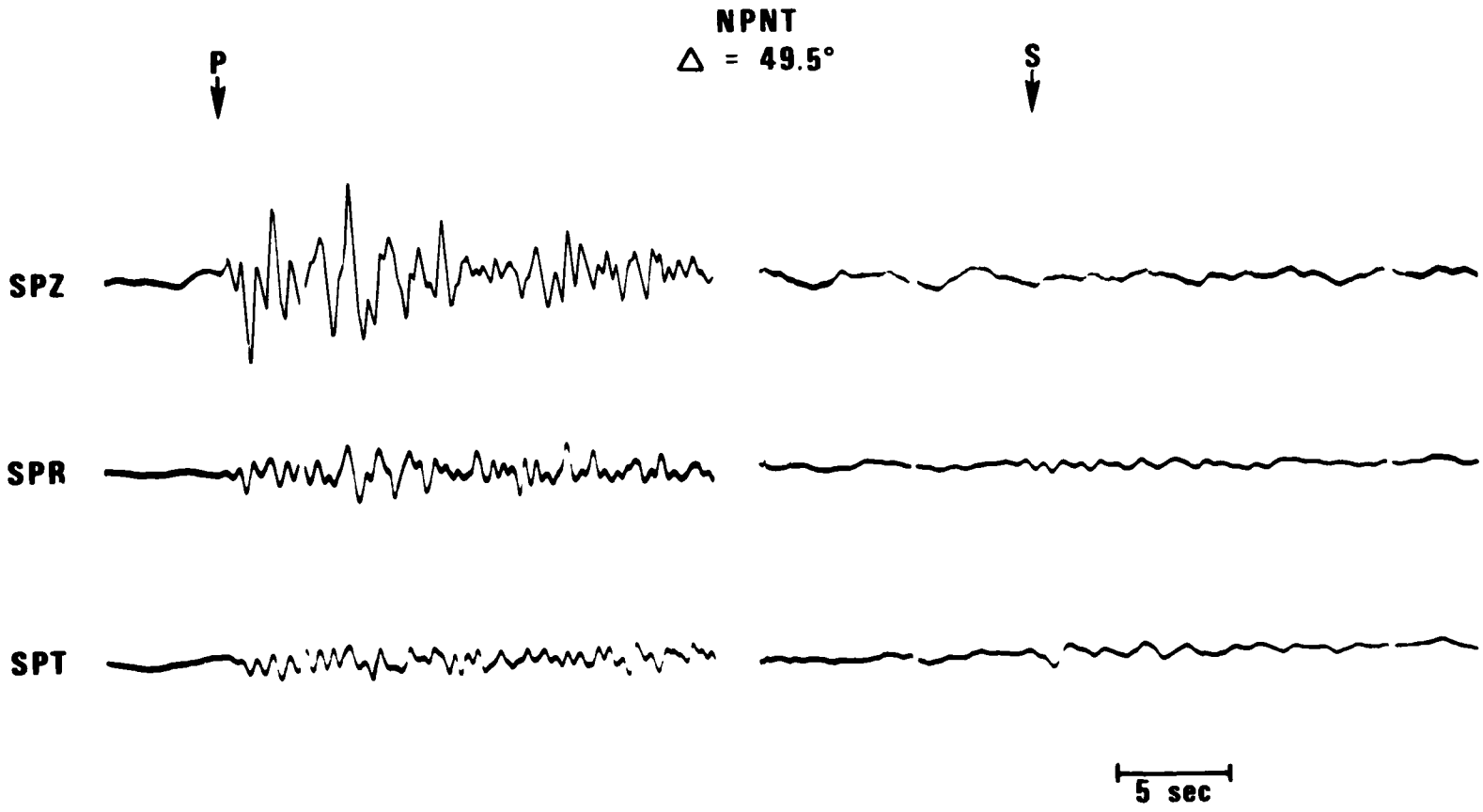

Figure 20. Short-period S wave from a shallow earthquake observed at the distance of 49.5° at NPNT. Time interval between time marks on the right is 20 sec.

well known fact that nuclear explosions in this area have been shown to generate high-frequency P waves at NORSAR with energy detectable above the noise level up to 10 Hz. Examples of such signals are shown in Figures 1 and 2 of this report. A widely used method for deriving detailed crust-upper mantle velocity profiles is the use of seismic profiles recorded at regional distances. The interpretation of such profiles was originally done by ray theory (Green and Hales, 1968; Hales, 1972; Archambeau et al., 1969; Massé et al., 1972, Massé and Alexander, 1974) and later by using generalized ray theory and various other more refined methods based on exact wave theory (Helmberger and Wiggins, 1971; Burdick and Helmberger, 1978). Most of the studies using ray theory, with the exception of Archambeau et al (1969), did not consider the effect of Q on the record section characteristics, and the generalized ray theory studies applied only a common attenuation operator to the whole trace without taking into account the differences in the attenuation affecting the various rays.

In any frequency-dependent and depth-dependent Q model, there will be changes of spectral content of P arrivals with distance; and due to the nature of the travel path, the spectral content of the arrivals along the various upper mantle travel time triplications will change in a manner that allows one to derive Q models of the mantle (Kennett, 1975; Archambeau et al., 1969).

The enclosed Figures 21 to 24 show profiles constructed from bandpass filtered recordings of nuclear explosions in the USSR obtained at NORSAR. The events we have used to make these include those analyzed by Massé and Alexander (1974), but newer events were also added. The fact that the general appearance of the record section is not much affected by the bandpass filtering, as shown by the invariance of the relative amplitudes of arrivals, the envelope shapes of the individual traces, and the change of amplitudes with distance (all amplitudes were normalized with respect to m_b and multiplied with a factor R to make the initial trace amplitudes comparable). Since recordings of nuclear explosions in the USSR commonly show significant energy up to 10 Hz at NORSAR in teleseismic upper mantle arrivals up to 35° in distance, the presence of low Q zones in the mantle should cause changes in the

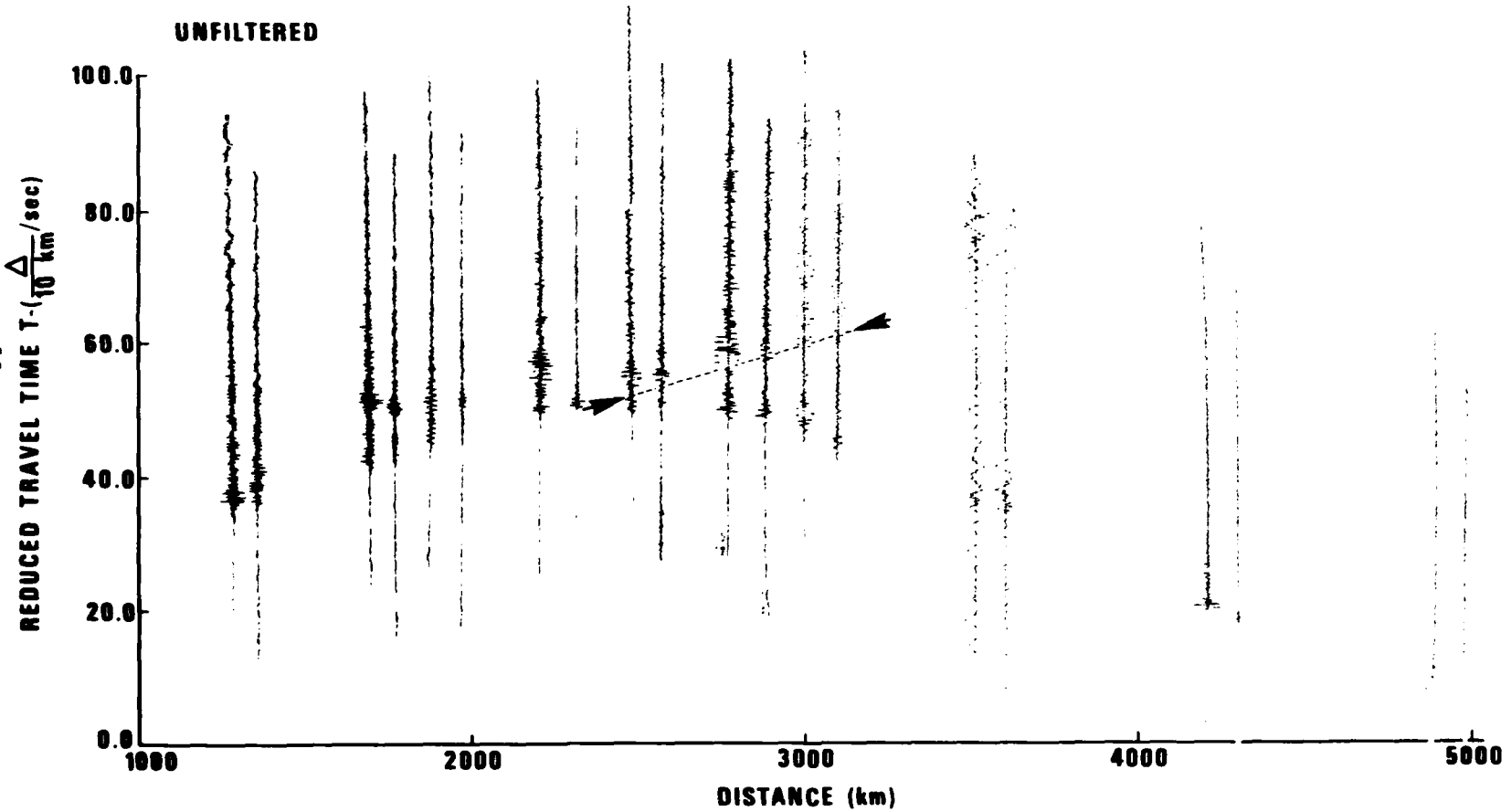

Figure 21. The record section constructed from P wave arrivals from nuclear explosions in Eurasia. Heavy arrows indicate travel time branches corresponding to the 400 km discontinuity and first arrivals. The relative amplitudes A/B and C/D can be strongly affected by details in the Q structure.

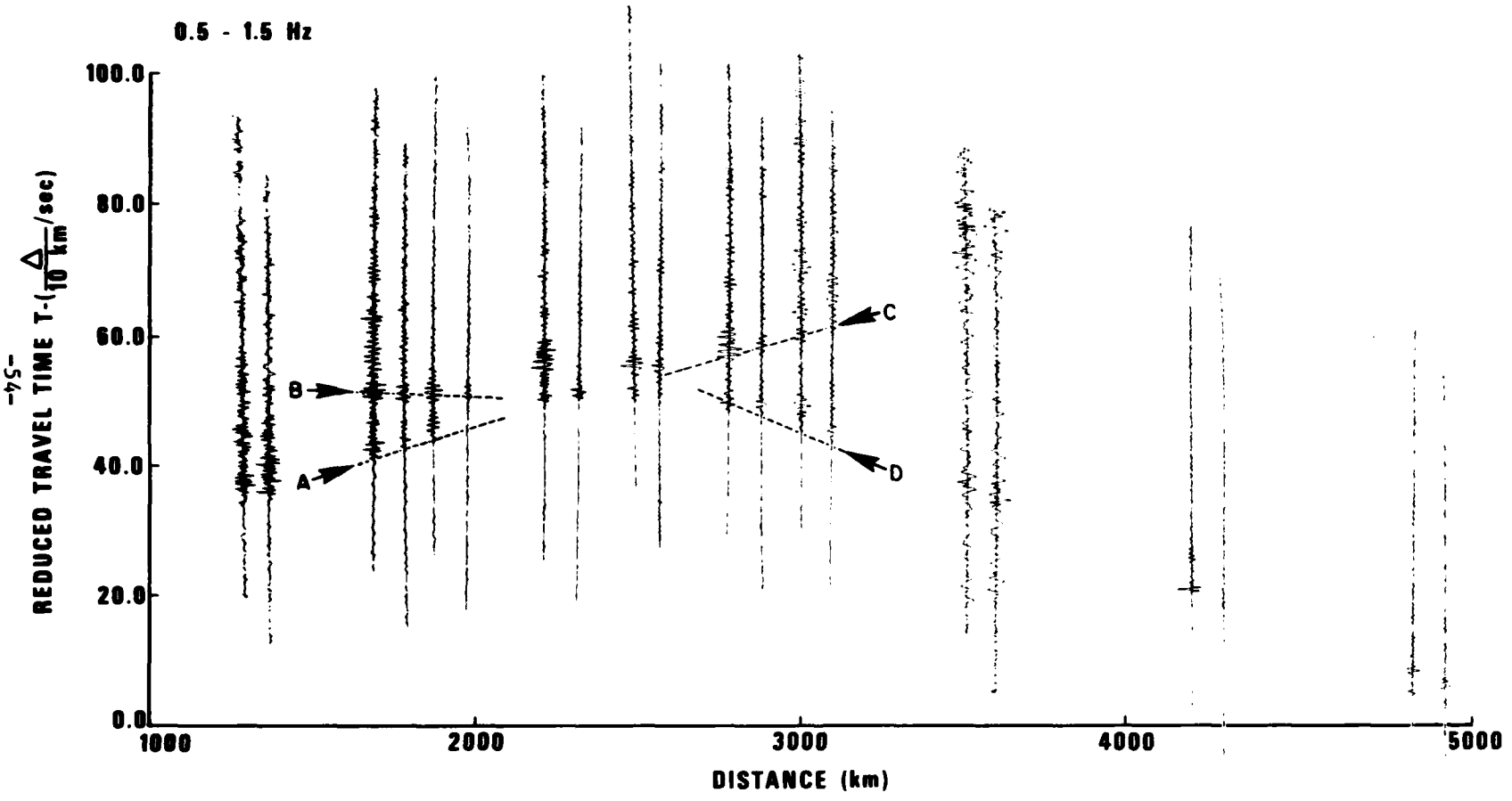

Figure 22. The record section in Figure 21 filtered by a 0.5-1.5 Hz bandpass filter. Heavy arrows indicate travel time branches corresponding to the 400 km discontinuity and first arrivals. The relative amplitudes A/B and C/D can be strongly affected by details in the Q structure.

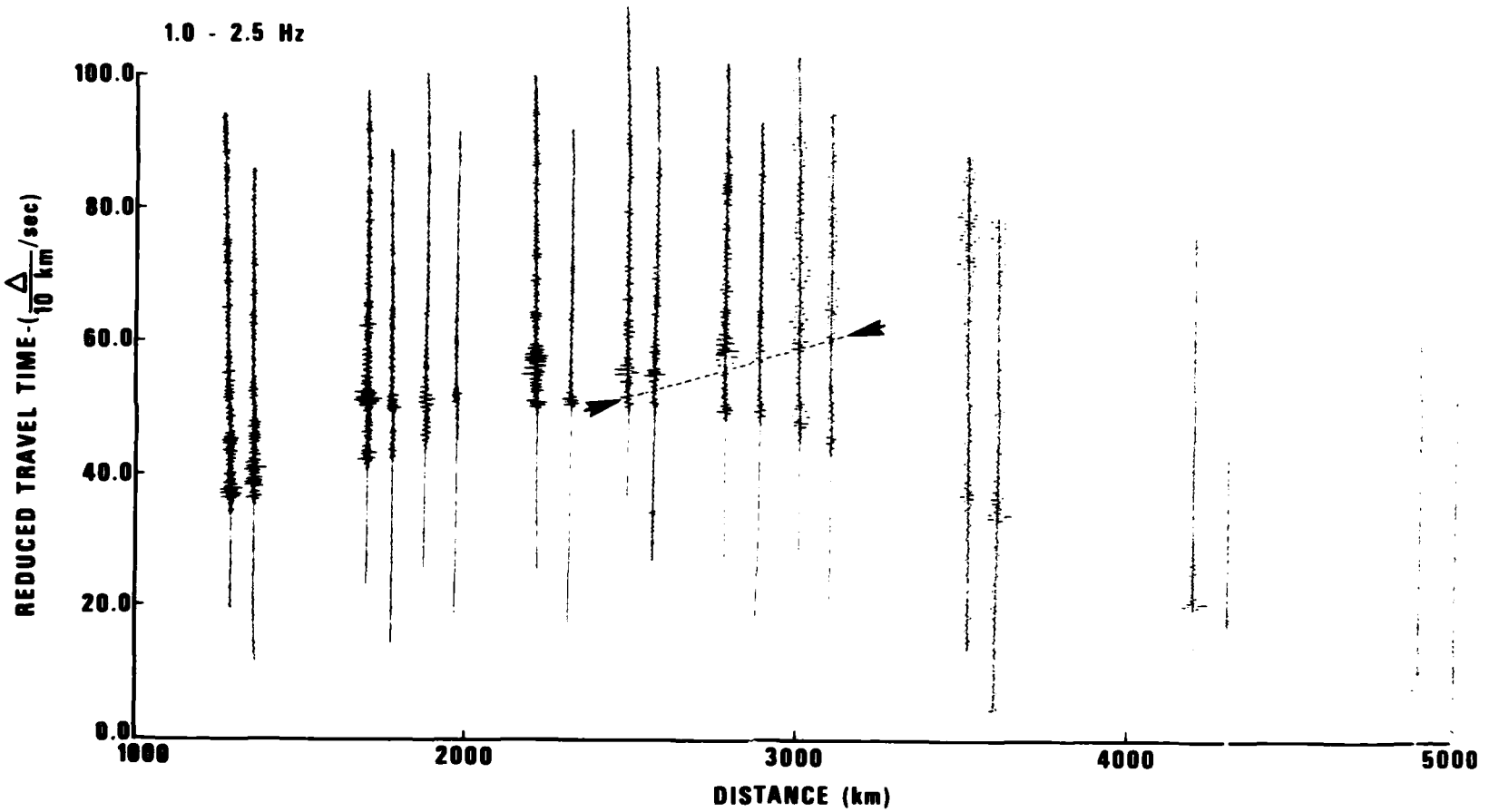

Figure 23. The record section in Figure 21 filtered by a 1.0-2.5 Hz bandpass filter. Heavy arrows indicate travel time branches corresponding to the 400 km discontinuity and first arrivals. The relative amplitudes A/B and C/D can be strongly affected by details in the Q structure.

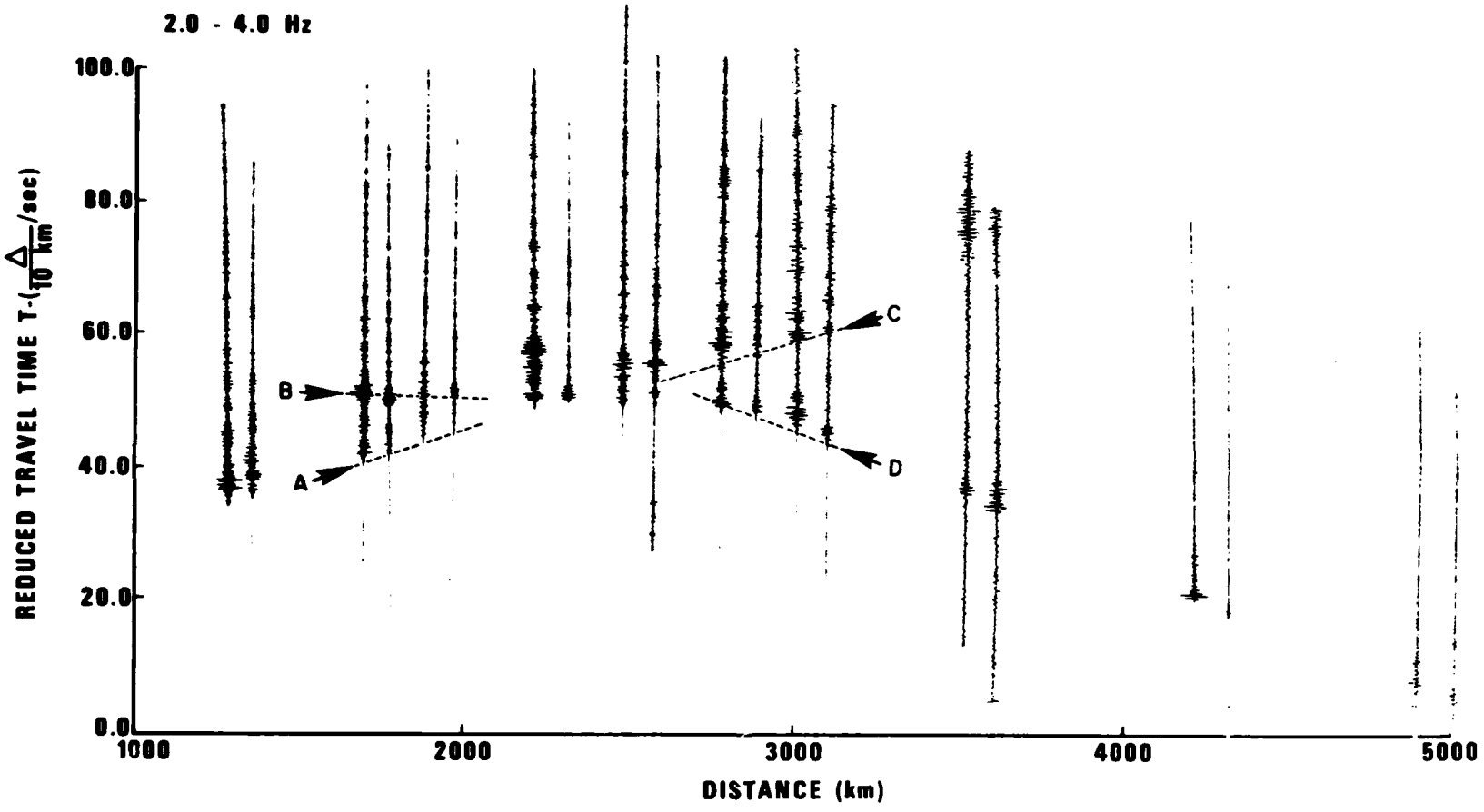

Figure 24. The record section in Figure 21 filtered by a 2.0-4.0 Hz bandpass filter. Heavy arrows indicate travel time branches corresponding to the 400 km discontinuity and first arrivals. The relative amplitudes A/B and C/D can be strongly affected by details in the Q structure.

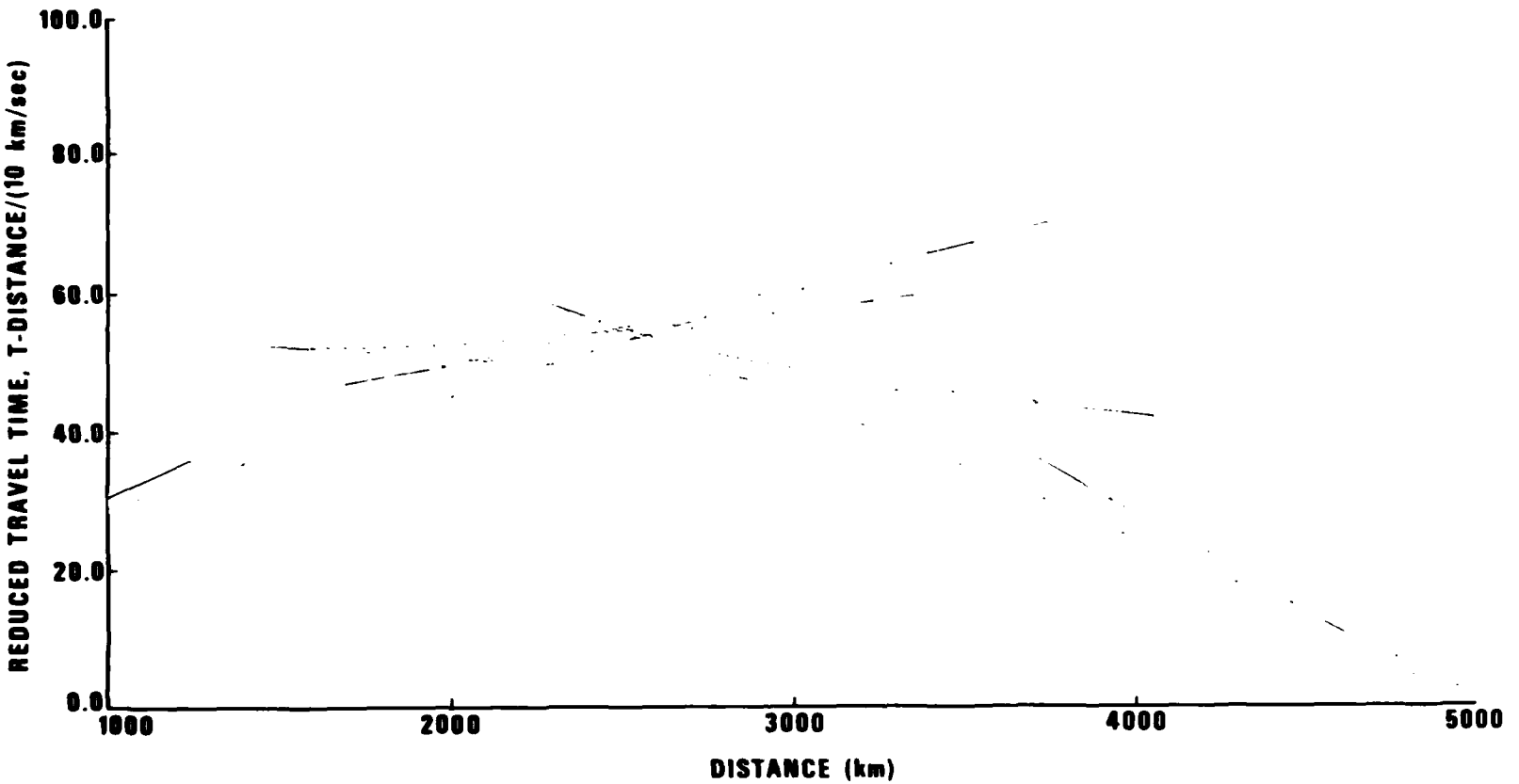

Figure 25. Interpretation of the record sections by Massé and Alexander (1974).

relative amplitudes of arrivals along various types of paths, if the recordings are filtered into narrow bands including frequencies higher than those in Figure 24. Points to look for are changes in the relative amplitudes between the primary arrivals A and the back branch of upper mantle triplication B between 1600 and 2000 km. There variations will reveal Q structure at depths in the upper 200 km of the mantle (Burdick and Helmberger, 1978). If this would be reflected in the changes of amplitudes in the primary arrivals at greater distances, D, relative to those of the forwarded branches of the 400 km triplications (Kennett, 1975; Mereu et al., 1974). Although these changes are small at low frequencies around 1 Hz (Burdick and Helmberger, 1978), they should be quite apparent at higher frequencies. The enclosed section 24 does seem to reveal some changes in the relative amplitudes A and B relative to those shown in Figure 22, but the change is small; this, together with the fact that the upper mantle transmits frequencies up to 10 Hz, indicates that the average Q is high under the region.

Given and Helmberger (1980) used a $\overline{t^*_p} = 1$ in their study of the same region. This t* is clearly too high, since it implies that Q under shields is the same as the worldwide average of approximately 1 sec. This also conflicts with global studies of Q at long period (Nakanishi, 1979; Mills, 1978) which indicate that Q under shields is higher than that for the average Earth ($\overline{t^*_p} < 1$). It also conflicts with our findings above. Moreover, the synthetic seismograms in the studies of Given and Helmberger (1980) and Burdick and Helmberger (1978) obtained with $\overline{t^*_p} = 1$ sec have visibly less high frequency content than the corresponding observed seismograms. This indicates a higher Q and lower t* than the values they used. In the studies of Given and Helmberger (1980) and Burdick and Helmberger (1979), values of 4 and 6 of the parameter B in the von Seggern and Blandford model (1972) were found by fitting waveforms. These values are physically impossible, because at these values the nuclear explosions cannot be contained, and the explosions in question were contained. This indicates that the methodology used by these authors for finding Q and explosion source parameters needs to be revised substantially.

The evidence shown above also indicates that frequency-dependent Q models that require a $\overline{t_p^*}$ near 1 sec around 1 Hz for shield paths are in conflict with the available data. If the high $\overline{t_p^*}$ values implied by some of the work of Given and Helmberger (1980) and Lay and Helmberger (1981) were valid for shields, then the high frequency content and the waveforms of teleseismic body waves would be quite different from the observed. The $\overline{t_p^*}$ versus frequency models favored by some workers (Burdick, 1980) that retain a high value near 1 sec at 1 Hz and then plunge rapidly at frequencies above 1 Hz are clearly in conflict with the type of data shown above. Instead, these data show that $\overline{t_p^*}$ is substantially below 1 sec in the roughly 0.3-2 Hz range, even adding the typical mean differentials of the shield relative to other types of tectonic environments, which amount to a few tenths of a second. Thus it can safely be said that $\overline{t_p^*}$ is below 1 sec for most paths in the Earth near 1 Hz.

Constraints on the Frequency Dependence of Q Imposed by Long-Period Data

Attenuation results in the long-period band that are applicable to the United States are numerous but quite confusing. Attenuation studies elsewhere in the world (especially in shield areas) may be assumed to be applicable to the EUS on the basis of similarities among shield regions worldwide. Global studies impose some limits on the possible variations of Q. Before tying our short-period results to long-period t* estimates in order to outline frequency dependence, some critical selection must be made among the numerous but mutually contradicting results.

A large number of $\overline{t^*_p}$ and $\overline{t^*_s}$ values in the recent literature come from studies involving time-domain matching of synthetic seismograms with recorded data traces. These studies obtain the fits using complex multiparametric models that contain various source parameters and mantle velocity models. The parameters are adjusted simultaneously until the time-domain fits are deemed satisfactory by largely subjective criteria. In general, these results cover the 0.03-1 Hz range. Strictly speaking, these $\overline{t^*}$ values are byproducts of source or mantle structure studies, and their validity is not essential to most of the conclusions of time-domain studies. We have expressed our reservations about this technique for estimating Q in the past (Der and McElfresh, 1980). Since most workers using this technique obtained Q values that are in conflict with spectral studies, we consider their results concerning Q invalid in the short-period band.

A variant of the time domain methods matches the relative amplitudes of short- and long-period recordings. We find the method acceptable for studying regional variations of Q if sufficiently large data bases are used to overcome the variability of short-period wave amplitudes (Lay and Helmberger, 1980). On the other hand, application of this method to small sets of stations can lead to invalid results. This is drastically demonstrated by the failure of Burdick (1978) to detect regional variations of Q under the United States, a phenomenon whose existence is obvious from even casual inspection of short-period S waves from deep earthquakes. Another illustration of this is a $\overline{t^*_p}$ estimate of 1.3 by Helmberger and Hadley (1981) from NTS to stable platform or shield

regions in the 0.3-0.7 Hz range as indicated by the dominant periods of P waves. To reconcile this measurement with the $\overline{t^*_p}$ of the order of 0.4-0.5 along similar paths determined by spectral methods (Der et al, 1977; von Seggern and Rivers, 1979; Noponen, 1975; Frasier and Filson, 1972), an unacceptably rapid variation of t^*_p with frequency in the short-period band would be required.

In our discussion of the frequency dependence of t* we shall consider the relative $\overline{t^*}$ differences determined by Lay and Helmberger (1981) and other studies using either spectral or combined time-domain and spectral methods, but we will exclude all work using time-domain waveform fitting alone. Although we do not have any direct proof that the long-period Q estimates in these studies are wrong, the repeated discrepancies we have found between these and our work in the short-period band make us suspicious about the validity of all Q values obtained by such methods. Hanks (1981) pointed out that limitations in the source models used in many of these studies may cause Q estimates to be too low.

Measurements of the Earth's free oscillations are also valid indicators of the anelastic losses in an average Earth, although the extraction of regional information from such data has barely begun (Jordan, 1978; Silver and Jordan, 1981; Dahlen, 1980; Woodhouse, 1980). On the average, $t^*_p \approx 1$ and $t^*_s \approx 4$ are required by such data (Anderson and Hart, 1977); Sailor and Dziewonski, 1978). It must be pointed out, however, that averaged Q models of the Earth may be biased by the grossly uneven regional distribution of anelastic losses in the Earth. If short-period Q data are any guide for this distribution, some areas behind island arcs, mid-ocean ridges, and rift zones must dissipate a disproportionate amount of energy relative to their physical dimensions, biasing the Q of an averaged model towards values lower than for most of the earth's volume. This possible bias makes it even more likely that the $\overline{t^*_p}$ involving shield type paths are considerably below one second throughout the seismic band. Moreover, some Q estimates obtained by spectral stacking methods in free oscillation studies may also be biased towards too low values by the lateral heterogeneities of the Earth (Sleep, Geller and Stein, 1981).

Regional variations of Q in the long-period band were studied by Solomon and Toksoz (1970) and Solomon (1972), who give a regional $\overline{t^*_p}$ differential of 0.5 sec or more between EUS and WUS. The studies of Lee and Solomon (1975, 1978, 1979) result in Q_β structures that imply a long-period $\overline{t^*_p}$ differential of only 0.25 sec. Ray tracing through the Q models given by these authors would give t^*_p of the order of 0.6 to 0.7 sec in the eastern U.S. (EUS) and close to unity for an EUS-WUS path. The absolute Q values in these models are, however, rather uncertain due to the inherent difficulties of measuring Q of surface waves over short paths. In any case, these studies indicate that the upper mantle Q varies regionally also in the long-period band. The work of Nakanishi (1979) and Mills (1978) provides further indications that the upper mantle Q measured in the 150 to 300 sec period range is high under shields. It appears from Nakanishi's results that, on the average, anelastic losses under the shields are less than those associated with model MM8 of Anderson et al (1965). At teleseismic distances, model MM8 gives a t^*_p of the order of 0.6 to 0.8 sec, and thus those values should be considered as upper limits of absolute t^*_p in the long-period band for shield type paths.

Numerous measurements of Q_β averages in the mantle have been provided by multiple ScS phases. Unfortunately, there are no studies of ScS that could be clearly associated with purely shield type paths and none under the eastern United States. Nevertheless, the average Q_{ScS} values of 600 for the whole mantle by Kovach and Anderson (1964) and 580 by Sato and Espinosa (1967) may be indicative of Q values in regions above the downgoing slab in South America that may have Q characteristics similar to shields (Sacks, and Okada, 1974). These Q values are considerably higher than those obtained from multiple ScS studies elsewhere (Sipkin and Jordan, 1980), but the corresponding t^*_p at teleseismic distances in such structures would still be 0.4 to 0.5 sec, twice the $\overline{t^*_p}$ from spectral ratios in the short-period band along similar paths. Q estimates obtained from core reflections may also be influenced by low Q regions near the core-mantle boundary and may not be directly applicable to the paths with epicentral distances less than 85° used in this study.

Indications of the frequency dependence of Q within the long-period band were found by Sipkin and Jordan (1979), Brune (1977), Yoshida and Tsijiura (1975), and Sato and Espinosa (1967) in other areas of the world.

Constraints on the Possible Forms of Frequency Dependence of Q Imposed by the Shapes of Spectral Ratios

There is now a widespread consensus that some kind of frequency dependence for Q must be adopted in order to reconcile the apparent discrepancies in Q values in the long- and short-period bands. It must be pointed out, however, that available data allow only a fairly restricted class of frequency dependences. Over the years, many workers used constant Q in both the long- and short-period bands and did not notice any peculiarities. This implies that Q is quasi-constant, i.e., it cannot change very rapidly as a function of frequency. For instance, let us examine what a simple absorption band model of the type described by Minster (1978a) would do to source-to-observed spectral ratios (Figure 26). If one attempts to fit a high t* value to an observed low apparent t* in the high-frequency end, one needs a rapid variation of Q with frequency. This in turn would introduce a peculiar curvature in the spectral ratios. The greater the gap between the long- and short-period apparent t* values, the more pronounced the curvature becomes. On the other hand, no such curvature has ever been observed, at least not consistently. Many researchers estimated Q in the short-period band, and the constant Q assumption was found to be quite satisfactory. In Figure 27 we show some observed-to-source spectral ratios (note the regional variations) for two nuclear explosions, MAST and GNOME. In all cases, the fit to a straight line in a log (amplitude)-linear frequency plot is quite good. Spectral ratios fluctuate quite a bit, and the figures showing actual spectral ratios serve only as representative illustrations of the fact that indications of a strong frequency dependence of Q have been found to be absent in practically all work on Q in the short-period band. Drastic effects such as those shown in Figure 26 would not have gone unnoticed. It appears that any variation of t* with frequency in the short-period band must be gradual, since rapid change is contradicted by the data. The

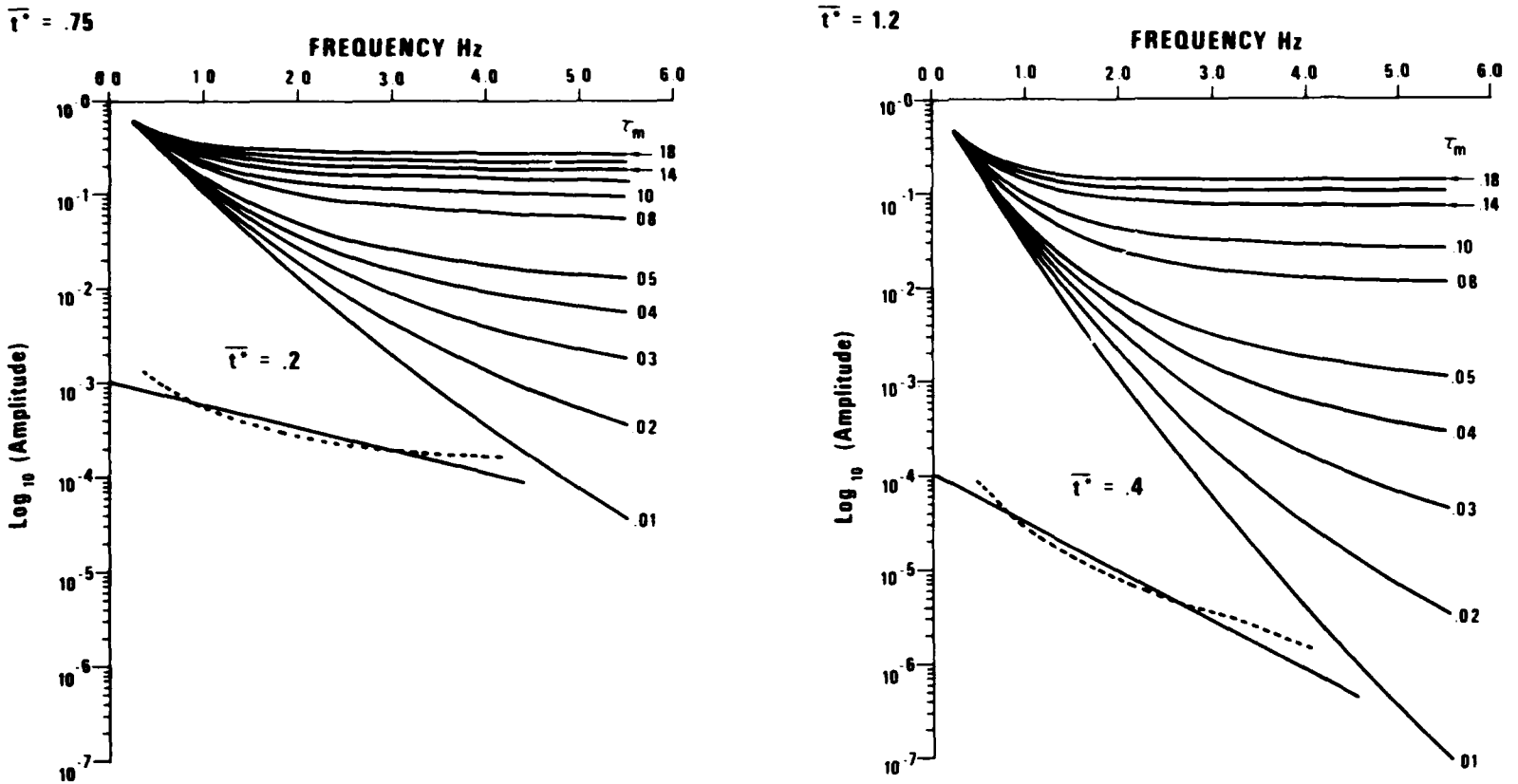

Figure 26. Forms of spectral ratios resulting from an absorption band model of Q according to Minster (1978a,b) assuming various long-period starting values for t_0^* and a variety of τ_m (τ_M of 1000 was assumed). The observed spectral ratio slopes of 0.2 and 0.4 are also shown with the shapes resulting from our preferred frequency dependent Q model superposed for comparison.

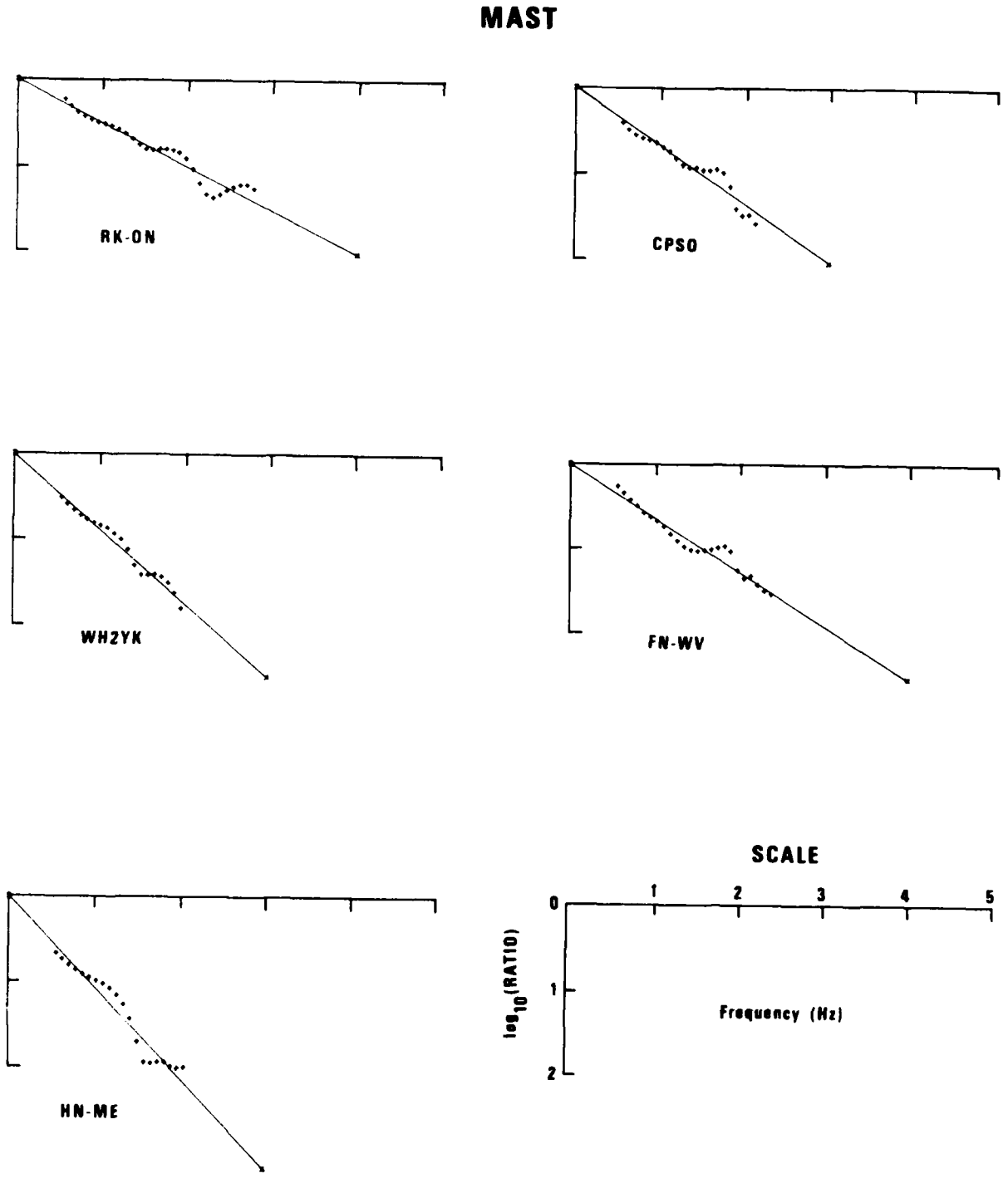

Figure 27a. Observed to source spectral ratios for MAST.

GNOME

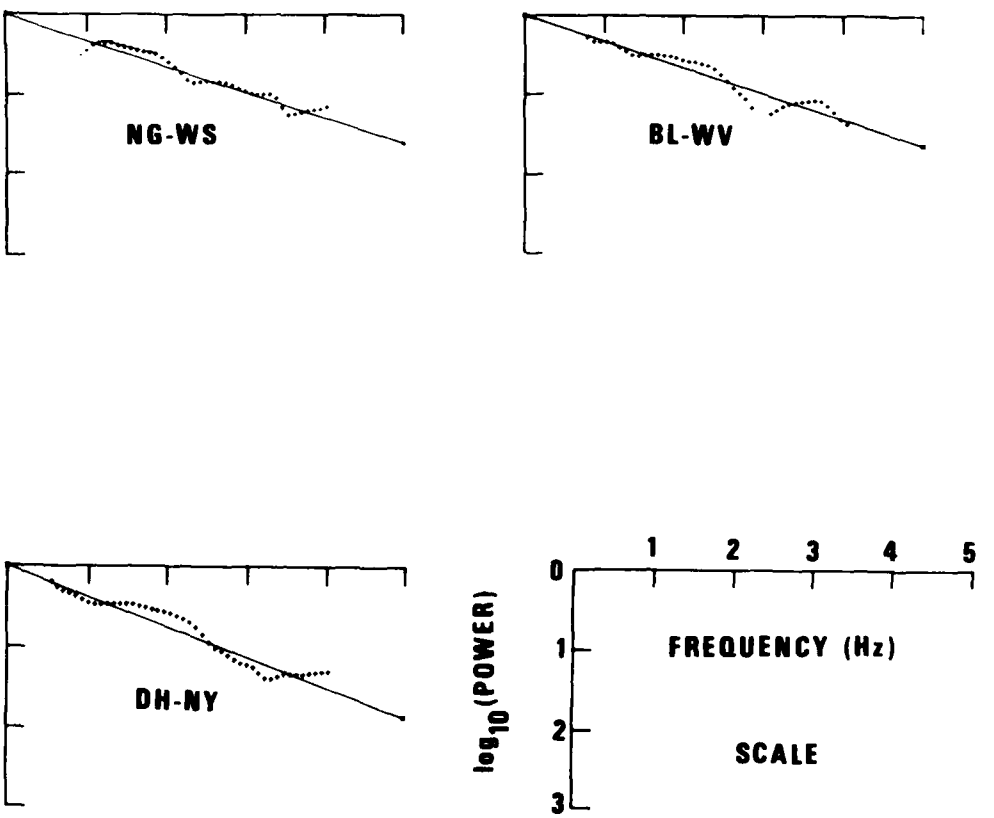

Figure 27b. Observed to source spectral ratios for GNOME.

extremely high t* estimates of 1.3 by Helmberger and Hadley (1981) would require an unacceptably rapid change of t^*_p with frequency to satisfy the spectral constraints. These can thus be ruled out by such arguments alone.

Frequency Dependence of Q for Shields

Strictly speaking, frequency dependence of Q can be established only if attenuation is measured in a wide frequency band using short- and long-period instruments over the same paths. Assumption of frequency dependence introduces a large number of additional parameters into studies of attenuation. It is possible that the form of frequency dependence changes from region to region, and the depth distribution of Q may be different at various frequencies (Solomon, 1972; Lundquist and Cormier, 1980). These uncertainties can be resolved only by further detailed studies.

The field of low-frequency Q studies in the earth is currently undergoing a change, and the trend is toward higher Q values than previously assumed. Recent studies (Sleep et al., 1981; Okal, 1980) indicate that Q estimates may be too low for some of the free oscillation studies. The spectral stacking technique used to enhance the data appears to introduce a negative bias in the Q estimates in a laterally inhomogeneous Earth.

Studies that would give incontrovertible indications of frequency dependence across the United States from a single data set do not exist. An example is the multiple ScS studies of Sipkin and Jordan (1979) in other regions. It must be noted, however, that core reflections traverse a region near the core-mantle boundary that, according to some studies, may have Q values much lower than the rest of the lower mantle. Therefore such measurements may yield lower Q than is appropriate for teleseismic raypaths that do not go that deeply into the lower mantle.

The results summarized in this paper put several restrictions on any model describing the frequency dependence of t* along shield type paths and shield-to-tectonic paths. These are as follows:

1) The apparent t_p^* must be in the range of 0.1-0.2 for shield paths in the 0.5-4.0 H_z band.

2) The absolute t_p^* changes slowly with frequency in the same band.

3) The apparent t_s^* must be less than 1.6 between 0.3-2 Hz, twice the value derived from deep earthquakes, for shield-to-shield paths.

4) The absolute t_s^* cannot change faster than the frequency.

5) The apparent t_p^* differential between shield-to-shield and shield-to-tectonic paths must be of the order of 0.2 sec in the 0.5-4 Hz range.

6) The apparent t_β^* differential between the two types of paths changes slowly with frequency.

7) The absolute t_p^* differential near 1 Hz must produce the observed magnitude and amplitude diferentials (0.26 magnitude units or a factor of approximately two in amplitude variation).

8) $t_s^* = 4t_p^*$ for both paths.

9) The difference in apparent t_β^* between the two types of paths must be 0.5 sec in the long-period band.

10) The absolute t_β^* in the long-period band should be considerably less than 1 sec, the worldwide average, for shield-to-shield type paths.

Figure 28 shows two regional t* versus frequency relationships that satisfy these constraints. These curves were drawn conservatively to set upper bounds on t_p^*. We made the shield-to-shield type t_p^* curve approach the value of 0.75 sec at the long-period end, corresponding to ray tracing results from the models of Lee and Solomon (1975, 1979) and exceeding those implied by the work of Nakanishi (1979). The curves are drawn with a rapid decrease beyond 1 H_z to keep them as high as possible, while still satisfying the constraints imposed by the apparent t* from the data in the 0.5-4.0 Hz band and also keeping the curvature in the spectral ratios reasonably low. The shield-to-shield curve can be fitted with an absorption band model described by Minster (1978) with the parameter τ_m of 0.08. This curve gives a $\overline{t_s^*}$ of about 1.6 in the 0.3-1.0 Hz range, which is twice the value of the $\overline{t_s^*}$ derived from deep earthquake data in Figure 19. Since the actual $\overline{t_s^*}$ must be less than twice the value derived from deep earthquakes, the curve for shield-to-shield paths must certainly be an upper bound. The t_p^* differential between the shield-to-shield and

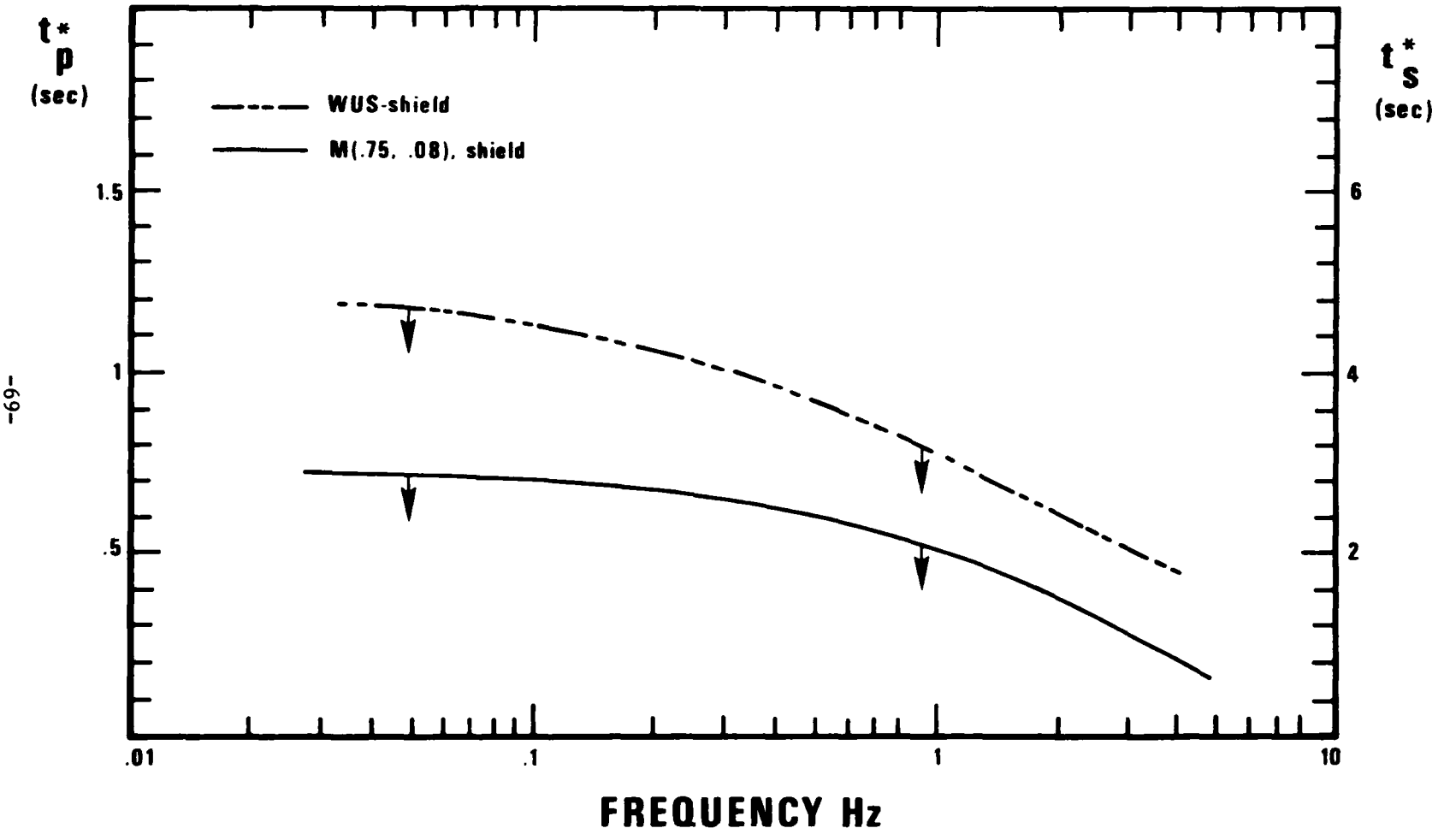

Figure 28. Upper limits of t_p^* and t_s^* for shield and shield-WUS type paths.

shield-tectonic curves at 1 Hz is dictated by regional EUS-WUS magnitude anomalies of the order of 0.26-0.33 magnitude units (Booth et al., 1974; Der et al., 1979). The shield-tectonic curve cannot be fitted with an absorption band model of the Minster type. A simple absorption band model starting out with high values at the long-period end would fall off too rapidly to be compatible with both the apparent constancy of Q in the short-period band and the t* differential compatible with the m_b variations across the United States.

In comparison with these curves, the t^*_p versus frequency relationships of Lundquist and Cormier (1980) were made to converge to 1 sec at the long-period end. The models of Lay and Helmberger (1980) converge to 0.8 at the long-period end. On the other hand, our models diverge toward the lower frequencies, and in this they are in better agreement with available evidence that both the absolute values and the regional differentials of t^*_p become larger in the long-period band. The majority of the constraints in the long-period band can be satisfied by almost any pair of smooth curves that retain the relative vertical spacing of our proposed limiting curves while remaining below them.

In spite of the fact that our upper bounds on absolute t* as functions of frequency provide a marginal fit to the constraints listed above, the quality of fits to the conditions imposed by the SH wave data from deep earthquakes and the near constancy of apparent t* can be markedly improved by lowering the low frequency limits by about 0.2 sec and putting more of the change in t* into the 0.1-1.0 Hz band, allowing the curves to level off above 1 Hz. This is allowed by some of the available new evidence in the long-period band (Kovach and Anderson, 1964; Sate and Espinosa, 1967; Geller et al., 1981).

Such t* versus frequency relationships would also have more variation at lower frequencies in accordance with some indications of frequency dependence there (Brune, 1977; Sato and Espinosa, 1967; Yoshida and Tsujiura, 1975). Such curves are shown in Figure 29, fitted to somewhat lower t* values at the low-frequency end. In contrast to those describing the upper limits of t* in Figure 29, the curvatures of spectral ratios associated with these curves are quite small (Figure 30) and agree better

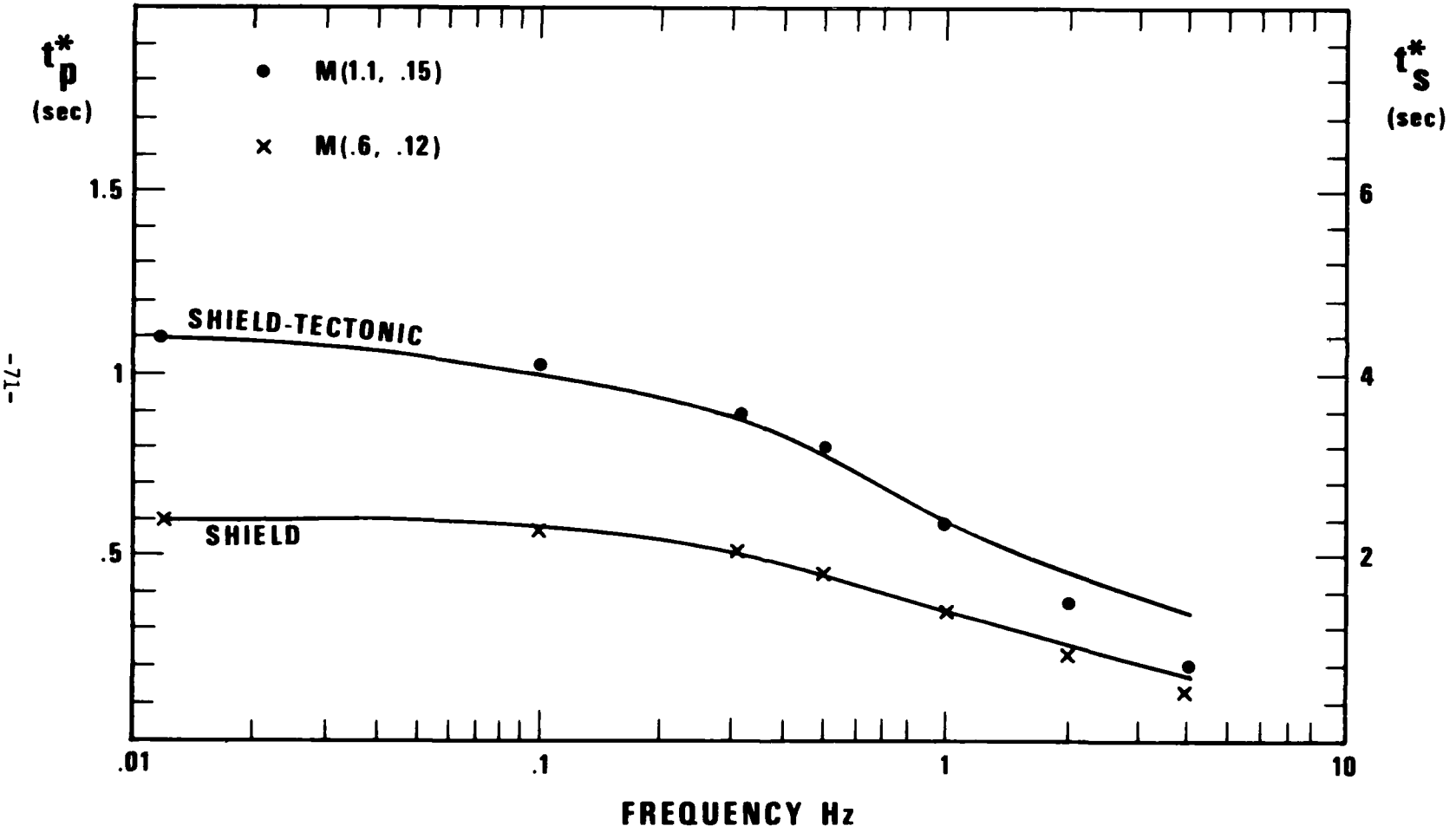

Figure 29. Alternate t* versus frequency models having less variation on the short-period band.

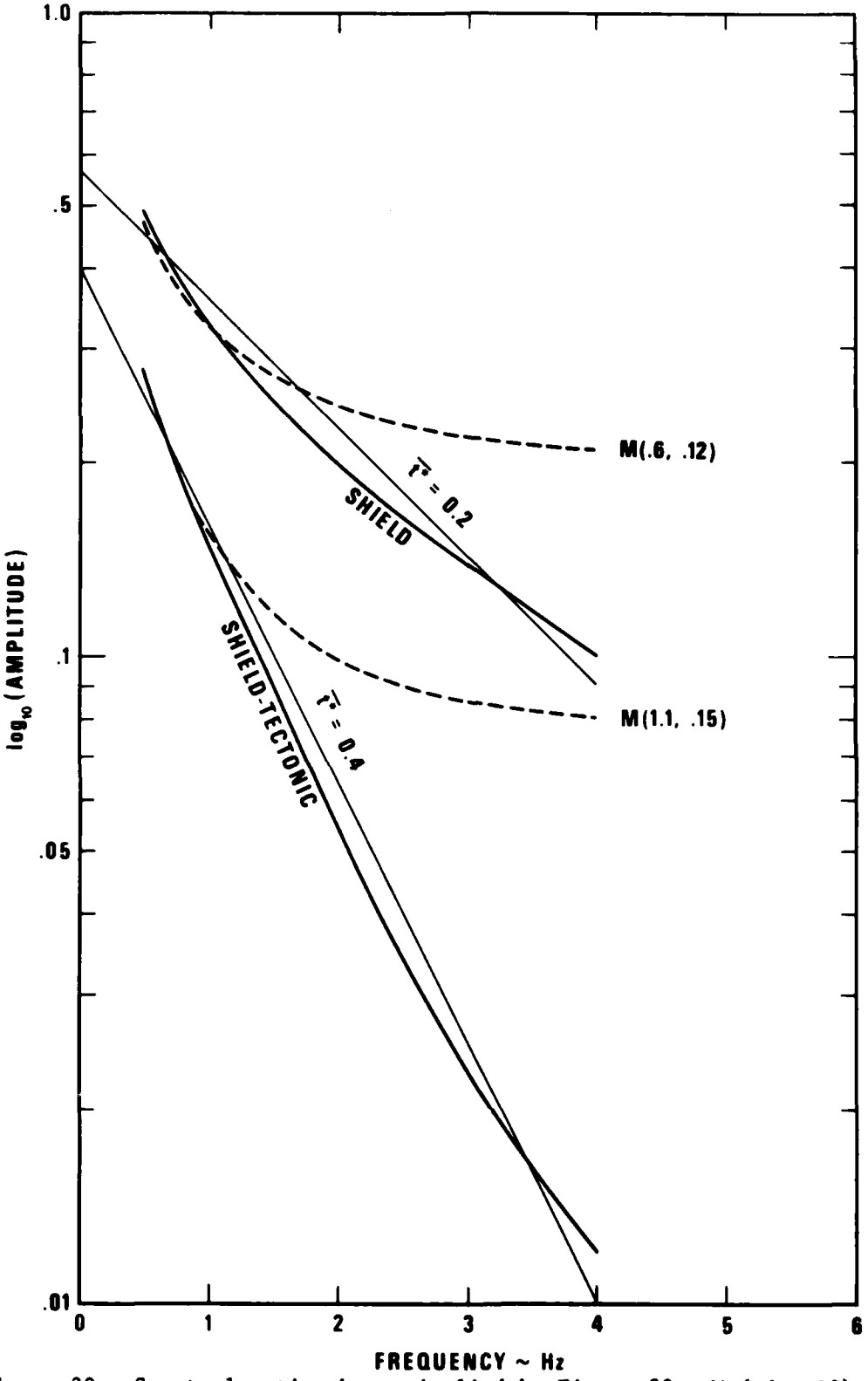

Figure 30. Spectral ratio shapes implied by Figure 29. M (.6, .12) refers to a single absorption band model with a long-period value of t* of .6 and a τ_m of .12. Heavy solid curves correspond to the t* versus frequency curves proposed by us and shown in Figure 29. Slopes corresponding to the t^*_p values of .2 and .4 are also indicated.

with the near constancy of apparent t* implied by spectral ratios such as those shown in Figure 27. As we did before, we also show some curves for a Minster type model fitted to the same low frequency limits (dashed lines in Figure 30). In general, moderate values of the parameter τ_m are needed to obtain the type of curves required; we used 0.15 and 0.12. For the types of paths investigated here, 0.5 would be too high. Although the Minster models fit the general trend of our curves, the spectral ratio curves in Figure 30 would not satisfy the near constancy of the apparent t* as shown in Figure 27. It appears therefore that any parameterization of the t* versus frequency relationships in the real Earth, in terms of a simple absorption band model with two parameters, is unsatisfactory in the short-period band, and more complex models are necessary.

The types of frequency dependences we have derived for the United States are likely to be applicable to other areas of the world as well. These vary smoothly with frequency and have differences in a similar sense over wide frequency bands. Since lateral variations of Q in the mantle are almost certainly related to temperature (Minster, 1980; Minster and Anderson, 1981; Lundquist and Cormier, 1980), it is likely that an increase of temperature will increase attenuation in a wide frequency band for waves passing through the upper mantle, although the maximum frequencies of attenuation may change with depth. This is also corroborated by most of the literature on seismic attenuation that shows that high attenuation in the short-period band in the mantle is usually accompanied by high attenuation of long-period surface waves in the same regions. Tibet and back-arc basins are typical examples. Therefore, models that involve peculiar, sharp variations of t* with frequency and that may bias t_p^* in a variety of ways relative to t_p^* in various regions, such as those discussed by Lundquist (1981), are not very likely in most areas of the world. The most notable exceptions may occur in subduction zones where severe mixing of mantle materials takes place. Models of the so called "absorption band shift" are also in conflict with the existing studies discussed above.

CONCLUSIONS

The regional variations of $\overline{t_p^*}$ correlate well with the lateral variations of the upper mantle low-velocity low-Q layer, as derived from studies of surface waves, travel times of body waves at regional and teleseismic distances, and the previous studies of attenuation.

The $\overline{t_p^*}$ data presented indicate low attenuation under shields and old oceans and higher attenuation under tectonic areas and new oceans. Deep earthquakes appear to have $\overline{t_p^*}$ of the same order as shallow earthquakes on shields, when both kinds of events are observed on a shield. This indicates that Q is higher under shields throughout most of the upper mantle. These findings are in harmony with the theory of plate tectonics and the presently prevailing view that mid-ocean ridges are underlain by partially molten material.

To reconcile short- and long-period estimates of mantle attenuation t_p^* must decrease with increasing frequency. This decrease must be gradual and may be considerably less than previously proposed since the values of t_p^* in the long period band may have been seriously overestimated.

The lack of a low Q layer under shields is also indicated by the observability at high frequencies of the prograde portions of the travel time triplication due to a velocity discontinuity or sharp gradients at 400 km depth. This part of the triplication would not be visible in the presence of a low Q layer in the mantle.

ACKNOWLEDGEMENTS

Phyllis Sobel and David von Seggern computed many of the t_p^* estimates used for the worldwide data set. Charmaine Mrazek, Michelle Silk, and Dave Racine assembled the record sections for the Russian Shield. Discussions with Robert Blandford and Shelton Alexander contributed greatly to this report. This research was supported by the Defense Advanced Research Projects Agency and is monitored by the VELA Seismological Center under contract F08606-79-C-0007.

REFERENCES

Aki, K. (1967). Scaling law of the seismic spectrum, J. Geophys. Res., 72, 1212-1231.

Anderson, D. L., A. Ben-Menahem, and C. B. Archambeau (1965). Attenuation of seismic energy in the upper mantle, J. Geophys. Res., 70, 1441-1448.

Anderson, D. L., and R. S. Hart (1978). The Q of the Earth, J. Geophys. Res., 83, 5869-5882.

Archambeau, C. B., E. A. Flinn and D. G. Lambert (1969). Fine structure of the upper mantle, J. Geophys. Res., 74, 5825-5865.

Asada, T. and K. Takano (1964). VESIAC report on Proceedings of the Lakewood Conference on High Frequency Seismic Energy, U. of Michigan, 4410-52-X.

Asada, T. and K. Takano (1963). Attenuation of short-period P waves in the mantle, J. Geophys. Earth, 11, 25-34.

Balakina, L. M. and N. V. Golubyeva (1979). Characterisitcs of focal mechanisms of deep earthquakes of Japan and Okhotsk seas, Izvestiya Acad. Sci. USSR, 15, 607-618 (English translation).

Barazangi, M. B. Isacks (1971). Lateral variations of seismic-wave attenuation in upper mantle above the in the inclined earthquake zone of the Tonga Island arc; Deep anomaly in the upper mantle, J. Geophys. Res., 76, 8493.

Barazangi, M., B. Isacks, and J. Oliver (1972). Propagation of seismic waves through and beneath the lithosphere that descends under the Tonga Island arc, J. Geophys. Res., 77, 952.

Barazangi, M., B. Isacks, J. Dubois and G. Pascal (1974). Seismic wave attenuation in the upper mantle beneath the southwest Pacific, Tectonophysics, 24, 1.

Barazangi, M., J. Oliver, and B. Isacks (1978). Relative excitation of the seismic shear waves S_n and L_g as a function of source depth and their propagation from Melanesia and Banda arcs to Australia, Annuli di Geofisica,

Barazangi, M., W. Pennington, and B. Isacks (1975). Global study of seismic wave attenuation in the upper mantle behind island arcs using pP waves, J. Geophys. Res., 80, 1075.

Billington, S., B. L. Isacks and M. Barazangi (1977). Spatial distribution and focal mechanisms of mantle earthquakes in the Hindu-Kush-Pamir region; A contorted Benioff zone, Geology, 5, 699-704.

Booth, D. C., P. D. Marshall and J. B. Young (1974). Long- and short-period amplitudes from earthquakes in the range 0° - 114°; Geophys. J. R. Astr. Soc., 39, 528-538.

Brune, J. N. (1970). Tectonic stress and the spectra of seismic shear waves, J. Geophys. Res., 75, 4997-5009.

Brune, J. N. (1977). Q of shear waves estimated from S-SS spectral ratios; Geophys. Res. Lett., 4, 179-181.

Burdick, L. J. (1980). Relative attenuation of P and S waves and the frequency dependence of Q, Annual Technical Report for the AFOSR, Columbia University, Lamont-Doherty Geological Observatory.

Burdick, L. J. and K. Kaufman (1980). The reproducing earthquakes of the Galapagos Islands, Bull. Seism. Soc. Am., 70, 1737.

Burdick, L. J. (1978). t* for S waves with a continental ray path; Bull. Seism. Soc. Am., 68, 1013-1030.

Burdick, L. J. and D. V. Helmberger (1979). Time functions appropriate for nuclear explosions, Bull. Seism. Soc. Am., 69, 951.

Burdick, L. J. and D. V. Helmberger (1978). The upper mantle P-velocity structure of the western United States, J. Geophys. Res., 83, 1699-1712.

Dahlen, F. A. (1980). The effect of laterally heterogeneous attenuation on the free oscillations of the Earth, Trans. Am. Geophys. Union EOS, 61, 303.

Der, Z. A., R. P. Masse, and J. P. Gurski (1975). Regional attenuation of short-period P and S waves in the United States, Geophys. J. R. Astr. Soc., 40, 85-106.

Der, Z. A. and T. W. McElfresh (1976a). Short-period P wave attenuation along various paths in North America as determined from P wave spectra of the SALMON nuclear explosion, Bull. Seism. Soc. Am., 66, 1609-1622.

Der, Z. A. and T. W. McElfresh (1976b). The effect of attenuation on the spectra of P waves from nuclear explosions in North America, SDAC-TR-76-7, Teledyne Geotech, Alexandria, Virginia.

Der, Z. A. and T. W. McElfresh (1977). The relationship between anelastic attenuation and regional amplitude anomalies of short-period P waves in North America, Bull. Seism. Soc. Am., 67, 1303-1317.

Der, Z. A., T. W. McElfresh, and C. P. Mrazek (1979). Interpretation of short-period P-wave magnitude anomalies at selected LRSM stations, Bull. Seism. Soc. Am., 69(4), 1149-1160.

Der, Z. A. and T. W. McElfresh (1980). Time domain methods, the values of t*p and t^*_s in the short-period band and regional variations of the same across the United States, Bull. Seism. Soc. Am., 70, 921-924.

Der, Z. A., T. W. McElfresh, and A. O'Donnell (1980a). Results of the SDAC experiment, SDAC-TR-80-4, Teledyne Geotech, Alexandria, Va.

Der, Z. A., E. Smart, and A. Chaplin (1980b). Short-period S wave attenuation in the United States, Bull. Seism. Soc. Am., 70, 101-126.

Fedotov, S. A. and O. V. Potapova (1974). Preliminary map of bodies at depths of 30-100 km in the upper mantle beneath Kamchatka, which screen P and S waves. In "Seismicity and Earthquake Prediction, the Properties of the Upper Mantle and their Relationship to Volcanism in Kamchatka." (S. A. Fedotov, editor) Nauka, Moscow.

Filson, J., and C. W. Frasier (1972). Multisite estimation of explosive source parameters, J. Geophys. Res., 77, 2045-2061.

Frasier, C. W. and J. Filson (1972). A direct measurement of Earth's short-period attenuation along a teleseismic ray path, J. Geophys. Res., 77, 3782-3787.

Given, J. W. and D. V. Helmberger (1981). Upper mantle structure of northwestern Eurasia, J. Geophys. Res., 85, 7183-7194.

Green, R. W. E. and A. L. Hales (1968). The travel time of P-waves to 30° in the central United States and upper mantle structure, Bull. Seism. Soc. Am., 58, 267-289.

Hanks, T. C. (1981). The corner frequency shift, earthquake source models and Q, Bull. Seism. Soc. Am., 71, 597-612.

Hanks, T. C. (1979). b values and $\omega^{-\gamma}$ seismic source models; Implications for tectonic stress variations along active crustal fault zones and estimation of high-frequency strong ground motion, J. Geophys. Res., 84, 2235-2242.

Helmberger, D. V. and D. M. Hadley (1981). Seismic source functions amd attenuation from local and teleseismic observations of the NTS events JORUM AND HANDLEY, Bull. Seism. Soc. Am., 71, 127-142.

Jordan, T. H. (1981). Global tectonic regionalization for seismological data analysis, Bull. Seism. Soc. Am., 71, 1131-1141.

Kennett, B. L. N. (1975). The effect of attenuation on seismograms, Bull. Seism. Soc. Am., 65, 1643.

Khalturin, V. I., Rautian, T. G. and P. Molnar (1977). Spectral content of Pamir-Hindu Kush intermediate depth earthquakes: Evidence for a high Q zone in the upper mantle, J. Geophys. Res., 82, 2231-2969.

Kovach, R. L., and D. L. Anderson (1964). Attenuation of shear waves in the upper and lower mantle; Bull. Seism. Soc. Am., 54, 1855-1865.

Kurita, T. (1968). Attenuation of short-period P-waves and Q in the mantle, J. Phys. Earth, 16, 61-78.

Langston, C. A. (1976). A body wave inversion of the Koyna, India earthquake of December 10, 1967, and some implications for body wave focal mechanisms, J. Geophys. Res., 81, 2517-2529.

Langston, C. A. (1978). Moments, corner frequencies, and the free surface, J. Geophys. Res., 83, 3422-3426.

Lay, T. and D. V. Helmberger (1980). Body wave amplitude patterns and upper mantle attenuation variations across North America; Annual Report for the Air Force Office of Scientific Research, 1 October 1979 - 30 September 1980 California Institute of Technology, Pasadena, California.

Lee, W. B. and S. C. Solomon (1975). Inversion schemes for surface wave attenuation and Q in the crust and the mantle, Geophys. J. R. Astr. Soc., 43, 47-71.

Lee, W. B. and S. C. Solomon (1979). Simultaneous inversion of surface wave phase velocity and attenuation, Rayleigh and Love waves over continental and oceanic paths, Bull. Seism. Soc. Am., 69, 65-96.

Lundquist, G. M. and V. C. Cormier (1980). Constraints on the absorption model of Q, J. Geophys. Res., 85, 5244-5256.

Lundquist, G. M. (1981). Inversion for t*, presented at the Air Force Office of Scientific Research review meeting, Las Vegas, Nevada.

Liu, H. L. and H. Kanamori (1980). Determination of source parameters of mid-plate earthquakes from the waveforms of body waves, Bull. Seism. Soc. Am., 70, 1989-2004.

Mereu, R. F., D. W. Simpson, and D. W. King (1974). Q and its effect on the observation of upper mantle travel-time branches, Earth and Planet. Sci. Letters, 21, 439-447.

Masse, R. P. and S. S. Alexander (1974). Compressional velocity distribution beneath Scandinavia and western Russia, Geophys. J. R. Astr. Soc., 39, 587.

Marshall, P. D., D. L. Springer and H. C. Rodean (1979). Magnitude corrections for attenuation in the upper mantle, Geophys. J. R. Astr. Soc., 57, 609-638.

Marshall, P. D., Douglas, A., Barley, B. J. and J. A. Hudson (1975). Short-period teleseismic S waves, Nature, 253, 181-182.

Marshall, P. D. and P. W. Basham (1972). Discrimination between earthquakes and underground explosions employing an improved M_s scale, Geophys. J. R. Astr. Soc., 28, 431-458.

Matumoto, T. (1971). Seismic body waves observed in the vicinity of Mount Katmai, Alaska, and evidence for the existence of molten chambers, Bull. Geol. Soc. Am., 82, 2905-2920.

McGarr, A. (1977). Seismic moments of earthquakes beneath island arcs, phase changes, and subduction velocities, J. Geophys. Res., 82, 256-264.

Mills, J. M. (1978). Great circle Rayleigh wave attenuation and group velocity, Part IV, Regionalization and pure-path models for shear velocity and attenuation, Phys. Earth Planet. Int., 17, 323-352.

Minster, J. B. (1978a). Transient and impulse responses of a one-dimensional linearly attenuating medium, - I. Analytical results, Geophys. J. R. Astr. Soc., 52, 479-501.

Minster, J. B. (1978b). Transient and impulse responses of a one-dimensional attenuating medium, II. A parametric study, Geophys. J. R. Astr. Soc., 52, 503-524.

Minster, J. B. (1980). Anelasticity and attenuation in "Physics of the Earth's Interior", Soc. Italiana di Fisica, Bologna, Italy.

Minster, J. B. and D. L. Anderson (1981). A model of dislocation-controlled rheology for the mantle, Phil. Trans. Roy. Soc. London, 299, 319-356.

Molnar, P., B. E. Tucker and J. N. Brune (1973). Corner frequencies of P and S waves and models of earthquake sources, Bull. Seism. Soc. Am., 63, 2091-2104.

Mitronovas, W., B. Isacks and L. Seeber (1969). Earthquake locations and seismic wave propagation in the upper 250 km of the Tonga Island arc, Bull. Seism. Soc. Am., 52, 1115.

Mitronovas, M. and B. Isacks (1971). Seismic velocity anomalies in the upper mantle beneath the Tonga-Kermadec Island arc, J. Geophys. Res., 76, 7154.

Molnar, P. and J. Oliver (1969). Lateral variations of attenuation in the upper mantle and discontinuities in the lithosphere, J. Geophys. Res., 74, 2648.

Mooney, H. M. (1970). Upper mantle inhomogeneity beneath New Zealand: Seismic evidence, J. Geophys. Res., 75, 285.

Nakanishi, I. (1979). Phase velocity of Q of mantle Rayleigh waves, J. Geophys. Res., 58, 35-59.

Nedgard, I. (1978). Seismological recordings of nuclear explosions in 1976 obtained at the Hagfors Observatory in Sweden, Forsvarets Forskningsanstalt, Stockholm, FOA Report C 2075-T1.

Noponen, I. (1975). Compressional wave-power spectrum from seismic sources, Institute of Seismology, University of Helsinki, ISNB-45-0538-7, Contract AFOSR-72-2377 (Final Report).

Pitt, A. M. (1974). Evidence from local earthquakes for the existence of a region of seismic body wave attenuation in the upper mantle crust under Yellowstone Caldera, EOS, Trans. Am. Geophys. Uni., 55, 1190.

Randall, M. J. (1964). Seismic energy generated by a sudden volume change, Bull. Seism. Soc. Am., 54, 1291-1298.

Rial, J. (1976). Seismic wave transmission across the Caribbean plate: high attenuation on concave side of Lesser Antilles arc, Bull. Seism. Soc. Am., 66, 1905.

Ryall, F. and A. Ryall (1981). Attenuation of P and S waves in a magma chamber in Long Valley Caldera, California, Geophys. J. R. Astr. Soc., 53, 559-581.

Sato, R. and A. F. Espinosa (1967). Dissipation in the earth's mantle and rigidity and viscosity in the earth's core determined from waves multiply reflected from the mantle-core boundary, Bull. Seism. Soc. Am., 57, 829-856.

Sengupta, M. K. and B. R. Julian (1976). P-wave travel times from deep earthquakes, Bull. Seism. Soc. Am., 66, 1555-1579.

Silver, P. G. and T. H. Jordan (1981). Fundamental spheroidal mode observations of aspherical heterogeneity, Geophys. J. R. Astr. Soc., 64, 605-634.

Sipkin, S. A. and T. H. Jordan (1980). Regional variations Q_{Scs}, Bull. Seism. Soc. Am., 70, 1071-1102.

Sipkin, S. A. and T. H. Jordan (1979). Frequency dependence of Q_{Scs}, Bull. Seism. Soc. Am., 69, 1055-1079

Sleep, N. H., R. J. Geller and S. Stein (1981). A constraint on the Earth's lateral heterogeneity from the scattering of spheroidal mode Q^{-1} measurements, Bull. Seism. Soc. Am., 71, 183-198.

Solomon, S. C. (1972). Seismic-wave attenuation and partial melting in the upper mantle of north America, J. Geophys. Res., 77, 1483-1502.

Solomon, S. C. and M. N. Toksoz (1970). Lateral variation of attenuation of P and S waves beneath the United States, Bull. Seism. Soc. Am., 60, 819-838.

Solomon, S. C. (1973). Shear wave attenuation and melting beneath the mid-Atlantic ridge, J. Geophys. Res., 78, 6044-6059.

Takano, K. (1971). A note on the attenuation short-period P and S waves in the mantle, J. Phys. Earth, 19, 155-163.

Trulio, J. G. (1978). Simple scaling and nuclear monitoring, Applied Science Inc., ATR-77-45-2, Los Angeles, California.

Toksoz, M. N. and P. Bird (1977). Formation and evolution of marginal basins and continental plateaus. In "Island Arcs, Deep Sea Trenches and Back-Arc Basins," Maurice Ewing Series #1, Manik Talwani and Walter C. Pitman, editors, American Geophysical Union, Washington, D.C.

Trehu, A. M., Nabelek, J. L. and S. C. Solomon (1981). Source characterization of two Revkianes Ridge earthquakes: Surface waves and moment tensors; P waveforms and nonorthogonal nodal planes, J. Geophys. Res, 86, 1701-1724.

von Seggern, D. H. and R. R. Blandford (1972). Source time functions and spectra from underground nuclear explosions, Geophys. J. R. Astr. Soc., 31, 83-97.

von Seggern, D. H. and D. W. Rivers (1979). Seismic discrimination of earthquakes and explosions with applications to the southwestern United States, SDAC-TR-77-10, Teledyne Geotech, Alexandria, Virginia.

Woodhouse, J. H. (1980). Time domain calculations of modal envelopes for slightly aspherical earth models, Trans. Am. Geophys. Union EOS, 61, 303.

Yoshida, M., and M. Tsujiura (1975). Spectrum and attenuation of multiply reflected core phases, J. Phys. Earth, 23, 31-42.

APPENDIX A

Event Data Set

(* denotes explosions)

	NO	DATE	ORIGIN	LAT	LONG	DEP	R	LOCATION
	1	5APR77	7 39 49.5	54.3N	161.5E	53	I	KAMCHATKA
	2	13APR77	18 20 38.3	51.5N	179.6W	46	I	RAT IS.
	3	15APR77	23 35 38.9	22.9S	68.8W	99	T	N. CHILE
	4	20APR77	20 4 29.7	30.7N	137.5E	493	N	JAPAN
	5	22APR77	0 52 5.2	52.5N	153.8E	390	T	KAMCHATKA
	6	23APR77	14 49 5.7	75.0N	134.9E	37	S	NEW SIBERIAN IS.
*	7	25APR77	4 6 59.9	49.8N	78.3E	0	S	E. KAZAKH
	8	14MAY77	6 4 45.9	1.6N	85.1W	33	N	ECUADOR COAST
*	9	29MAY77	2 57 0.4	49.9N	78.9E	0	S	E. KAZAKH
	10	2JUN77	16 50 36.1	20.9S	68.6W	107	T	CHILE-BOLIVIA BORDER
	11	5JUN77	2 46 6.8	24.0S	70.5W	32	T	NEAR COAST N. CHILE
	12	5JUN77	6 41 17.9	42.4N	142.8E	66	I	HOKKAIDO, JAPAN
	13	24JUL77	19 55 38.9	19.4N	144.9E	409	I	MARIANA ISLANDS
	14	25JUL77	4 51 37.7	17.8N	81.6W	33	I	CARIBBEAN SEA
	15	30MAY77	15 16 5.1	52.3N	169.7W	33	I	FOX IS. ALEUTIANS
	16	12JUN77	8 48 5.1	43.0N	142.3E	108	I	JAPAN
	17	13JUN77	5 28 32.2	12.7N	90.5W	111	T	CENT. AMER. CST.
	18	13JUN77	8 2 13.4	22.2S	70.0W	149	T	N. CHILE CST.
	19	15MAY77	0 21 4.1	49.9N	152.8E	221	I	KURILES
	20	15MAY77	15 50 44.1	52.5N	168.2W	33	I	FOX IS.
	21	22JUN77	7 11 30.2	35.4N	140.4E	35	I	JAPAN
	22	22JUN77	8 50 31.2	53.7N	160.7E	33	I	KAMCHATKA
	23	19JUL77	6 35 35.7	29.1S	69.7W	111	T	CHILE-ARGENTINA BDR
	24	20JUL77	13 24 21.1	50.6N	161.9W	53	N	ALASKA PEN.
	25	7AUG77	23 26 55.0	52.2N	176.2W	125	I	ANDREANOF IS.
	26	8AUG77	7 0 6.3	6.9N	77.8W	33	T	CST OF COLUMBIA
	27	13AUG77	3 13 35.1	44.3N	147.9E	67	I	KURILES
	28	13AUG77	19 33 11.7	43.2N	145.4E	62	I	JAPAN
	29	14AUG77	10 58 9.5	19.8S	73.6W	33	T	N. CHILE CST
	30	14AUG77	23 49 15.7	41.8N	138.6E	33	N	SEA OF JAPAN
*	31	20AUG77	22 0 0.6	64.1N	99.8E	0	S	CENT. SIBERIA
	32	21AUG77	5 19 39.2	35.1N	141.1E	42	I	HONSHU CST
	33	21AUG77	11 33 41.7	13.6N	90.1W	84	T	GUATEMALA CST
	34	23AUG77	3 12 55.6	21.5S	68.3W	99	T	CHILE BOLIVIA BDR
	35	26AUG77	7 16 0.8	51.0N	176.1E	34	I	RAT IS
	36	28AUG77	15 40 56.7	5.1N	81.4W	20	N	S. PANAMA
	37	30AUG77	6 50 41.7	63.2N	151.2W	130	T	CENT. ALASKA
*	38	1SEP77	3 0 0.0	73.3N	54.3E	0	S	NOVAYA ZEMLYA
	39	1SEP77	17 37 0.9	6.9N	76.1W	28	T	N. COLUMBIA
	40	2SEP77	7 9 53.8	0.7N	91.1W	33	N	GALAPAGOS IS
	41	4SEP77	15 40 59.7	51.0N	178.4E	34	I	RAT IS
	42	4SEP77	16 39 47.5	33.2N	140.6E	17	I	S. HONSHU
	43	4SEP77	17 10 37.0	50.9N	178.3E	31	I	RAT IS.
	44	4SEP77	17 24 50.5	50.9N	178.1E	8	I	RAT IS
	45	4SEP77	18 0 11.2	51.0N	178.3E	50	I	RAT IS
	46	4SEP77	18 25 55.1	51.1N	177.9E	41	I	RAT IS
	47	4SEP77	19 23 1.1	51.0N	177.7E	35	I	RAT IS
	48	4SEP77	23 20 48.0	51.0N	178.5E	41	I	RAT IS
	49	5SEP77	12 52 14.9	51.0N	177.8E	33	I	RAT IS
	50	9SEP77	2 35 6.2	43.0N	131.3E	499	T	RUSSIA-CHINA BDR
	51	10SEP77	4 39 5.6	14.3S	76.1W	58	T	PERU CST.
	52	10SEP77	10 21 9.1	14.1N	91.5W	78	T	GUATEMALA
	53	13SEP77	4 55 32.3	41.5N	142.3E	49	I	JAPAN
	54	17SEP77	16 28 48.4	50.0N	173.8W	33	I	ALEUTIANS
	55	20DEC77	8 50 40.6	48.5N	152.9E	140	I	KURILE IS.
	56	30DEC77	17 35 11.9	40.0N	15.5E	283	T	S. ITALY

	NO	DATE	ORIGIN	LAT	LONG	DEP	R	LOCATION
	57	31DEC77	7 53 21.8	14.7S	71.6W	158	T	PERU
	58	10JAN78	0 50 19.5	46.8N	152.3E	65	I	KURILE IS.
	59	13JAN78	20 3 5.0	44.6N	149.8E	50	I	KURILE IS.
	60	17JAN78	11 33 15.3	31.2S	67.8W	20	T	ARGENTINA
	61	2JAN78	20 57 35.1	51.1N	178.4W	52	I	ANDREANOF IS.
	62	16FEB78	3 47 33.1	5.5N	77.8W	16	T	W CST COLUMBIA
	63	22FEB78	6 7 37.1	14.4N	91.2W	68	T	GUATEMALA
	64	26FEB78	0 5 42.2	49.2N	155.5E	44	I	KURILE IS.
	65	26FEB78	9 16 52.6	26.5S	113.6W	33	N	EASTER IS. REG.
	66	22MAR78	0 50 34.9	43.8N	148.9E	60	I	KURILE IS.
	67	9MAY78	7 31 6.0	52.5N	158.1E	111	I	KAMCHATKA
	68	11MAY78	0 23 38.0	51.6N	176.0W	57	I	ANDREANOF IS
*	69	29SEP76	3 0 0.0	73.5N	53.7E	0	S	N.Z.
	70	30SEP76	8 4 10.9	24.2S	68.2W	131	T	CHILE-ARG. BORDER
	71	22SEP76	2 30 30.8	51.6N	175.9W	43	I	ALEUTIANS
	72	22SEP76	8 20 27.6	23.3N	142.1E	129	I	VOLCANO IS.
	73	4OCT76	23 36 6.0	0.2S	77.5W	55	T	ECUADOR
	74	8OCT76	14 38 27.9	49.8N	155.7E	69	I	KURILES
*	75	23NOV76	5 3 0.0	50.0N	79.0E	0	S	E.KAZ
	76	9OCT76	12 31 6.6	10.7N	85.8W	85	T	COSTA RICA
	77	9OCT76	2 52 24.3	45.1N	153.5E	34	I	KURILES
	78	9OCT76	16 2 26.9	9.4N	77.5W	33	T	N.COLUMBIA
	79	9OCT76	21 10 24.1	10.3S	79.5W	64	T	PERU COAST
	80	9OCT76	23 48 9.0	10.0N	91.0W	33	N	C. AMER. COAST
	81	10OCT76	2 58 56.6	45.4N	151.0E	38	I	KURILES
	82	10OCT76	14 32 4.9	43.2N	147.7E	21	I	KURILES
	83	12OCT76	4 24 52.1	31.2N	141.5E	29	I	S. HONSHU, JAPAN
	84	12OCT76	23 49 24.3	2.8N	77.5W	90	T	W CST COLUMBIA
	85	13OCT76	17 35 45.1	10.5N	62.2W	55	T	VENEZUELA
	86	22OCT76	4 4 22.6	12.1N	87.6W	59	T	CST OF NICARAGUA
	87	22OCT76	5 53 50.9	13.2N	88.2W	83	T	EL SALVADOR
	88	22OCT76	18 35 23.9	56.1N	153.3W	26	I	KODIAK REG
	89	24OCT76	17 19 55.5	63.0N	149.0W	75	T	CEN. ALASKA
	90	26OCT76	5 59 56.4	46.1N	150.8E	120	I	KURILE IS
	91	28OCT76	9 59 21.3	14.6S	73.7W	86	T	PERU
	92	2NOV76	19 23 2.7	47.0N	151.0E	33	I	KURILE IS
	93	15NOV76	14 14 26.6	45.0N	148.0E	147	I	KURILES
	94	22NOV76	20 9 2.7	7.0N	72.0W	33	T	VENEZUELA
	95	26NOV76	23 43 12.6	2.0S	77.0W	196	T	PERU-ECUADOR BDR
	96	1DEC76	14 15 33.2	10.0N	85.0W	58	T	COSTA RICA
	97	1DEC76	17 44 33.8	12.0N	90.0W	85	T	CST OF CENT. AMER.
	98	3DEC76	5 27 34.4	21.0S	69.0W	71	T	CHILE-BOLIVIA
	99	3DEC76	23 10 23.1	22.0S	69.0W	93	T	N. CHILE
	100	30NOV76	0 40 57.0	21.0S	69.0W	88	T	CHILE-BOLIVIA
	101	4DEC76	5 6 29.7	21.0S	69.0W	78	T	N. CHILE
	102	4DEC76	12 32 35.4	20.0S	69.0W	72	T	N. CHILE
	103	5DEC76	22 1 22.1	23.0N	140.0E	366	I	BONN IS.
	104	6DEC76	19 46 2.4	34.0S	112.0W	33	N	EASTER IS.
	105	7DEC76	9 36 41.4	34.0N	137.0E	342	I	S. HONSHU
	106	19DEC76	14 37 30.0	45.0N	154.0E	91	I	KURILES
	107	20DEC76	10 18 58.0	7.0N	75.0W	66	T	COLUMBIA
	108	15DEC76	12 26 4.0	30.0N	131.0E	3	I	JAPAN
	109	20DEC76	21 22 25.0	56.0N	124.0W	33	T	BR. COLUMBIA
	110	22DEC76	1 1 42.0	24.0N	142.0E	33	I	VOLCANO IS.
	111	13DEC76	23 1 28.0	32.0N	145.0E	33	O	N. PACIFIC
	112	14DEC76	16 6 56.0	31.0N	130.0E	60	I	JAPAN

NO	DATE	ORIGIN			LAT	LONG	DEP	R	LOCATION
113	27DEC76	18	8	8.0	42.0N	145.0E	60	I	JAPAN
114	31DEC76	9	16	37.0	40.0N	145.0E	107	I	JAPAN
115	1JAN77	11	33	42.4	30.6N	137.2E	476	N	JAPAN
116	5JAN77	10	37	33.6	25.7N	142.5E	21	I	VOLCANO IS.
117	5JAN77	22	44	57.0	23.3N	143.8E	33	I	VOLCANO IS.
118	6JAN77	7	55	55.5	49.3N	155.4E	33	I	KURILES
119	6JAN77	16	2	3.6	51.3N	175.4W	38	I	ANDREANOF IS.
120	22SEP76	0	16	9.3	44.8N	149.1E	64	I	KURILE IS.
121	17JAN77	6	23	42.6	26.7N	142.6E	33	I	BONIN IS.
122	17JAN77	9	42	22.5	53.6N	158.7W	22	N	S. OF ALASKA
123	24JAN77	6	11	30.0	45.5N	150.9E	33	I	KURILE IS
124	3FEB77	21	30	59.0	43.0N	130.0E	506	T	RUSSIA-CHINA BDR
125	6FEB77	0	31	29.0	24.0N	48.0W	33	N	N. ATLANTIC
126	13FEB77	5	51	11.0	52.0N	160.0E	167	I	KAMCHATKA
127	16FEB77	0	50	18.0	32.0N	25.0W	33	N	N ATLANTIC OCEAN
128	16FEB77	1	5	48.0	38.0N	150.0E	33	O	N PACIFIC OCEAN
129	17FEB77	13	32	7.0	56.0N	166.0E	33	I	KORANDORFSKI
130	18FEB77	20	51	26.0	34.0N	142.0E	42	I	JAPAN
131	19FEB77	5	51	1.0	51.0N	156.0E	23	I	KAMCHATKA
132	19FEB77	22	47	7.0	49.0N	175.0E	30	I	ALEUTIANS
133	20FEB77	7	2	0.0	56.0N	152.0W	51	I	KODIAK IS. REG.
134	20FEB77	8	0	36.0	51.0N	174.0E	42	I	ALEUTIANS
135	8MAR77	22	46	44.0	8.0S	63.0W	33	S	W. BRAZIL
136	12MAR77	2	58	55.0	32.0N	41.0W	33	N	N. ATLANTIC RIDGE
137	13MAR77	4	55	55.0	2.0S	58.0W	33	S	BRAZIL
138	15MAR77	21	28	9.0	9.0N	83.0W	95	T	COSTA RICA
139	19MAR77	10	56	6.0	43.0N	149.0E	70	I	KURILES
140	4MAR77	19	21	40.0	44.0N	26.0E	94	T	RUMANIA
141	7MAR77	0	29	11.0	43.0N	114.0E	33	T	N.E. CHINA
142	7MAR77	9	11	55.0	39.0N	149.0E	24	O	N. PACIFIC
143	21MAR77	4	36	38.0	23.0N	143.0E	56	I	VOLCANO IS.
144	23MAR77	2	11	25.0	11.0N	69.0W	164	T	CST. VENEZUELA
145	26MAR77	4	36	10.0	52.0N	168.0W	38	I	FOX IS.
*146	29MAR77	3	57	0.0	50.0N	78.0E	0	S	E. KAZAKH
147	20OCT77	8	18	7.0	56.4N	164.1E	40	I	KAMCHATKA
148	31OCT77	9	40	38.5	56.0N	162.8E	26	I	KAMCHATKA
149	2DEC77	12	57	10.7	52.9N	159.7E	15	I	KAMCHATKA
151	10DEC77	21	58	51.3	51.4N	156.6E	130	I	KAMCHATKA
152	16DEC77	9	8	59.7	51.6N	159.5E	33	I	KAMCHATKA
153	18DEC77	6	57	33.3	55.3N	160.6E	125	I	KAMCHATKA
154	18DEC77	19	9	15.7	51.0N	157.8E	65	I	KAMCHATKA
155	21DEC77	16	39	33.0	52.9N	159.8E	136	I	KAMCHATKA
156	22DEC77	14	5	45.1	53.0N	159.9E	33	I	KAMCHATKA
157	16OCT77	21	5	37.3	49.4N	155.4E	41	I	KURILES
158	19OCT77	21	20	41.6	49.3N	155.6E	52	I	KURILES
159	29OCT77	10	33	56.7	47.1N	153.2E	58	I	KURILES
160	2DEC77	16	15	44.9	44.6N	146.5E	163	I	KURILES
161	4DEC77	11	39	2.8	48.3N	146.6E	479	I	KURILES
162	8DEC77	13	57	4.4	50.4N	149.8E	502	T	KURILES
163	16DEC77	7	11	41.6	43.2N	146.8E	40	I	KURILES
164	1NOV77	3	54	26.0	55.4N	130.5E	33	T	SIBERIA
*165	20AUG77	21	59	58.7	64.2N	99.6E	0	S	SIBERIA
166	18NOV77	21	55	39.7	60.1N	143.4E	33	T	SIBERIA
167	30OCT77	21	38	38.5	45.5N	146.0E	165	I	KURILES
*168	10AUG77	21	59	58.7	50.9N	110.8E	2	T	LAKE BAIKAL
*169	10SEP77	16	0	3.3	57.3N	106.2E	33	S	LAKE BAIKAL

NO	DATE	ORIGIN	LAT	LONG	DEP	R	LOCATION
170	26NOV77	22 46 52.2	39.5N	117.9E	106	T	E. CHINA
171	3DEC77	17 6 21.9	41.9N	131.1E	540	T	E. CHINA
172	31DEC77	3 24 38.6	39.2N	91.1E	3	T	CENT. CHINA
173	4NOV77	23 54 44.7	30.7M	81.3E	15	T	TIBET
174	13NOV77	21 2 29.3	26.5N	93.1E	33	T	TIBET
175	18NOV77	5 20 11.3	32.7N	88.4E	33	T	TIBET
176	18NOV77	11 27 27.6	32.7N	88.5E	33	T	TIBET
177	18NOV77	15 10 41.8	32.7N	88.3E	33	T	TIBET
178	18NOV77	17 23 24.4	32.6N	88.3E	33	T	TIBET
179	18NOV77	23 12 49.5	32.7N	88.4E	33	T	TIBET
180	20NOV77	23 40 35.9	32.4N	87.8E	33	T	TIBET
181	7DEC77	16 19 33.9	35.7N	94.5E	33	T	TIBET
182	16DEC77	10 15 27.5	33.3N	97.6E	33	T	TIBET
183	26DEC77	5 15 21.3	39.9N	72.0E	38	T	TIBET
184	28OCT77	21 15 1.9	39.6N	73.4E	78	T	TIEN SHAN
185	6DEC77	10 52 53.5	41.4N	69.7E	33	T	TIEN SHAN
186	18DEC77	16 47 17.1	39.9N	77.3E	33	T	TIEN SHAN
187	18DEC77	20 43 5.9	39.7N	77.7E	33	T	TIEN SHAN
188	19DEC77	18 12 25.9	39.8N	77.7E	33	T	TIEN SHAN
189	20DEC77	7 27 38.9	39.8N	69.3E	20	T	TIEN SHAN
190	23DEC77	9 9 54.1	39.6N	77.4E	34	T	TIEN SHAN
*191	30JUL77	1 56 58.0	49.8N	78.2E	0	S	E. KAZAKH
*192	17AUG77	4 26 57.7	49.8N	78.2E	0	S	E. KAZAKH
*193	5SEP77	3 2 57.8	50.1N	79.0E	0	S	E. KAZAKH
*194	29OCT77	3 6 57.7	49.8N	78.2E	0	S	E. KAZAKH
*195	30NOV77	4 6 57.5	50.0N	78.9E	0	S	E. KAZAKH
*196	26DEC77	4 2 57.7	49.9N	78.1E	0	S	E. KAZAKH
197	20MAR76	4 3 39.3	50.1N	77.3E	0	S	E. KAZAKH
*198	29MAR77	3 56 57.7	49.8N	78.1E	0	S	E. KAZAKH
*199	13DEC75	4 56 57.3	49.8N	78.2E	0	S	E. KAZAKH
*200	19MAY76	2 56 57.9	49.9N	78.0E	0	S	E. KAZAKH
201	1NOV77	17 56 42.7	36.6N	68.7E	104	T	PAMIRS - HINDU KUSH
202	6NOV77	13 31 41.1	36.3N	71.1E	163	T	PAMIRS - HINDU KUSH
203	12NOV77	12 27 5.3	35.8N	71.3E	167	T	PAMIRS - HINDU KUSH
204	15NOV77	20 20 46.6	38.2N	74.2E	119	T	PAMIRS - HINDU KUSH
205	13OCT77	20 38 52.1	37.3N	78.1E	140	T	PAMIRS - HINDU KUSH
206	19NOV77	11 51 14.2	36.5N	71.3E	97	T	PAMIRS - HINDU KUSH
207	19OCT77	5 1 57.0	36.4N	71.3E	233	T	PAMIRS - HINDU KUSH
208	20NOV77	20 57 33.1	37.4N	71.8E	114	T	PAMIRS - HINDU KUSH
209	22NOV77	6 56 14.2	36.5N	71.2E	76	T	PAMIRS - HINDU KUSH
210	15DEC77	5 15 42.3	36.5N	71.2E	77	T	PAMIRS - HINDU KUSH
211	21DEC77	20 17 13.6	36.2N	68.7E	53	T	PAMIRS - HINDU KUSH
212	29OCT77	6 26 40.6	40.3N	63.5E	33	T	TURKMEN
213	16DEC77	17 55 14.2	36.9N	59.8E	9	T	TURKMEN
214	15DEC77	15 7 51.8	43.2N	45.2E	16	T	CAUCASUS
215	15DEC77	15 23 30.7	43.6N	45.4E	26	T	CAUCASUS
216	16DEC77	23 17 17.7	43.1N	47.1E	33	T	CAUCASUS
217	21DEC77	8 30 46.3	42.0N	47.9E	33	T	CAUCASUS
218	23DEC77	7 31 44.2	44.8N	32.8E	10	T	CAUCASUS
*219	26JUL77	16 59 57.6	69.5N	90.6E	0	S	N.W. RUSSIA
*220	1SEP77	2 59 57.5	73.4N	54.6E	0	S	N.W. RUSSIA
*221	9OCT77	11 0 0.3	73.6N	53.2E	0	S	N.W. RUSSIA
222	14JUN71	13 48 55.7	56.2N	123.6E	16	T	E. RUSSIA
223	15JAN72	18 7 57.8	57.4N	120.7E	16	T	E. RUSSIA
224	9AUG72	19 42 17.3	52.9N	107.5E	20	T	LAKE BAIKAL
225	25NOV72	13 42 34.4	56.3N	123.5E	23	T	E. RUSSIA

NO	DATE	ORIGIN	LAT	LONG	DEP	R	LOCATION
226	21JUN74	20 56 48.7	56.5N	117.3E	14	T	E. OF LAKE BAIKAL
227	5NOV76	4 0 3.4	61. N	113. E	0	S	S. SIBERIA
228	24NOV71	8 23 24.6	38.7N	73.4E	10	T	TADZHIK-SINKIANG BDR
229	12DEC71	22 27 41.1	39.5N	73.2E	17	T	TADZHIK-SINKIANG BDR
230	20FEB74	11 43 3.9	40.7N	73.2E	20	T	TADZHIK-SINKIANG BDR
231	11AUG74	8 2 54.0	39.3N	73.9E	14	T	TADZHIK-SINKIANG BDR
232	11AUG74	9 8 58.5	39.2N	73.8E	12	T	TADZHIK-SINKIANG BDR
233	11AUG74	23 18 58.3	39.5N	73.6E	15	T	TADZHIK-SINKIANG BDR
234	14AUG74	22 6 52.9	39.2N	73.9E	30	T	TADZHIK-SINKIANG BDR
235	21AUG74	18 8 29.0	39.3N	73.9E	7	T	TADZHIK-SINKIANG BDR
236	28JUN71	10 53 45.7	42.4N	43.3E	16	T	TURKEY-USSR BDR
237	3FEB72	2 29 21.9	40.7N	48.4E	23	T	E. CAUCASUS
238	14DEC73	9 11 46.3	41.9N	49.0E	75	T	CASPIAN SEA
239	9JAN75	23 9 46.6	42.9N	47.0E	30	T	E. CAUCASUS
*241	20CT69	22 6 0.0	51.4N	179.2W	0	I	ALUETIANS
243	26FEB74	6 23 45.3	53.3N	159.7E	53	I	E. CST. KAMCHATKA
244	2JAN72	10 27 34.9	41.8N	84.5E	11	T	S. SINKIANG PROV.
*245	15AUG73	1 59 57.8	42.7N	67.4E	0	T	CENT. KAZAKH
246	27DEC59	15 52 54.0	56. N	162.5E	33	I	E. CST. KAMCHATKA
247	5MAR60	13 49 18.0	1. N	129. E	33	I	HALMAHERA
248	15OCT59	6 15 34.0	0.5N	120.5E	33	I	N. CELEBES
249	2DEC59	9 34 16.0	1. S	123. E	33	I	CELEBES
250	9FEB60	23 55 49.0	4. S	128. E	33	I	BANDA SEA
251	24FEB60	21 37 4.0	7.5S	156. E	33	I	SOLOMON IS.
252	3NOV59	9 40 5.0	10.5S	111. E	33	I	S. OF JAVA
253	29MAR60	6 30 54.0	17. S	167. E	33	I	NEW HEBRIDES IS.
254	24APR60	12 14 26.0	28. N	54.5E	33	T	S. IRAN
255	22MAY61	13 44 35.8	21.3S	174.4W	91	I	TONGA IS.
256	22MAY61	17 32 21.6	22.8S	176.1W	35	I	S. OF FIGI IS.
257	14AUG61	18 50 55.3	24.2S	175.7W	21	I	S. OF TONGA IS.
258	14SEP59	14 9 50.0	28.5S	177. W	33	I	KERMADEC IS.
259	25APR60	4 1 15.0	45.5N	144.5E	360	I	HOKKAIDO, JAPAN
260	5NOV59	14 59 40.0	30.5N	129.3E	240	I	KYUSHU, JAPAN
261	9JAN62	22 13 50.4	48.3N	147.5E	480	T	SEA OF OKHOTSK
262	31MAY62	6 28 26.1	22.1N	142.6E	257	I	VOLCANO IS.
263	29DEC59	20 35 8.0	18. N	145. E	350	I	MARIANA IS.
264	19NOV59	11 8 47.0	5.5S	146. E	160	I	E. NEW GUINEA
265	30APR60	22 10 8.0	6. S	124.5E	600	I	MINDANAO, PHILLIPPINES
266	22MAY62	8 6 38.8	12.3S	166.6E	151	I	SANTA CRUZ IS.
267	19FEB60	10 36 46.0	36. N	70.5E	200	T	HINDU KUSH
268	9JAN60	7 24 3.0	36. N	69. E	150	T	HINDU KUSH
269	3JUN60	13 23 42.8	17.5S	179.5W	600	I	FIJI IS.
270	20MAR61	15 53 26.1	18.4S	175.2W	175	I	TONGA IS.
271	20FEB62	10 7 26.9	25.9S	178.4E	655	I	S. OF FIJI IS.
272-274	REGIONAL AVERAGES OF NOPONEN					T	CRIMEA-CAUCASUS
275-288	REGIONAL AVERAGES OF NOPONEN					T	GREECE
289-296	REGIONAL AVERAGES OF NOPONEN					T	TURKEY
297-300	REGIONAL AVERAGES OF NOPONEN					T	ITALY
301-305	REGIONAL AVERAGES OF NOPONEN					N	GULF OF CALIFORNIA
*306-313	REGIONAL AVERAGES OF NOPONEN					S	E. KAZAKH
*314	23JUL76		22.7S	138.6W	0	N	MURUROA
315	2JAN72	10 27 59.0	44.1N	82.6E	33	T	N. SINKIANG PROV.
316	15JAN72	20 22 15.0	41.4N	77.7E	33	T	KIRGIZ-SINKIANG BDR.
317	26FEB72	23 30 48.0	48.7N	100.2E	33	T	MONGOLIA

NO	DATE	ORIGIN	LAT	LONG	DEP	R	LOCATION
318	4MAR72	18 24 14.0	39.9N	73.5E	130	T	TADZHIK-SINKIANG BDR.
319	10MAR72	14 35 59.0	32.7N	75.3E	45	T	KASHMIR-INDIA BDR.
320	17MAY72	10 6 13.0	34.2N	71.4E	33	T	W. PAKISTAN
321	12JUN72	13 33 51.0	38.1N	43.0E	33	T	TURKEY
322	20JUN72	5 26 0.0	36.5N	71.7E	110	T	AFGHAN-USSR BDR.
323	24JUN72	15 29 26.0	36.7N	69.4E	47	T	HINDU KUSH
324	27JUN72	6 39 48.0	29.6N	70.1E	12	T	W. PAKISTAN
325	6AUG72	1 13 2.0	26.9N	61.8E	33	T	S. IRAN
326	8AUG72	19 9 44.0	27.0N	62.0E	41	T	S. IRAN
*327	26AUG72	3 46 59.0	49.5N	78.0E	0	S	E. KAZAKH
328	31AUG72	14 3 4.0	50.8N	96.7E	33	T	USSR-MONGOLIA BDR.
329	4SEP72	13 42 20.0	36.0N	73.4E	33	T	N.W. KASHMIR
330	10SEP72	20 58 17.0	41.1N	79.4E	33	T	KIRGIZ-SINKIANG BDR.
331	14JUN72	4 35 17.0	37.8N	43.2E	33	T	TURKEY
332	7OCT75	8 28 9.5	0.9N	26.8W	33	N	MID-ATLANTIC RIDGE
333	12JAN72	18 37 24.0	38.7N	74.6E	84	T	TADZHIK-SINKIANG BDR.
334	10NOV63	1 0 38.8	9.2S	71.5W	600	S	PERU-BRAZIL BDR.
335	8DEC62	21 27 18.	27.0S	63.0W	620	S	ARGENTINA

APPENDIX B

Station Data and t* Values

NO	STA	REG	DIST	t*	NO	STA	REG	DIST	t*
1	RK-ON	S	57.8	0.	45	RK-ON	S	51.9	0.1
2	RK-ON	S	50.7	0.2	46	RK-ON	S	52.1	0.
3	RK-ON	S	76.8	0.2	46	HN-ME	S	67.7	0.1
4	RK-ON	S	87.0	0.2	47	RK-ON	S	52.2	0.1
5	RK-ON	S	62.2	0.3	48	RK-ON	S	51.8	0.1
6	RK-ON	S	50.2	0.3	48	HN-ME	S	67.5	0.2
7	RK-ON	S	79.3	0.1	49	RK-ON	S	52.2	0.1
8	RK-ON	S	49.8	0.4	50	RK-ON	S	78.3	0.2
9	RK-ON	S	79.0	0.1	50	HN-ME	S	89.6	0.1
9	HN-ME	S	79.7	0.2	51	RK-ON	S	66.9	0.3
10	RK-ON	S	75.0	0.2	52	RK-ON	S	36.8	0.4
11	RK-ON	S	77.6	0.3	52	HN-ME	S	37.6	0.4
11	HN-ME	S	70.2	0.4	53	RK-ON	S	75.6	0.2
12	RK-ON	S	74.6	0.1	54	RK-ON	S	48.4	0.2
13	RK-ON	S	93.0	0.2	55	IF-ME	S	78.8	0.2
14	RK-ON	S	34.4	0.5	55	HN-ME	S	78.8	0.2
15	RK-ON	S	45.0	0.4	56	IF-ME	S	58.4	0.2
15	HN-ME	S	61.0	0.3	56	HN-ME	S	58.4	0.2
16	RK-ON	S	74.3	0.2	57	IF-ME	S	60.9	0.3
17	RK-ON	S	38.2	0.2	57	HN-ME	S	60.9	0.3
18	RK-ON	S	75.9	0.3	57	TQ-MS	S	48.7	0.2
19	RK-ON	S	64.5	0.3	58	IF-ME	S	80.6	0.2
19	HN-ME	S	78.0	0.3	58	HN-ME	S	80.6	0.2
20	RK-ON	S	44.1	0.2	59	IF-ME	S	83.3	0.2
21	RK-ON	S	81.5	0.3	59	HN-ME	S	83.3	0.2
22	RK-ON	S	58.4	0.3	60	IF-ME	S	77.2	0.3
23	RK-ON	S	82.7	0.2	60	HN-ME	S	77.2	0.3
24	RK-ON	S	39.8	0.2	61	TQ-MS	S	65.6	0.5
24	HN-ME	S	55.9	0.2	62	IF-ME	S	41.4	0.5
25	RK-ON	S	48.5	0.2	62	HN-ME	S	41.5	0.4
26	RK-ON	S	45.9	0.3	63	IF-ME	S	37.0	0.3
26	HN-ME	S	40.2	0.3	63	HN-ME	S	37.2	0.3
27	HN-ME	S	84.1	0.1	64	IF-ME	S	77.5	0.2
28	RK-ON	S	72.9	0.2	64	HN-ME	S	77.4	0.2
29	RK-ON	S	72.8	0.2	65	IF-ME	S	83.4	0.7
30	RK-ON	S	76.8	0.2	65	HN-ME	S	83.6	0.7
31	RK-ON	S	64.6	0.	66	IF-ME	S	84.3	0.2
31	HN-ME	S	69.3	0.1	66	HN-ME	S	84.3	0.3
32	RK-ON	S	81.5	0.5	67	IF-ME	S	73.7	0.2
33	RK-ON	S	37.3	0.2	67	HN-ME	S	73.7	0.
34	RK-ON	S	75.7	0.3	68	IF-ME	S	64.4	0.3
35	RK-ON	S	53.0	0.2	68	HN-ME	S	64.4	0.3
35	HN-ME	S	68.3	0.2	69	RK-ON	S	54.4	0.1
36	RK-ON	S	46.9	0.3	69	HN-ME	S	54.7	0.1
37	RK-ON	S	32.3	0.	70	RK-ON	S	78.3	0.4
38	RK-ON	S	53.9	0.1	71	RK-ON	S	48.6	0.
38	HN-ME	S	54.5	0.2	71	HN-ME	S	64.3	0.2
39	RK-ON	S	46.3	0.3	72	RK-ON	S	91.1	0.3
40	RK-ON	S	50.2	0.5	73	RK-ON	S	52.8	0.3
41	RK-ON	S	51.9	0.1	73	HN-ME	S	47.1	0.5
41	HN-ME	S	67.6	0.3	74	RK-ON	S	63.3	0.1
42	RK-ON	S	83.3	0.4	74	HN-ME	S	76.8	0.1
43	RK-ON	S	52.0	0.1	75	RK-ON	S	79.2	0.
43	HN-ME	S	67.7	0.3	75	HN-ME	S	79.2	0.2
44	RK-ON	S	52.1	0.2	76	RK-ON	S	40.6	0.3
44	HN-ME	S	67.8	0.2	76	HN-ME	S	38.5	0.2

NO	STA	REG	DIST	t*	NO	STA	REG	DIST	t*
77	RK-ON	S	67.9	0.4	123	RK-ON	S	66.4	0.2
78	RK-ON	S	43.6	0.4	123	HN-ME	S	79.8	0.3
78	HN-ME	S	37.7	0.3	124	RK-ON	S	78.7	0.
79	RK-ON	S	62.3	0.3	125	RK-ON	S	44.1	0.3
80	RK-ON	S	40.9	0.1	126	RK-ON	S	59.9	0.1
81	RK-ON	S	68.7	0.2	126	HN-ME	S	73.5	0.1
81	HN-ME	S	82.2	0.4	127	HN-ME	S	36.0	0.4
82	RK-ON	S	71.9	0.2	128	RK-ON	S	75.1	0.1
83	RK-ON	S	84.6	0.3	129	RK-ON	S	54.6	0.3
84	RK-ON	S	49.9	0.2	130	RK-ON	S	82.0	0.4
84	HN-ME	S	44.1	0.	130	HN-ME	S	95.0	0.3
85	RK-ON	S	47.8	0.2	131	RK-ON	S	62.3	0.2
86	RK-ON	S	39.1	0.2	132	RK-ON	S	54.8	0.2
86	HN-ME	S	37.9	0.3	133	RK-ON	S	34.1	0.3
87	RK-ON	S	37.9	0.1	134	RK-ON	S	54.1	0.2
88	RK-ON	S	34.8	0.3	135	RK-ON	S	64.5	0.4
89	HN-ME	S	46.4	0.4	136	RK-ON	S	42.6	0.2
90	RK-ON	S	68.3	0.3	137	RK-ON	S	60.9	0.1
90	HN-ME	S	81.6	0.1	138	RK-ON	S	42.7	0.2
91	RK-ON	S	67.8	0.3	139	RK-ON	S	71.5	0.3
92	HN-ME	S	80.8	0.4	139	HN-ME	S	85.0	0.
93	HN-ME	S	83.0	0.1	140	RK-ON	S	71.7	0.3
94	RK-ON	S	47.3	0.1	141	RK-ON	S	83.1	0.2
95	RK-ON	S	55.2	0.	142	RK-ON	S	74.7	0.1
96	RK-ON	S	41.6	0.3	143	RK-ON	S	90.9	0.2
96	HN-ME	S	39.0	0.5	144	RK-ON	S	44.7	0.
97	RK-ON	S	38.7	0.1	145	RK-ON	S	44.3	0.3
98	RK-ON	S	74.7	0.1	146	RK-ON	S	78.9	0.1
99	RK-ON	S	76.5	0.4	147	NAO	S	61.2	0.8
100	RK-ON	S	74.5	0.3	147	BFAK	T	24.8	0.4
100	HN-ME	S	66.6	0.3	147	KSRS	T	30.7	0.1
101	RK-ON	S	74.8	0.1	147	CTAO	T	77.7	0.3
102	RK-ON	S	74.5	0.1	147	KAAO	T	64.6	0.3
103	RK-ON	S	87.8	0.2	147	MAIO	T	67.9	0.3
104	RK-ON	S	86.9	0.7	147	ILPA	T	72.6	0.4
105	RK-ON	S	84.3	0.1	148	NAO	S	61.5	0.3
106	RK-ON	S	67.9	0.1	148	BFAK	T	25.7	0.5
107	RK-ON	S	46.5	0.4	148	KAAO	T	64.1	0.2
107	HN-ME	S	39.6	0.4	149	BFAK	T	29.1	0.5
108	RK-ON	S	90.0	0.4	149	KSRS	T	26.9	0.5
109	RK-ON	S	19.0	0.5	149	CHTO	T	57.7	0.3
110	RK-ON	S	91.0	0.5	149	CTAO	T	73.6	0.5
111	RK-ON	S	82.4	0.2	149	KAAO	T	63.7	0.1
112	RK-ON	S	89.5	0.4	149	ILPA	T	72.7	0.7
113	RK-ON	S	74.0	0.	151	BFAK	T	31.5	0.5
114	RK-ON	S	75.7	0.3	151	KSRS	T	24.6	0.2
115	RK-ON	S	87.6	0.3	151	CHTO	T	55.5	0.4
116	RK-ON	S	86.5	0.2	152	NAO	S	65.1	0.3
117	RK-ON	S	90.7	0.4	152	BFAK	T	30.1	0.5
118	RK-ON	S	64.3	0.3	152	KAAO	T	64.1	0.1
118	HN-ME	S	78.2	0.3	153	NAO	S	61.8	0.1
119	RK-ON	S	49.7	0.	153	BFAK	T	27.1	0.4
120	RK-ON	S	70.0	0.3	153	CTAO	T	76.0	0.4
120	HN-ME	S	83.3	0.2	153	KAAO	T	63.2	0.1
121	RK-ON	S	85.6	0.5	153	HN-ME	S	70.6	0.2
122	RK-ON	S	36.1	0.2	154	BFAK	T	31.3	0.6

NO	STA	REG	DIST	t*	NO	STA	REG	DIST	t*
154	CHTO	T	56.2	0.3	165	RK-ON	S	64.8	0.2
154	KAAO	T	63.4	0.2	166	BFAK	T	31.1	0.7
154	ILPA	T	72.8	0.1	166	RK-ON	S	60.3	0.2
155	KSRS	T	27.0	0.5	167	BFAK	T	40.6	0.3
155	CHTO	T	57.8	0.2	167	KAAO	T	57.8	0.1
155	MAIO	T	67.6	0.1	167	MAIO	T	63.0	0.2
155	KAAO	T	63.7	0.1	167	MAJO	I	9.7	0.2
155	ILPA	T	72.7	0.5	167	ILPA	T	69.1	0.3
156	BFAK	T	29.0	0.5	168	NAO	S	51.6	0.4
156	KSRS	T	27.1	0.4	168	KSRS	T	18.2	0.3
156	CHTO	T	57.9	0.2	168	KAAO	T	34.2	0.3
157	BFAK	T	33.5	0.4	168	HN-ME	S	82.9	0.4
157	KSRS	T	23.1	0.4	168	RK-ON	S	76.1	0.1
157	CHTO	T	54.3	0.3	169	BFAK	T	46.3	0.3
157	HN-ME	S	76.9	0.4	169	KAAO	T	33.8	0.1
158	NAO	S	65.5	0.2	169	ILPA	T	42.7	0.2
158	KSRS	T	23.0	0.4	169	HN-ME	S	76.8	0.2
158	CHTO	T	54.5	0.2	169	RK-ON	S	71.0	0.4
158	CTAO	T	69.6	0.5	170	BFAK	T	57.2	0.4
158	KAAO	T	61.8	0.2	170	CHTO	T	26.4	0.5
158	MAIO	T	66.2	0.4	170	KAAO	T	39.0	0.6
158	NWAO	S	89.4	0.3	170	MAIO	T	45.5	0.4
158	ILPA	T	71.6	0.3	170	ILPA	T	52.4	0.3
158	HN-ME	S	77.6	0.1	170	HN-ME	S	96.8	0.2
158	RK-ON	S	64.0	0.1	171	BFAK	T	49.8	0.3
159	NAO	S	68.2	0.2	171	KSRS	T	5.1	0.1
159	BFAK	T	36.2	0.3	171	CHTO	T	35.8	0.2
159	MAJO	I	15.4	0.4	171	KAAO	T	48.4	0.1
160	CHTO	T	47.1	0.4	171	ILPA	T	61.0	0.1
160	KAAO	T	58.5	0.2	172	BFAK	T	66.9	0.3
161	NAO	S	65.6	0.1	172	CHTO	T	21.4	0.3
161	BFAK	T	38.2	0.1	172	KAAO	T	18.2	0.2
161	KSRS	T	17.4	0.2	172	MAIO	T	25.1	0.5
161	CHTO	T	48.4	0.2	173	NAO	S	55.2	0.2
161	KAAO	T	57.4	0.1	173	BFAK	T	78.8	0.6
161	ILPA	T	68.1	0.3	173	KSRS	T	39.3	0.4
162	NAO	S	64.3	0.3	173	ILPA	T	26.4	0.1
162	BFAK	T	35.1	0.4	174	KAAO	T	22.2	0.2
162	KAAO	T	58.8	0.2	174	MAIO	T	30.2	0.3
162	ILPA	T	68.9	0.2	174	MAJO	I	41.2	0.4
163	NAO	S	70.3	0.1	174	ILPA	T	37.2	0.2
163	BFAK	T	42.1	0.3	175	NAO	S	56.1	0.5
163	KSRS	T	15.5	0.4	175	BFAK	T	73.8	0.3
163	CTAO	T	63.0	0.4	175	KSRS	T	32.5	0.2
163	KAAO	T	59.1	0.2	175	CHTO	T	16.7	0.4
163	MAIO	T	64.5	0.2	175	ILPA	T	31.2	0.6
163	ILPA	T	70.7	0.4	175	HN-ME	S	98.7	0.3
163	RK-ON	S	72.3	0.5	176	CHTO	T	16.6	0.5
164	NAO	S	54.7	0.6	176	KAAO	T	16.3	0.2
164	BFAK	T	39.3	0.4	176	MAIO	T	24.1	0.8
164	KAAO	T	46.5	0.2	177	CHTO	T	16.8	0.5
164	ILPA	T	56.2	0.3	177	KAAO	T	16.2	0.3
165	KSRS	T	31.7	0.3	178	BFAK	T	73.9	0.6
165	CHTO	T	45.4	0.2	178	CHTO	T	16.7	0.3
165	ILPA	T	41.1	0.2	178	KAAO	T	16.2	0.3
165	HN-ME	S	69.5	0.2	178	MAIO	T	24.0	0.6

NO	STA	REG	DIST	t*	NO	STA	REG	DIST	t*
178	ILPA	T	31.2	0.4	193	KAAO	T	17.2	0.1
179	CHTO	T	16.7	0.4	193	TATO	I	41.2	0.1
179	KAAO	T	16.2	0.5	193	ILPA	T	25.2	0.5
179	MAIO	T	24.1	0.5	193	HN-ME	S	79.9	0.1
180	KAAO	T	15.8	0.4	193	RK-ON	S	79.3	0.4
180	MAIO	T	23.6	0.2	194	NAO	S	38.2	0.1
181	NAO	S	56.7	0.7	194	BFAK	T	60.3	0.1
181	BFAK	T	69.1	0.5	194	KSRS	T	37.2	0.3
181	KAAO	T	20.9	0.3	194	CTAO	T	91.8	0.3
181	MAIO	T	28.3	0.5	194	KAAO	T	16.9	0.1
182	BFAK	T	70.2	0.6	194	MAIO	T	19.4	0.1
182	KSRS	T	25.0	1.0	194	MAJO	I	44.6	0.3
182	KAAO	T	23.7	0.2	194	NWAO	S	89.0	0.2
182	MAIO	T	31.3	0.5	194	ILPA	T	24.1	0.3
183	NAO	S	42.4	0.7	195	BFAK	T	60.2	0.1
183	BFAK	T	71.3	0.6	195	KSRS	T	36.9	0.3
183	KSRS	T	43.1	1.0	195	CHTO	T	34.9	0.3
183	KAAO	T	5.8	0.1	195	CTAO	T	91.5	0.4
184	KAAO	T	5.7	0.1	195	KAAO	T	17.0	0.2
184	MAIO	T	10.4	0.1	195	ILPA	T	25.2	0.4
184	ILPA	T	18.5	0.1	195	HN-ME	S	80.1	0.2
185	KSRS	T	44.3	0.7	195	RK-ON	S	79.4	0.3
185	CHTO	T	33.6	0.2	196	NAO	S	38.1	0.1
185	CTAO	T	93.6	0.3	196	BFAK	T	60.5	0.3
185	KAAO	T	6.9	0.1	196	KAAO	T	16.7	0.1
185	MAIO	T	9.5	0.1	196	MAIO	T	19.2	0.1
186	NAO	S	45.0	0.4	197	KSRS	T	38.2	0.4
186	BFAK	T	70.1	0.4	197	MAIO	T	18.7	0.2
186	KSRS	T	39.2	0.4	198	NAO	S	37.9	0.1
186	CHTO	T	28.0	0.4	198	KSRS	T	37.5	0.4
186	CTAO	T	87.6	0.3	198	CTAO	T	92.1	0.6
186	MAIO	T	14.5	0.1	199	NAO	S	38.2	0.1
186	ILPA	T	21.5	0.6	200	HN-ME	S	79.9	0.1
186	HN-ME	S	88.6	0.6	201	MAIO	T	7.2	0.1
187	NAO	S	45.3	0.2	202	KAAO	T	3.0	0.1
188	MAIO	T	14.7	0.1	203	MAIO	T	9.2	0.1
189	NAO	S	41.2	0.1	204	KAAO	T	5.2	0.1
189	BFAK	T	72.0	0.5	204	MAIO	T	11.7	0.1
189	ILPA	T	15.4	0.5	205	MAIO	T	10.9	0.2
190	MAIO	T	14.5	0.1	206	ILPA	T	16.7	0.1
190	ILPA	T	21.5	0.2	207	BFAK	T	74.8	0.7
191	BFAK	T	60.6	0.1	207	KAAO	T	2.9	0.1
191	CHTO	T	35.1	0.3	207	ILPA	T	16.7	0.2
191	KAAO	T	16.6	0.1	207	RK-ON	S	92.1	0.1
191	MAIO	T	19.1	0.1	208	NAO	S	44.2	0.6
191	MAJO	I	44.4	0.1	208	BFAK	T	73.7	0.3
191	HN-ME	S	79.7	0.2	208	KAAO	T	4.2	0.1
191	RK-ON	S	79.2	0.2	208	MAIO	T	10.3	0.1
192	NAO	S	38.2	0.1	208	ILPA	T	17.1	0.3
192	BFAK	T	60.2	0.3	209	NAO	S	44.7	0.3
192	KSRS	T	37.4	0.1	209	ILPA	T	16.7	0.2
192	KAAO	T	16.7	0.2	210	KAAO	T	2.3	0.1
192	HN-ME	S	79.7	0.3	210	MAIO	T	9.2	0.1
193	KSRS	T	36.9	0.3	211	NAO	S	43.7	0.2
193	CHTO	T	35.0	0.3	211	KSRS	T	46.8	0.2
193	CTAO	T	91.6	0.4	211	CHTO	T	31.7	0.2

NO	STA	REG	DIST	t*	NO	STA	REG	DIST	t*
211	MAIO	T	7.4	0.1	247	TSK	I	36.5	0.1
211	ILPA	T	14.6	0.3	248	TSK	I	39.9	0.3
212	BFAK	T	72.6	0.1	249	TSK	I	40.3	0.
212	KAAO	T	7.7	0.2	250	TSK	I	41.6	0.
212	MAIO	T	5.7	0.1	251	TSK	I	46.0	0.
213	KAAO	T	7.9	0.1	252	TSK	I	54.0	0.1
214	NAO	S	27.0	0.1	253	TSK	I	58.7	0.2
214	KAAO	T	20.5	0.3	254	TSK	I	70.8	0.2
214	MAIO	T	13.0	0.2	255	TSK	I	71.6	0.5
214	ILPA	T	8.9	0.2	256	TSK	I	71.8	0.
215	BFAK	T	71.5	0.2	257	TSK	I	73.2	0.2
215	KAAO	T	20.4	0.5	258	TSK	I	76.0	0.2
216	ILPA	T	8.1	0.1	259	TSK	I	81.4	0.
217	ILPA	T	6.9	0.1	260	TSK	I	10.7	0.3
218	NAO	S	20.6	0.3	261	TSK	I	13.3	0.
218	MAIO	T	21.9	0.6	262	TSK	I	14.2	0.
219	BFAK	T	40.0	0.2	263	TSK	I	18.6	0.
219	CHTO	T	51.0	0.5	264	TSK	I	41.9	0.1
219	KAAO	T	36.8	0.1	265	TSK	I	44.5	0.
219	MAIO	T	37.3	0.4	266	TSK	I	54.3	0.1
219	MAJO	I	41.6	0.3	267	TSK	I	55.1	0.
220	KSRS	T	49.8	0.5	268	TSK	I	56.2	0.
220	CHTO	T	59.9	0.3	269	TSK	I	65.7	0.1
220	KAAO	T	39.6	0.1	270	TSK	I	68.8	0.2
220	MAJO	I	53.4	0.2	271	TSK	I	71.6	0.1
220	TATO	I	59.7	0.6	272	NAO	S	21.0	0.2
220	ILPA	T	38.1	0.1	273	NAO	S	21.0	0.2
220	HN-ME	S	54.5	0.1	274	NAO	S	21.0	0.2
220	RK-ON	S	54.2	0.3	275	NAO	S	21.0	0.3
221	NAO	S	20.2	0.1	276	NAO	S	21.0	0.3
221	BFAK	T	41.2	0.5	277	NAO	S	21.0	0.3
221	HN-ME	S	54.0	0.2	278	NAO	S	21.0	0.3
221	RK-ON	S	53.8	0.4	279	NAO	S	21.0	0.3
222	NAO	S	51.9	0.2	280	NAO	S	21.0	0.3
223	NAO	S	50.0	0.2	281	NAO	S	21.0	0.3
224	NAO	S	48.8	0.2	282	NAO	S	21.0	0.3
225	NAO	S	51.8	0.2	283	NAO	S	21.0	0.3
226	NAO	S	49.6	0.2	284	NAO	S	21.0	0.3
227	NAO	S	44.7	0.	285	NAO	S	21.0	0.3
228	NAO	S	44.0	0.1	286	NAO	S	21.0	0.3
229	NAO	S	43.3	0.	287	NAO	S	21.0	0.3
230	NAO	S	42.4	0.2	288	NAO	S	21.0	0.3
231	NAO	S	43.8	0.2	289	NAO	S	25.0	0.4
232	NAO	S	43.8	0.2	290	NAO	S	25.0	0.4
233	NAO	S	43.5	0.3	291	NAO	S	25.0	0.4
234	NAO	S	43.9	0.1	292	NAO	S	25.0	0.4
235	NAO	S	43.8	0.	293	NAO	S	25.0	0.4
236	NAO	S	26.9	0.3	294	NAO	S	25.0	0.4
237	NAO	S	30.5	0.3	295	NAO	S	25.0	0.4
238	NAO	S	29.8	0.3	296	NAO	S	25.0	0.4
239	NAO	S	28.1	0.1	297	NAO	S	20.0	0.3
241	EKA	S	73.6	0.2	298	NAO	S	20.0	0.3
243	NAO	S	63.6	0.2	299	NAO	S	20.0	0.3
244	NAO	S	47.0	0.	300	NAO	S	20.0	0.3
245	NAO	S	38.0	0.2	301	NAO	S	80.0	0.5
246	TSK	I	25.0	0.2	302	NAO	S	80.0	0.5

NO	STA	REG	DIST	t*
303	NAO	S	80.0	0.5
304	NAO	S	80.0	0.5
305	NAO	S	80.0	0.5
306	NAO	S	30.0	0.2
307	NAO	S	30.0	0.2
308	NAO	S	30.0	0.2
309	NAO	S	30.0	0.2
310	NAO	S	30.0	0.2
311	NAO	S	30.0	0.2
312	NAO	S	30.0	0.2
313	NAO	S	30.0	0.2
314	HFS	S	137.8	0.1
315	NAO	S	44.4	0.2
316	NAO	S	44.0	0.2
317	NAO	S	48.9	0.2
318	NAO	S	43.1	0.1
319	NAO	S	49.7	0.2
320	NAO	S	46.5	0.2
321	NAO	S	30.4	0.2
322	NAO	S	44.9	0.2
323	NAO	S	43.6	0.2
324	NAO	S	49.8	0.2
325	NAO	S	48.1	0.4
326	NAO	S	48.1	0.3
327	NAO	S	38.3	0.1
328	NAO	S	45.8	0.3
329	NAO	S	46.1	0.1
330	NAO	S	45.1	0.2
331	NAO	S	30.7	0.2
332	NAO	S	58.0	0.8
333	NAO	S	44.6	0.
334	HHND	S	62.6	0.2
335	WNSD	S	77.8	0.
335	CFWS	S	76.4	0.1
335	NGWS	S	75.9	0.1